5-2012

Synthesis and Characterization of Mesoporous Silica Membranes Modified by Atomic and Molecular Layer Deposition

David Emmett Cassidy

SYNTHESIS AND CHARACTERIZATION OF MESOPOROUS SILICA MEMBRANES MODIFIED BY ATOMIC AND MOLECULAR LAYER DEPOSITION

By

David Emmett Cassidy

B.S. Clarkson University, 2006

A THESIS

Submitted in Partial Fulfillment of the

Requirements for the Degree of

Doctor of Philosophy

(in Chemical Engineering)

The Graduate School

The University of Maine

May, 2012

Advisory Committee:

William J. DeSisto, Associate Professor of Chemical Engineering, Advisor

Michael D. Mason, Associate Professor of Chemical Engineering

Douglas M. Ruthven, Professor of Chemical Engineering

Brian G. Frederick, Associate Professor of Chemistry

Susan G. Mackay, CEO of Cerahelix

THESIS ACCEPTANCE STATEMENT

On behalf of the Graduate Committee for David Cassidy I affirm that this manuscript is the final and accepted thesis. Signatures of all committee members are on file with the Graduate School at the University of Maine, 42 Stodder Hall, Orono, Maine.

_____

William J DeSisto, Associate Professor of Chemical Engineering Date:

LIBRARY RIGHTS STATEMENT

In presenting this thesis in partial fulfillment of the requirements for an advanced degree at The University of Maine, I agree that the Library shall make it freely available for inspection. I further agree that permission for "fair use" copying of this thesis for scholarly purposes may be granted by the Librarian. It is understood that any copying or publication of this thesis for financial gain shall not be allowed without my written permission.

Signature:

Date:

SYNTHESIS AND CHARACTERIZATION OF MESOPOROUS SILICA MEMBRANES MODIFIED BY ATOMIC AND MOLECULAR LAYER DEPOSITION

By

David Emmett Cassidy

Thesis Advisor: William DeSisto

An Abstract of the Thesis Presented
in Partial Fulfillment of the Requirements for the
Degree of Doctor of Philosophy
(in Chemical Engineering)
May, 2012

Inorganic membranes offer a means for chemical separations in a variety of applications including chemical processing, drug delivery systems, battery separators and fuel cells. There is currently a "pore size gap" in silica membranes between 1-2 nanometers. Synthesizing membranes with a fine control of the pore size and distribution within that gap is a significant challenge. This thesis reports findings on using atomic and molecular layer deposition as new synthesis approaches to controlling pore size and chemical functionality of silica membranes. Mesoporous silica membranes, prepared using surfactant-templates with pore diameters ~4nm, were modified using atomic layer deposition and molecular layer deposition. Atomic layer deposition was carried out using trimethyl aluminum and water as precursors and molecular layer deposition used trimethyl aluminum and oxalic and o-phthalic acid. These methods involved a separate pulse/purge sequence for each reactant that resulted in surface-limited film growth within the pores.

It was determined that the growth rate of atomic layer deposition of alumina within mesoporous silica membranes was not linear, with a higher growth rate during the first 7 cycles and a lower rate afterwards. Alumina deposition was favored in larger pores within

the pore size distribution of the support. The He/N_2 selectivity of the membrane was improved by removing defects, although still in the Knudsen range. In preliminary work, the hydrothermal stability of the membrane increased as a result of the addition of alumina into the silica pore network.

In the molecular layer deposition study, higher growth rates were observed when using oxalic acid as a precursor. Both oxalic and o-phthalic acid were able to increase the selectivity of the membrane above the He/N_2 Knudsen value. Analysis of the permeance of several light gases suggested that pore size reduction occurred and that the modification was confined to a small layer within the support.

ACKNOWLEDGEMENTS

I would like to first thank Dr. William J. DeSisto, my thesis advisor for providing me with this opportunity to study here at the University of Maine. I also greatly appreciate the funding received during my time at the University of Maine provided by the NSF CAREER award 0547103 and the Pulp and Paper Foundation. I would like to thank all my friends and family that have made my time at the University of Maine so great. Finally, Nick Hill, who not only helped me fabricate and design my ALD reactor but help me any random projects both for work and not.

TABLE OF CONTENTS

LIST OF TABLES

LIST OF FIGURES

CHAPTER 1

INTRODUCTION

1.1 Motivation for Research

Separating gases and liquids is a necessary means for production of chemicals and gases today. These separations range from air separation into pure forms of nitrogen and oxygen, to purification of chemicals such as gasoline and ethanol. Chemical separations are costly, typically a result of the large energy costs required to achieve the desired products. For example, distillation is a workhorse in chemical separations throughout the chemical process industries, however, it is an energy intensive process. Therefore, it is prudent to investigate alternative technologies that do not rely heavily on energy to achieve the desired separations.

Membranes provide an alternative to distillation for chemical separation. Unlike distillation, which separates chemicals based on boiling point differences and thermodynamic equilibrium, membranes separate based on the transport of molecules through a sieve. This latter separation is based on molecular size and affinity for the membrane surface, and can often provide superior separation relative to distillation. Membrane separations are relatively energy efficient, but the cost scales linearly with throughput. For most separations, distillation will continue to be used for large throughputs, but membranes are the economical choice for lower throughputs. In addition, membranes have unique applications beyond chemical processing that are highly relevant today, including applications in drug delivery, battery technology, and fuel cell technology, among others.

Membrane technologies can be divided into two different types: inorganic and organic membranes. Organic membranes are typically polymer membranes and have been studied extensively. The drawbacks for polymer membranes are their sensitivity to high

temperature and chemical instability. Inorganic membranes are more chemically and thermally stable, but have not been studied or implemented as extensively as polymer membranes. In this thesis, the focus is on inorganic membranes.

An ideal membrane will have a thin, uniform separation layer to permit a high throughput, a uniform pore size to increase molecular sieving effects, and a tailored surface chemistry to enhance surface adsorption of one chemical species relative to another. This presents a great challenge to the membrane research community. In addition, there exists a pore size gap in one class of inorganic membranes, silica membranes, between 1 and 2 nm, which has not been adequately addressed and is potentially important for separating larger organic and bio-molecules. In this thesis, research was focused on investigating new synthesis methods to address these needs.

A series of new membranes were synthesized and characterized by carrying out controlled reactions of chemical precursors within small pores (4 nanometers in diameter) of a supported silica membrane. These reactions allowed for both a controlled pore size reduction and a change in the surface chemistry of the membrane. The controlled reactions were carried out by sequentially pulsing in and purging out reactants that combined to form a very thin layer within the porous material, thereby reducing the diameter of the pores by about 0.1 nanometers per reaction cycle. Selected reactants led to the formation of a purely inorganic layer, aluminum oxide, and a hybrid organic-inorganic layer containing aluminum oxide units spaced with organic linkers such as oxalic and o-phthalic acid. A fundamental understanding of the membrane modification process as well as membrane properties for this new class of membranes is presented.

1.2 Thesis Organization

This thesis is organized in the following manner. First, background material is provided on the mesoporous silica membranes used for modification. Next, background

material is provided on the methods used to achieve the controlled chemical modification of the membranes, namely atomic and molecular layer deposition. Background material is also provided on membrane characterization methods used to quantify pore size distribution and permeance properties. The results of this research are presented in chapters 5-9. These include the synthesis and characterization of mesoporous silica membranes, atomic layer deposition reactor design and fabrication, atomic layer deposition modification of silica membranes with aluminum oxide, molecular layer deposition modification of silica membranes using oxalic and o-phthalic acid as organic linkers for aluminum oxide, and finally, preliminary results on the hydrothermal stability of modified and unmodified silica membranes. Recommendations for future work are included in the conclusions section of the thesis.

CHAPTER 2

MESOPOROUS SILICA MEMBRANES

2.1 History of Mesoporous Silica Membranes

Porous inorganic membranes offer many attractive features for separation processes that are not available in polymeric membranes. Inorganic membranes are chemically and thermally stable, are more robust, and the pore size distribution and structure are relatively uniform. Porous materials, such as inorganic membranes for gas separations, can be divided into three categories: microporous, mesoporous, and macroporous. Microporous materials have the smallest pores, typically less than 2 nm in diameter. In pores of this size, molecular sieve effects are important. Mesoporous materials have pores between 2-100 nm in diameter. In this regime, transport occurs by both Knudsen diffusion and viscous flow and perm-selectivities are generally close to the square root of the ratio of molecular weight. Macroporous materials have pores with diameters between 50nm-1μm in which viscous flow is dominant with little perm-selectivity. [1]

Mesoporous membranes have applications in nanofiltration, pervaporation, bio-separations, drug delivery, as well as other processes. The early development of inorganic mesoporous silica materials was through production of highly porous powders. The earliest patents date from the late 1960s and early 1970s. The rapid development of these materials, however did not start until the early 1990s.[2] These powders had a relatively uniform pore size distribution and offered an alternative to the smaller pore sizes of zeolites. One of the first developments of ordered silica mesoporous materials was Mobil Composition of Matter No. 41(MCM-41) a sol-gel derived material. It was developed at the Mobil labs in 1992 to produce a material with a very high surface area (over 1000 $m^2 g^{-1}$) with the ability to control the pore size between 2 and 20nm in pore diameter. The pore size was adjusted by using different length organic surfactants in their sol-gel process. The

longer the surfactant, the larger the pore diameter of the material produced.[3, 4] These materials were known to have a high degree of crystallographic ordering of pores, with the initial MCM-41 having a hexagonal structure and MCM-48, an expansion of these materials, having a cubic structure.[5-8] The field of mesoporous materials expanded with the first synthesis of SBA-15. SBA-15, while also a hexagonal structure, can be synthesized with uniform pores up to 30 nm. SBA-15 has thicker pore walls than those of MCM-41, with the result that it has better thermal and hydrothermal stability.[9]

2.2 Membrane Support Structure

The application of these new high porosity mesoporous materials to membranes required the development of a process of sol-gel dip coating these materials onto a support. In order to achieve this, a continuous thin film had to be produced and deposited on the top layer of a highly porous support. Some of the initial studies in templating these new materials were developed by Yang, in which a sol-gel membrane was deposited onto a porous alumina support.[10] McCool was also one of the first to examine depositing mesoporous silica membranes on an alumina support, using dip-coating and hydrothermal deposition techniques.[11]

Traditionally, sol-gel membranes are produced using an asymmetric porous membrane. Figure 2.1 shows the typical structure of an asymmetric membrane with three distinct layers. The bulk of the membrane is the macroporous layer which is typically composed of alumina. Alumina powder is sintered, producing a tortuous network of pores greater than 1 μm in diameter, through the void spaces of the macrostructure. On top of the macroporous layer is an intermediate layer consisting of smaller particles of alumina and yielding pores between 100-1500 nm. This intermediate layer is needed to smooth the surface thus allowing the top active layer to bond adherently to the surface, while minimizing the thickness. For sol-gel membranes this top mesoporous layer is typically dip-

coated from a sol-gel solution onto the intermediate surface. This mesoporous layer is called the active layer because the chemical separation occurs within it. The pore size of mesoporous sol-gel membranes are typically between 3-100 nm[1].

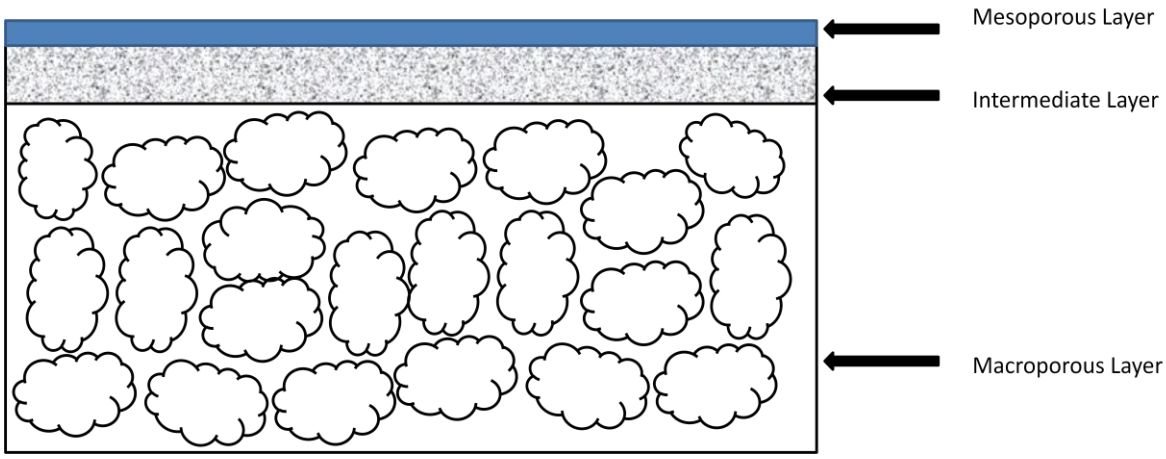

Figure 2.1 - Asymmetric porous membrane

2.3 Sol-Gel Synthesis

To produce a sol-gel membrane on the surface of a ceramic support, a sol-gel solution that is dip-coated onto the support must be prepared. A typical recipe for this solution (also used in this thesis) is described here. The solution contains a molecular silica source, tetraethyl orthosilicate (TEOS), a volatile organic that evaporates quickly, ethanol, a surfactant, cetyltrimethylammonium bromide (CTAB), an acid, dilute HCl, to suppress the sol-gel solution from polymerizing, and water. The silica to surfactant ratio is adjusted to produce the desired pore ordering. The sol-gel solution is then allowed to age for a period of time to allow the surfactant to organize into micelles. The micelles produce uniform rods, in which the hydrophobic ends are all at the center of the rod and the hydrophilic ends are all on the outside of the rod.[12]

Silica sol-gel membranes are produced using a technique called evaporation induced self-assembly. The solution is usually dip coated onto a support, where the volatile organic (ethanol) starts to evaporate. During the evaporation of the volatile organic, the surfactant

micelles organize as the concentration of surfactants increases due to the loss of the volatile organic solvent. After the concentration reaches a certain point, the micelles attain a cubic order and the micelles form a connected structure. The remaining water and ethanol is then removed by evaporation, leaving behind the solid sol-gel material deposited onto a ceramic support. The membrane is then calcined to remove the surfactant, to produce the ordered porous membrane with the pore size closely tied to the length of the surfactant molecule. [11, 13, 14]

During the development of the mesoporous silica membranes it was initially noted that these highly porous materials also have a degree of order to them. In the initial development of MCM-41 the material was hexagonally ordered while MCM-48 had cubic structure,[3, 4, 6, 7] but in MCM-48 it was noted the material would convert from a lamellar phase to a hexagonally ordered phase over time.[5] Control over the ordering of the materials became a study in itself extensively examined by Hillhouse and many other groups.[15] By varying the conditions of the aging time of the sol, the humidity during the evaporation, and the concentrations of the surfactant and silica source, the ability to alter the order of the material was established. The measured phase diagram is shown for a silica film in Figure 2.2. The Si:EO ratio is the silica to poly(ethylene oxide)-b-poly(propylene oxide)-b-alkyl surfactant ratio.[13-15] Figure 2.2 shows how the crystallographic order can change with variations in the aging time, and the concentration of the surfactants and silica sources. The rate of evaporation plays a key role in the production of an evenly coated film with uniform order.

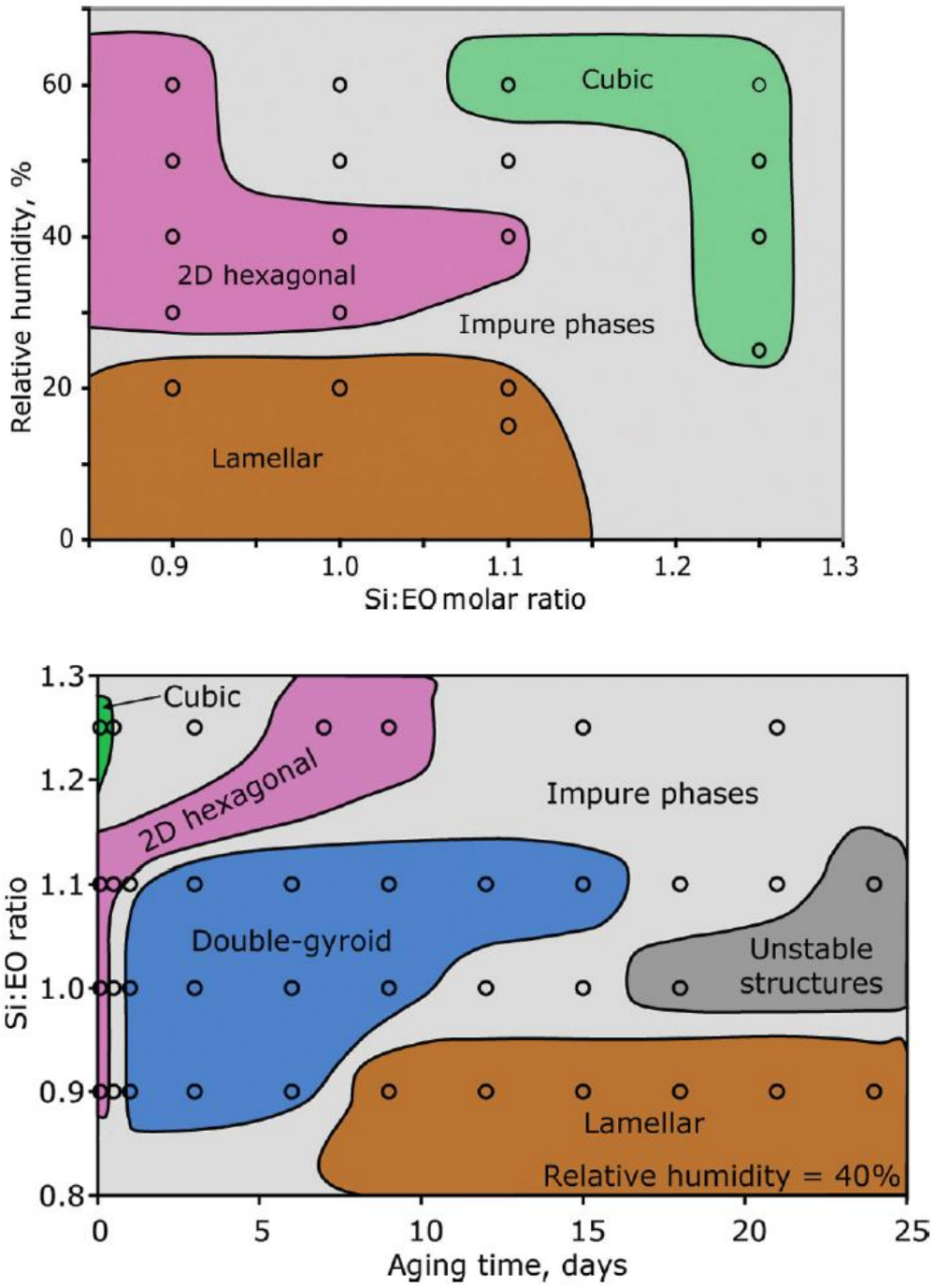

Figure 2.2 - Examples of the effect of humidity, silica to ethylene ratio, and aging time on the order of dip-coated membranes[15]

CHAPTER 3

ATOMIC LAYER DEPOSITION (ALD)

3.1 History of ALD

Atomic Layer Deposition (ALD) is a method used to deposit layers of atoms uniformly over a surface by sequential cycle of self-limiting surface reactions. Initial studies were carried out in the 1970s[16, 17] and initial applications were in the semiconducting industry for the manufacturing of 1 gigabyte DRAM computer memory [18]. The need for thin, uniform, and complete coatings for the semiconductor industry helped drive this development. ALD reactions have been carried out under a variety of reaction conditions including under vacuum, in a viscous flow reactor, and by advanced techniques including the use of plasma.[19] After the initial development of ZnTe ALD[17], a variety of different chemistries were developed for ALD , including SiO_2 and Al_2O_3. These materials were synthesized using different reactions. For example SiO_2 ALD has been synthesized using different silicon sources including silicon tetrachloride, tetraethyl orthosilicate, and tetramethyl orthosilicate.[20, 21]

3.2 ALD Chemistry

One of the most widely studied reactions of ALD is Al_2O_3 growth using trimethyl aluminum (TMA) and water as precursors.[20, 22-24] This reaction occurs at room temperature instead of at conditions above 400 °C that are required for many other chemistries. The reaction is divided into two half reactions, A and B, where * indicates a surface species.

$AlOH^* + Al(CH_3)_3 \rightarrow -O-Al(CH_3)_2^* + CH_4$ (A)

$AlCH_3^* + H_2O \rightarrow AlOH^* + CH_4$ (B)

Figures 3.1-3.3 show the steps of alumina ALD on a flat silica surface. Figure 3.1 shows the first half reaction involving component A, TMA, reacting with the surface hydroxyl groups.

If given enough time and precursor, the TMA will replace all the surface hydroxyl groups with alumina methyl groups. The TMA does not react with the methyl group, so the reaction is self-limited to a single layer. The only by-product is methane, which is purged together with any excess TMA either by pumping or purging with an inert gas.

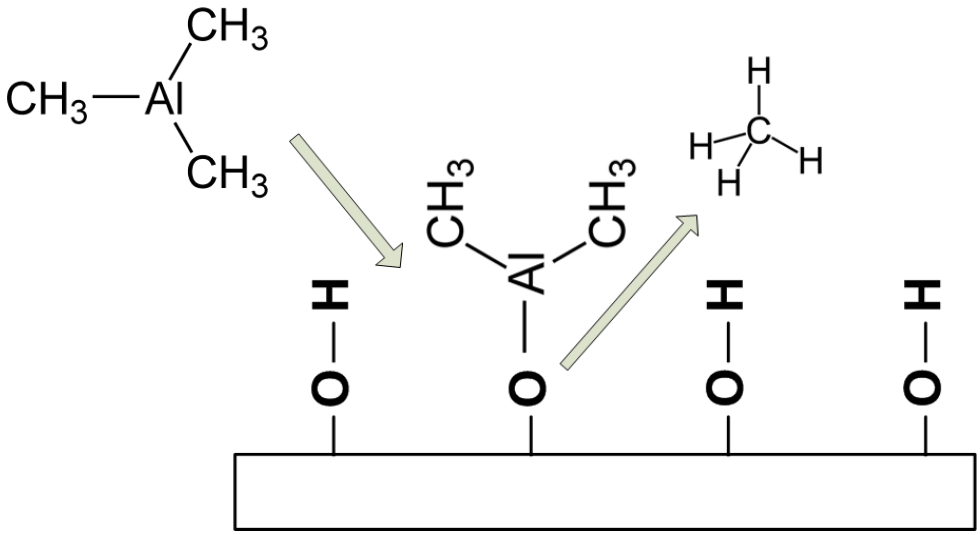

Figure 3.1 – Trimethyl aluminum ALD reaction with surface hydroxyls

In the second half-reaction, shown in Figure 3.2, water (component B) reacts with all of the methyl groups to produce surface hydroxyls and methane. Some of the water will react with two adjacent methyl groups to create an oxygen bridge. The overall concentration of free surface hydroxyls remains constant after each subsequent cycle of ALD.

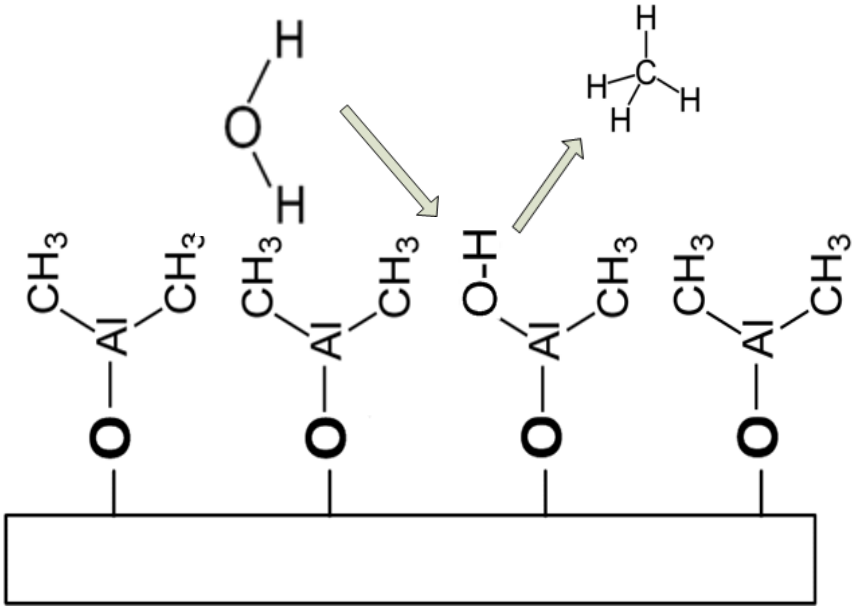

Figure 3.2 – Water ALD reaction with surface methyl groups

The excess water and methane are purged leaving behind surface hydroxyl groups that allow the process to continue as shown in Figure 3.3. Sequential deposition of repeated half-reaction cycles builds up a layer of finite thickness related to the growth rate per ALD cycle and total number of ALD cycles. The key difference between Chemical Vapor Deposition (CVD) and ALD is that in ALD all of the unused precursors are purged before the other precursor is exposed.[18, 20]

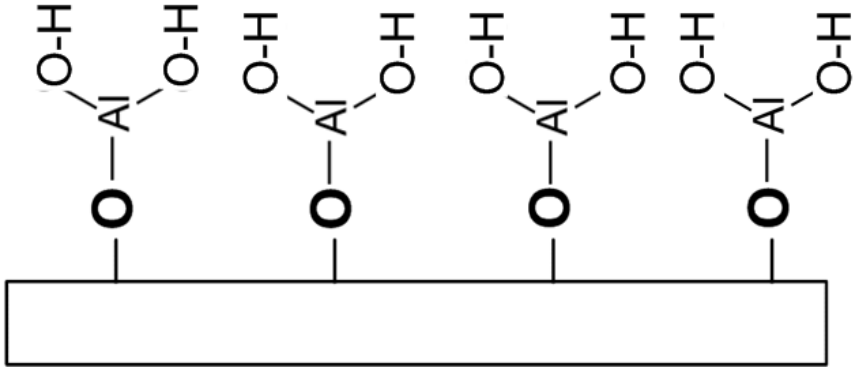

Figure 3.3 – Structure of complete surface layer of alumina ALD[25]

3.3 Types of ALD Reactors

There are two primary reactor types for ALD, a viscous flow reactor and a low-pressure reactor.[18] In an inert gas, or viscous flow reactor, a carrier gas provides the primary transport means for the precursors and byproducts. This helps to speed up the entire ALD cycle. The reactor pressure remains constant both during the precursor exposure and during removal. Viscous reactors are typically used for ALD on flat surfaces, or those typical of the semiconductor industry.

In highly porous material, such as membranes, a vacuum ALD reactor is used. Instead of using a carrier gas to bring the precursors to the reactor, transport occurs by Knudsen or molecular diffusion. This technique is helpful to access the active sites inside small pores where diffusion rates are slow. The overall reaction cycle is slower due to the longer purge times required. An inert gas is still used to help sweep out residual precursors and byproducts, but the reactor must be evacuated to less than 10 millitorr before the next exposure.[23]

3.4 Applications of ALD

Initial studies focused on modification of silicon wafers and high aspect trenches, including the production of DRAM capacitor dielectrics for memory chips over 1 gigabyte.[26, 27] In order to make these capacitors small enough to accommodate the large amounts of data on the memory chip, deep trenches were coated using ALD to make a thin uniform insulating surface of SiO_2 on the capacitor. An additional potential application of ALD is membrane modification, a particular focus of this thesis.

3.4.1 Modification of Membranes

An important approach to the modification of inorganic membranes requires coating of the surface with a uniform and very thin layer of material. This allows a controlled reduction in the pore size. ALD is one of several methods used for pore size

reduction. Some of the other techniques available for pore size reduction are: chemical vapor deposition (CVD), colloidal silica deposition, and supercritical CO_2 silanation.[28-30] CVD provides a good way of growing material quickly over a surface, but the surface growth is not always even and it is difficult to reduce pore size of small pores without closing them. The colloidal deposition and supercritical CO_2 methods allow the surface to be coated with new organic chains that reduce the pore size. This approach offers great flexibility for changing the surface chemistry of an inorganic membrane, but it does not yield the same even layers. Gold templating offers a way to coat porous materials evenly but is limited to pores greater than 80 nm due to diffusion limitations.[31] ALD offers the potential of modifying pores in the mesoporous regime of 2-50 nm in diameter while adding an even layer to both large and small pores alike.

3.4.1.1 ALD Modification of Ceramic Membranes

Using atomic layer deposition for modification on membranes was initially developed in the 1990s.[22, 32] George's group applied this technique to modify tubular ceramic membranes with TMA and water (Al_2O_3 ALD).[21, 33] These studies involved modifying a 50 Å pore diameter alumina membrane with 50 cycles of ALD. For all the experiments, the precursor exposure times were higher than those reported for ALD of flat surfaces (typically 2-30 seconds)..[18] They correlated a pore size reduction using a relationship assuming all Knudsen flux by comparing the changes in the conductance and with the pressure drop across the membrane. After 35 cycles of Al_2O_3 ALD they assumed that the pores had closed. This produced an average pore diameter reduction of 2.5 Å per cycle. This pore size reduction is comparable to the growth rate on a flat surface of 1.2 Å per cycle, since the reduction in the diameter of a cylinder occurs at twice the rate of growth for a flat surface. One of the interesting factors in their analysis was they correlated pore closer during conductance measurements at 500 K but at 298 K they correlated a pore size

between5-10 Å. Also after 17 cycles of ALD the membrane's pores showed no further reduction in pore size at 298 K, but for the same membrane at 500 K the pore diameters continued to decrease for between 18-35 cycles. One of the major deficiencies in their analysis is that it takes no account of pore size distribution and changes in porosity throughout the modification cycles. They assumed all the pores were uniformly modified during ALD, which may or may not be true.[22, 23] Even though the conductance dropped by over 99%, there was still a residual flux through the membrane even after 50 layers, with a conductance of $1.78 * 10^{-8}$ mol $m^{-2}s^{-1}Pa^{-1}$ at a pressure drop of 175 torr. This residual flux is probably due to the presence of a few larger pores that had not been closed, even though all the smaller pores were sealed off. Alternatively it is possible that all pores eventually approach a minimum size.

Cameron et al also later studied other ALD chemistries on the same alumina membranes using silicon tetrachloride/water (SiO_2 ALD) and titanium tetrachloride/water (TiO_2 ALD).[33] For SiO_2 ALD the pores closed after 25 cycles and for TiO_2 ALD the pores closed after 16 cycles, producing growth rates of 1.3 Å per cycle and 3.1 Å per cycle, respectively. They reported the pore size shift in terms of the conductance shift as for the Al_2O_3 study. In these studies, they also assumed that the pores closed, but the residual conductance after 24 cycles and through 30 cycles of SiO_2 ALD was over 10% of the original conductance. This remaining flux means that pore closure was incomplete and either the pores approached a minimum pore size, or there were still some large pores that remained open and contributing to the membrane flux.[21]

Klaus et al continued to the study ALD reactions in the late 1990s, including the implementation of catalyzed ALD. Many of the initial studies of ALD were carried out at high temperatures in excess of 500 K. In some of the ALD applications, the temperature could be reduced without changing the reaction chemistry, specifically TMA and water ALD.

For SiO_2 ALD an operating temperature in excess of 800 K was required. George's group was able to lower the temperature to 300K by adding a catalyst for the ALD reaction. By adding pyridine to the AB cycle (for $SiCl_4$ and water) they were able to grow SiO_2 ALD at 300K. The exposure required for the precursors also dropped from 10^7 to 10^4 Langmuir (10^{-6} torr s). Pyridine was combined with the exposure for both $SiCl_4$ and H_2O. [34-36] The amine group on the pyridine catalyzes the reaction of the precursor with the respective surface groups during the ALD cycle. Implementing this catalyzed ALD technique at room temperature almost doubles the growth rate from 1.1 Å per cycle to 2.1Å per cycle. This increased growth rate per cycle was attributed to the higher growth rates for most ALD applications at lower operating temperatures due to a reduction in the density of free surface hydroxyls at higher temperatures, not a direct effect of the pyridine catalyst. .

3.4.1.2 ALD Modification of Mesoporous Sol-gel Membranes

In 2004 McCool et al studied the effect of catalyzed ALD on mesoporous silica using pyridine, silicon tetrachloride, and water. McCool used the catalyst to serve two different purposes. The addition of the catalyst reduces the temperature and exposure time required. The results also suggest that the catalyst may have a limiting effect on the minimum pore size. The pyridine needs to be present for ALD to occur at lower temperatures, so in small pores from which pyridine is sterically excluded, ALD would stop. This would cause a minimum pore size corresponding to the size of the pyridine molecule. During the study they examined the effects of ALD on the permeance of the membrane. The viscous flux through the membrane was reduced from 3 to 1 % of the total permeance, due to the loss of pores larger than 20 nm in which there is viscous flow. Comparing the fluxes of o-xylene and p-xylene, a final pore size of 10 Å was estimated. There was no analysis of the pore size of the membrane produced except for the initial nitrogen isotherm of the sol-gel used for dipping onto the support. Since the membranes are not completely

homogeneous in pore size, the larger pores could have been modified since the diffusion rates of the precursors and catalyst were not fully completely studied. A permporometry analysis would yield a better understanding of the pore size distribution than the hypothesis of 10Å final pore diameter with no larger pores remaining.[37, 38]

Other research groups, including Dai's, have examined the effect of TiO_2 ALD on the pore size distribution of mesoporous silica with this approach. They were able to reduce the pore diameter of SBA-15 from 67 Å to 32 Å over 18 cycles of TiO_2 ALD. This corresponds to a pore size reduction of 1.8 Å per cycle, which is less than the 3.1 Å per cycle referenced by George in the modification of alumina membranes.[33] The surface area of the silica was reduced from 650 m^2/g to 20 m^2/g, which corresponds to a large drop in the porosity and a reduction in the total number of pores, not just a reduction in the pore diameter. The pore size distribution was measured in the standard way using nitrogen isotherms at low temperatures. Nitrogen isotherms offer an excellent way to measure the bulk porosity and pore size distribution of mesoporous materials. The application of nitrogen isotherms on dip-coated mesoporous silica is limited. For an asymmetric membrane most of the pore volume is associated with the macroporous support layer so the properties of the mesoporous silica layer are masked.[21, 39]

Lin's group studied mesoporous membranes using alumina ALD to reduce the pores of a sol-gel alumina membrane from 4 nm to sub 2 nm diameter pores for water/oxygen separations.[24] They used the ALD technique to modify sol-gel membranes to this size in order to overcome the problems of producing microporous membranes of high permeance and the limited range of surfactants that can produce pores in this regime. ALD modification allowed for the water permeance to remain high, reducing by a factor of 2, while the oxygen permeance reduced by a factor of 30. Water permeated faster than oxygen due to its larger kinetic diameter of 3.46 Å compared to 2.75 Å for water. The ALD

technique was able to reduce the pore size sufficiently to increase the separation factor of the sol-gel alumina membrane from 11 to 71 for water/oxygen. In future studies of sol-gel α-alumina membranes separation factors over 250 were obtained, whereas other microporous materials like P-zeolites have separation factors of only about 50. These increases in the separation factor were obtained without sacrificing the permeance, with the final permeance of a modified membrane being 3.0×10^{-7} mol $m^{-2}s^{-1}Pa^{-1}$. [24, 29]

CHAPTER 4

MEMBRANE CHARACTERIZATION

4.1 SEM

The production of ordered mesoporous silica membranes on dip-coated ceramic supports by dip-coating has been fairly well studied.[11, 40] A variety of techniques have been developed for characterization of mesoporous silica membranes. One of the more prevalent methods of characterization is through SEM. SEM imaging allows the top surface and a cross section of the membrane to be viewed, thus yielding a detailed picture of the membrane structure. SEM imaging techniques typically do not determine a bulk pore size distribution due to limits of the resolution of ~1 nm. The image shows only a very small part of the bulk membrane and may therefore miss regions of heterogeneity. SEM images cannot determine a pore size distribution for the top layer of mesoporous silica membranes due to the reduced resolution of images for insulating materials such as silica.

4.2 Permeance

In permeance measurements of light gases the flux through a membrane is measured and normalized for the pressure drop. The permeance of a membrane is derived from Fick's first law, Equation 4.1. The flux across the membrane (J) depends on the diffusivity, D, the change in concentration, C, and the membrane thickness, z. According to Henry's Law, the concentration, C = K*P, where K is the Henry's constant of the gas which relates P, the partial pressure, to C, the adsorbed quantity of the gas. Combining Henry's law with Fick's first law yields Equation 4.2.

$$J = -D * \frac{dC}{dz} \tag{4.1}$$

$$J = -D * K \frac{dP}{dz} \tag{4.2}$$

Integrating Equation 4.2 for dP and dz, respectively yields Equation 4.3.

$$\pi = \frac{J}{\Delta P} = \frac{D*K}{z} \quad (4.3)$$

$$\pi_t = -\frac{J_t}{\Delta P} = \frac{Q}{RT*SA}\frac{P_{atm}}{\Delta P} \quad (4.4)$$

The flux across the membrane is divided by the pressure drop to determine the permeance across the membrane, π.[41] Experimentally, the permeance across the membrane is calculated from Equation 4.4. The measurement is based on the flow rate through the membrane, Q, the ideal gas constant, R, the temperature of the membrane, T, the surface area of the membrane, SA, and the pressure drop across the membrane, ΔP; producing a permeance value with units of $\frac{mol}{area \cdot time \cdot pressure\ drop}$.

To measure the permeance across the membrane for different light gases involves measuring the flow rate for different pressure drops across the membrane. The gas flow into the membrane cell was held constant at 500 sccm using a mass flow controller (MKS). The pressure drop across the membrane was set using a back pressure regulator (MKS) between 30-1800 torr. Excess gas that did not permeate across the membrane was purged to the atmosphere. A soap-film meter was hand timed using a stop watch to determine the flow rate.

In pores greater than 20nm in diameter viscous flow is significant. In this region gas molecules flowing through a pore interact primarily with other molecules, rather than with the pore wall. As a result the effective diffusivity is pressure dependent. In instances in which the molecules interact with each other rather than with the pore wall the membrane will have a negligible selectivity.[1] The relationship of permeance for viscous flow is given by Equation 4.5.

$$\pi_V = \frac{\varepsilon}{\tau z}\frac{Pr^2}{8\mu RT} \quad (4.5)$$

The viscous permeance (π_v) is dependent on the pore radius, r_p, the mean pressure of the membrane system, P, the viscosity of the gas, μ, the porosity of the membrane, ε, the

tortuosity of the pores, τ, and the length of the pore, z.[42] Knudsen diffusion typically occurs in pores ranging from 2-100 nm in diameter, which corresponds to the pore size range of mesoporous sol-gel membranes. In the Knudsen diffusion regime there is no pressure dependence as the gas molecules interact primarily with the pore walls due to the low relative pressure.[1] The Knudsen permeance relationship shown in Equation 4.6 can be derived from the kinetic theory of gases.

$$\pi_k = \frac{97}{R}\frac{\varepsilon\bar{r}}{\tau z}\frac{1}{\sqrt{TM}} \qquad (4.6)$$

The Knudsen permeance relationship depends on the molecular weight of the gas, M, and the mean pore radius, $\bar{r}$. Since the permeance is independent of pressure, the membrane selectivity in the Knudsen regime is given by Equation 4.7.

$$\alpha = \sqrt{\frac{M_2}{M_1}} \qquad (4.7)$$

The theoretical Knudsen selectivity, α, of a binary gas mixture is simply the inverse ratio of the square-roots of the molecular weights. This is also equal to the ratio of the single-gas permeances.[1]

Membranes typically have a heterogeneous pore size distribution, so it is important to determine what fraction of the bulk permeance is due to viscous flow along with defects such as cracks and pinholes. The total permeance is a combination of the viscous permeance and the Knudsen permeance, which fits the parallel resistance model shown in Equation 4.8.[1]

$$\frac{1}{\pi_t} = \frac{1}{\pi_v} + \frac{1}{\pi} \qquad (4.8)$$

If a significant fraction of the pores are smaller than the mesoporous regime, micropore diffusion can occur. Micropores are less than 2 nm in diameter and as a consequence of molecular sieving effects, the selectivity is often much higher than the Knudsen limit, particularly for molecules of a size similar to the pore size. These

microporous membranes are used in natural gas purification, hydrogen, and other separations.[43, 44] Sol-gel membranes made using surfactants have pores larger than 2 nm and require a post synthesis modification to enhance the selectivity.

4.3 Hexane Permporometry

One method used to determine the pore size distribution of a sol-gel membrane is permporometry. Permporometry determines the pore size distribution by gradually increasing the partial pressure of a condensable vapor flowing across a membrane, while measuring the permeance of a permanent gas through the membrane. The vapor will condense by capillary condensation inside the smallest pores first, eventually blocking them, and then sequentially block larger and larger pores (Figure 4.1). The resulting permeance data can be used to generate a pore size distribution. This offers a more complete comparison for membranes than traditional permeance measurements.[40]

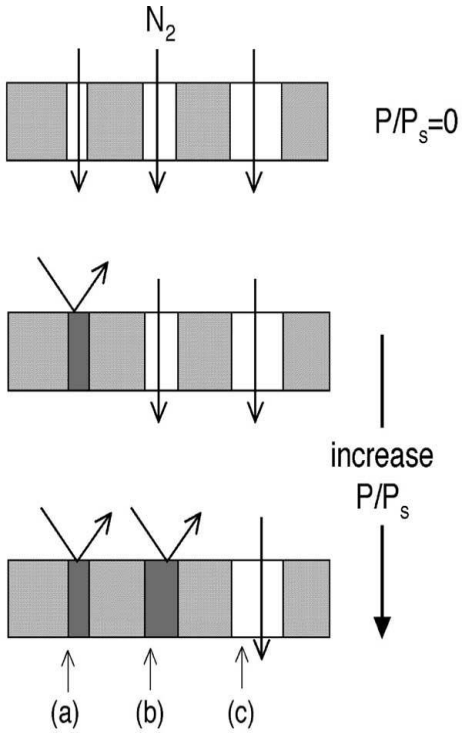

Figure 4.1 – Effect of increasing hexane concentration during permporometry measurement

The effect, of hexane condensing in the pores, can be mathematically evaluated using the Kelvin equation, Equation 4.9.

$$R_p = \frac{-4\sigma V_m}{RT * \ln(a)} + t \qquad (4.9)$$

Hexane will condense and block a pore up to the size, R_p, corresponding to the hexane activity, a, the surface tension, σ, the molecular volume of hexane, V_m, the ideal gas constant, R, the temperature, T, and the thickness of the absorbed monolayer, t.[40] This activity is corresponds to the partial pressure of the hexane.

To quantify the pore size distribution requires a model that describes pore geometry, adsorption of the condensable vapor and the transport of the permanent gas. Cao et al developed a simple model that assumes cylindrical pores, Knudsen transport through the pore and the Kelvin equation for capillary condensation. [45] At a specific pore radius the Knudsen permeance, P(r) is given by Equation 4.10, where f(r) is the pore size distribution, r is the specific radius, ν is the molar volume, T is the temperature, τ is the tortuosity, and l is the pore length. The differential relationship of the permeance provides the pore size distribution f(r) using Equation 4.11.

$$P(r) = \frac{2\pi\nu}{3RT\tau l}\int_r^\infty r^3 f(r)dr \qquad (4.10)$$

$$f(r) = \frac{-3RT\tau l}{2\pi\nu r^3}\frac{dP}{dr} \qquad (4.11)$$

This relationship can be applied to determine the pore size distribution from 1.7-200 nm. The lower limit of the pore size distribution is constrained by limits of the Kelvin equation for condensation of hexane and the limits of control of the partial pressure of hexane. The upper limit of the pore size distribution is constrained experimentally by the need for a pressure drop across the membrane to measure the permeance. This pressure drop causes the hexane in the large pores to be stripped and not be blocked by the hexane. Integrating

this pore size distribution allows the dimensionless porosity of the membrane with a surface area of S_A to be determined using Equation 4.12.

$$\Phi = \frac{\int \pi r * P(r) dr}{2S_A} \qquad (4.12)$$

4.4 Nitrogen Isotherm

One way to measure the porosity and surface area of porous materials is to measure how nitrogen condensing inside the pores of the material. A BJH analysis of this data correlates a pore sizes by using a modified Kelvin equation for nitrogen condensation.[46] For analysis of silicas, like the CTAB-derived sol-gel membranes, the BJH analysis underestimates pore size. Kruk-Jaroniec-Sayari correction was developed to better approximate the pore size of silica MCM-41.[47] Nitrogen isotherms can measure the properties of bulk powders but cannot be easily applied to sol-gel membranes dip-coated onto an asymmetric supports.

CHAPTER 5

SYNTHESIS OF MESOPOROUS SILICA MEMBRANES

5.1 Introduction

Mesoporous silica membranes were used as a support layer for further modification by ALD methods. In the overall membrane architecture the mesoporous silica layer, with a mean pore radius ~2.5 nm, is present as the top layer (~2 μm thick) on an asymmetric alumina membrane of high permeance. This top layer of mesoporous silica provides a smaller pore membrane for ALD modification, reducing the number of ALD reaction cycles required for modification, which can be examined with light gas permeance. The mesoporous silica membrane also provided a more uniform support membrane for ALD modification.

The synthesis of mesoporous silica membranes in the literature has been reviewed in the background section of this thesis (Chapter 2). It is very important to prepare a support layer that is both reproducible and defect-limited, as the presence of large defects will negate any attempts to modify the membrane permeance properties selective to ALD modification. In this chapter, the synthesis and characterization of the mesoporous silica support layer is described. The membranes were synthesized under controlled environmental conditions for reproducibility. The surfactant-template used was CTAB, which led to MCM-type membranes. The resulting membranes have light gas permeance properties essentially governed by Knudsen diffusion.

5.2 Sol-gel Solution Synthesis

During this study, improving the repeatability of the synthesis of dip-coated sol-gel membranes was emphasized. First, a solution for dip-coating was prepared and then aged. After dip-coating the layers were calcined. This process was repeated to eliminate cracks and defects. The sol-gel solution consisted of a mixture with a molar ratio of 1 TEOS:20.52

EtOH:5.25 H_2O:0.144 CTAB:0.00409 HCl. To produce this solution, 7.04 g of TEOS, 4.73 g EtOH, 0.617 g H_2O, and 0.57 g of 0.03 M HCl were refluxed at 60 °C for 1 hour. 10 mL of the refluxed solution was combined with 1.3 g of CTAB, 20.24 g of EtOH, 1.75 g of H_2O, and 0.1 g of 1M HCl and then aged in a sealed container for 1 week at 3 °C to aid in the formation of micelles.[11, 37, 48] HCl was added to the solution to prevent the surfactant molecules from polymerizing, while the proper ratio of water allowed formation of the desired micelle structures inside the solution.

During initial studies of synthesizing sol-gel mesoporous membranes, the dip-coating process was done at room temperature under varying humidity.[11, 40] It was noted that there were variations in the consistency of production of the dip-coated membranes throughout the year as the ambient temperature and humidity changed. An environmentally controlled chamber was then introduced for the dip-coating process, shown in Figure 5.1. This made it possible to maintain a constant temperature and humidity throughout the dip-coating and evaporation steps. Through experiments in the University of Maine lab under a range of controlled conditions, the optimal temperature and humidity for sol-gel synthesis was found to be, 30°C and 50% humidity for MCM-48 type cubic ordered films.[49]

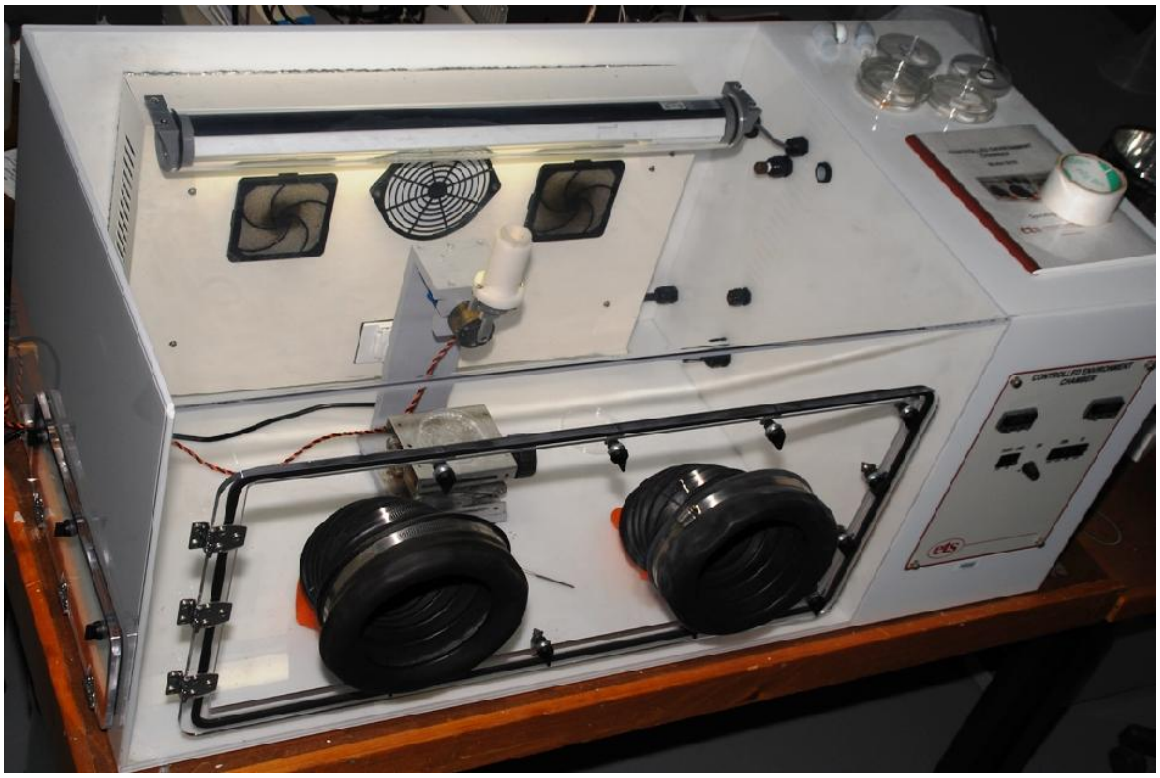

Figure 5.1 – Environment controlled chamber with dipping apparatus

The dipping process involved first bringing the chamber, the dipping apparatus, and sol-gel solution up to the operating temperature of 30 °C, along with the humidity inside the chamber to 50%. The solution was filtered, using a 0.8 μm syringe filter to remove any large particle contaminants were removed before dipping and placed into a petri dish from which the supports were dip-coated. The supports chosen were commercially produced α-alumina (HiTK) with a macroporous base layer and a 10 μm thick intermediate layer (pore size 0.1 μm). The supports were placed into the custom built dipping apparatus and the top active layer of the support was dipped into the sol-gel solution for 15 s. Any excess solution was removed using bibulous paper and the membrane was allowed to dry for 24 hrs at 30 °C and 50% humidity. The membrane was calcined in air for 4 hrs at 500 °C with a ramp rate of 1 °C min^{-1}. The calcination process was done to remove the CTAB surfactant and leave behind the silica mesoporous network on top of the support. Even with the

improvements in the control of the evaporation rate of the membranes, it was necessary to dip coat more than one layer of sol-gel mesoporous membrane on the alumina support. After each dip-coating cycle the membrane must be calcined. Calcination thermally decomposes the surfactant, removing it from the film and leaving a porous network. During calcination, cracks in the layer can appear due to thermal stresses. The minimum number of dip-coated layers required for the support to be completely coated and essentially crack free was found to be three. During experiments reported in this thesis, 4 layers were added to ensure that the majority of defects were coated. [11, 37, 40] The remaining sol-gel solution after dip-coating was also dried for 24 hrs. This material was ground using a mortar and pestle, and calcined for nitrogen BET isotherm analysis of the sol-gel layer.

5.3 SEM Analysis

The dip-coated membranes were analyzed using SEM to determine the thickness of the dip-coated layer and the conformal properties. The SEM images of a cross section of the mesoporous silica membrane dip coated onto a support are shown in Figures 5.2-5.4. For all of the images, the membrane was dip-coated, then mechanically snapped in half to develop the cross sectional view of the fractured membrane. Figure 5.2 shows clearly the two layers of the HiTK support. The bulk of the support is the macroporous alumina, with pores in excess of 500 nm and ~ 3 mm thick. On top of this layer is a thinner layer with smaller pores to provide a smooth surface for dip-coating. This intermediate layer is ~20 μm thick with 100 nm pores. The top layer is the mesoporous silica layer.

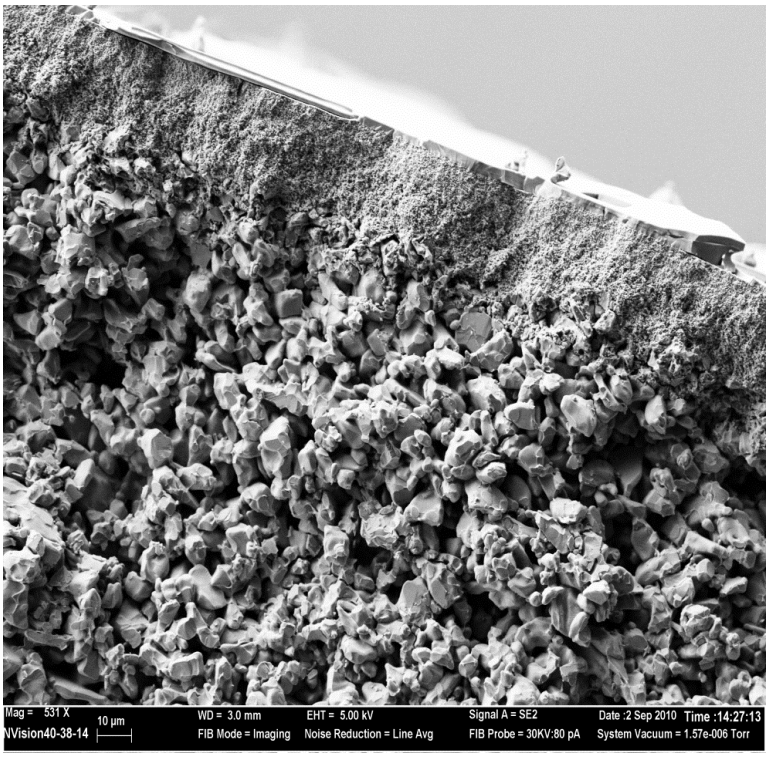

Figure 5.2 – SEM of α-alumina support

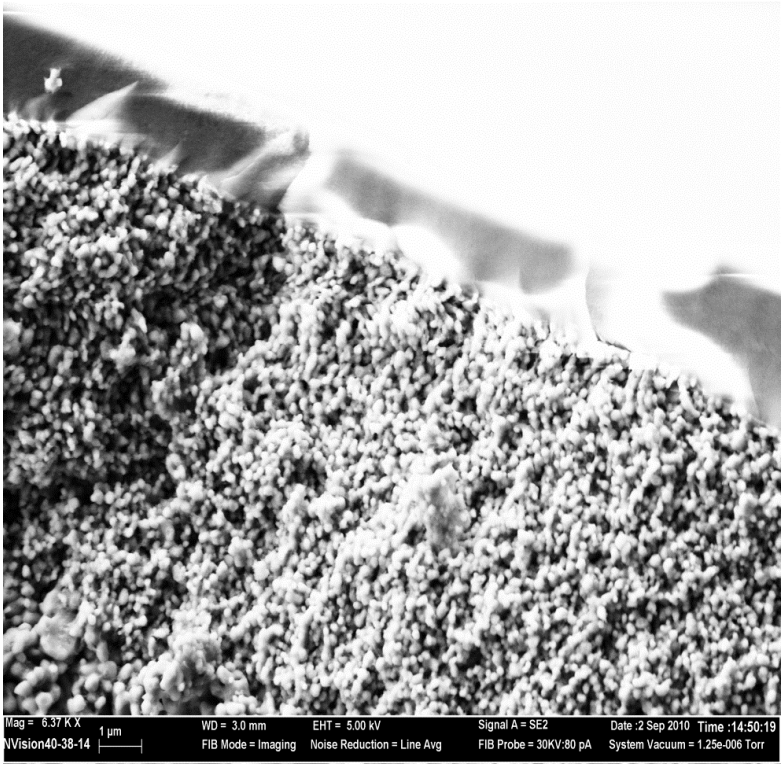

Figure 5.3 – SEM of 100 nm intermediate layer and sol-gel layer

Figure 5.3 shows a higher magnification view of the intermediate layer and the sol-gel layer. In this image, the microstructure of the intermediate layer and the dense layer of the mesoporous silica on top are more evident. Due to the nature of silica and alumina membranes acting as insulators, charging occurred on the surfaces during the SEM, lowering the image quality. A method to dissipate the surface charging was to sputter coat the membrane with gold before imaging. Figure 5.4 shows the surface silica layer cross section after sputter coating the surface with 5 nm of gold. The image clearly shows the mesoporous silica layer adhered on top of the 100 nm intermediate layer. The sol-gel layer did not penetrate into the support and was attached relatively defect free. The average thickness of the sol-gel layer was 2 μm, but varied in thickness from 1 to 3 μm. This variation in the thickness was attributed to areas where the sol-gel layer did not stay attached to the support during the dip-coating/calcination cycle, thus the need for repeated cycles of at least 3 dip-coatings on the support. The permeance of the membrane is inversely related to the thickness of the active layer of the membrane for both Knudsen diffusion and viscous flow. The areas with a thicker layer have lower permeance values than the areas with a thinner layer. The bulk of the membrane deposited had a relatively even layer of 2 μm and was used for the permeance and permporometry calculations.

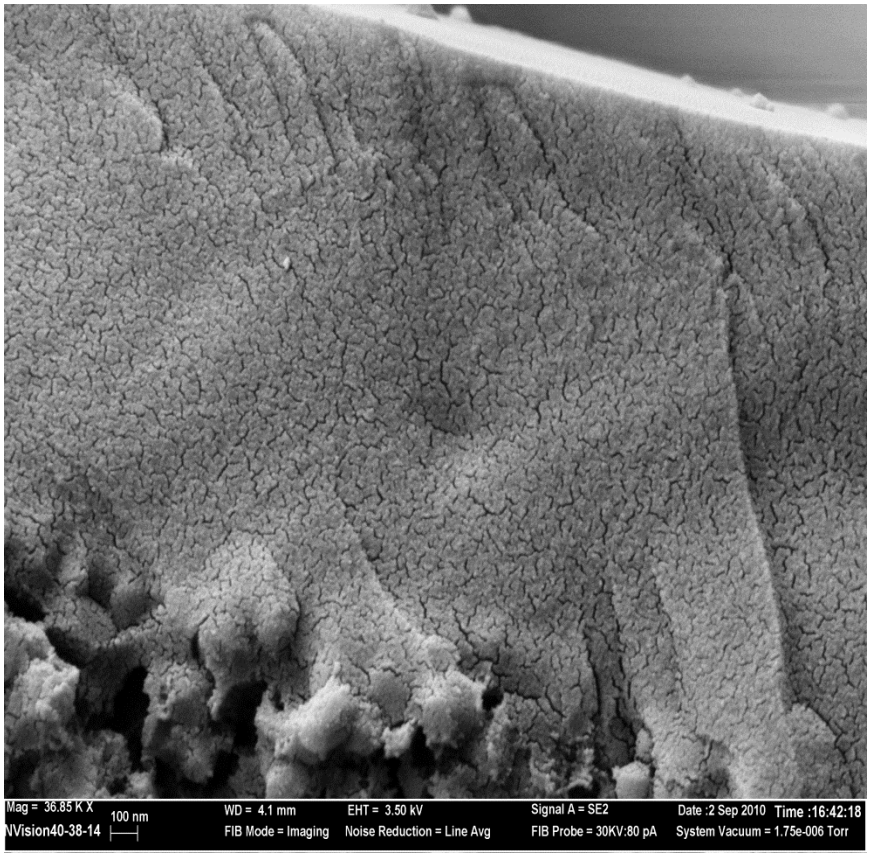

Figure 5.4 – SEM of gold templated sol-gel layer at 100 nm resolution

5.4 Permeance

A plot of the membranes permeance versus pressure drop is shown in Figure 5.5 for helium and nitrogen at room temperature. Helium had a higher permeance than nitrogen presumably due to its smaller size and molecular weight. The relationship of the permeance versus pressure drop for both gases showed a minimal pressure dependence on the permeance across the membrane. This minimal pressure dependence indicates that the flow through the membrane occurs by Knudsen diffusion rather than by viscous flow. By comparing the permeance of helium and nitrogen at 760 torr, $2.2 * 10^{-6}$ mol $m^{-2}s^{-1}Pa^{-1}$ and $1.0 * 10^{-6}$ mol $m^{-2}s^{-1}Pa^{-1}$, respectively, an ideal separation factor can be determined. The separation factor for the mesoporous silica membrane is 2.1 which is less than the Knudsen

theoretical ratio of 2.65, suggesting there must be a small viscous contribution to the total permeance. This is consistent with the small pressure dependence seen in Figure 5.5.

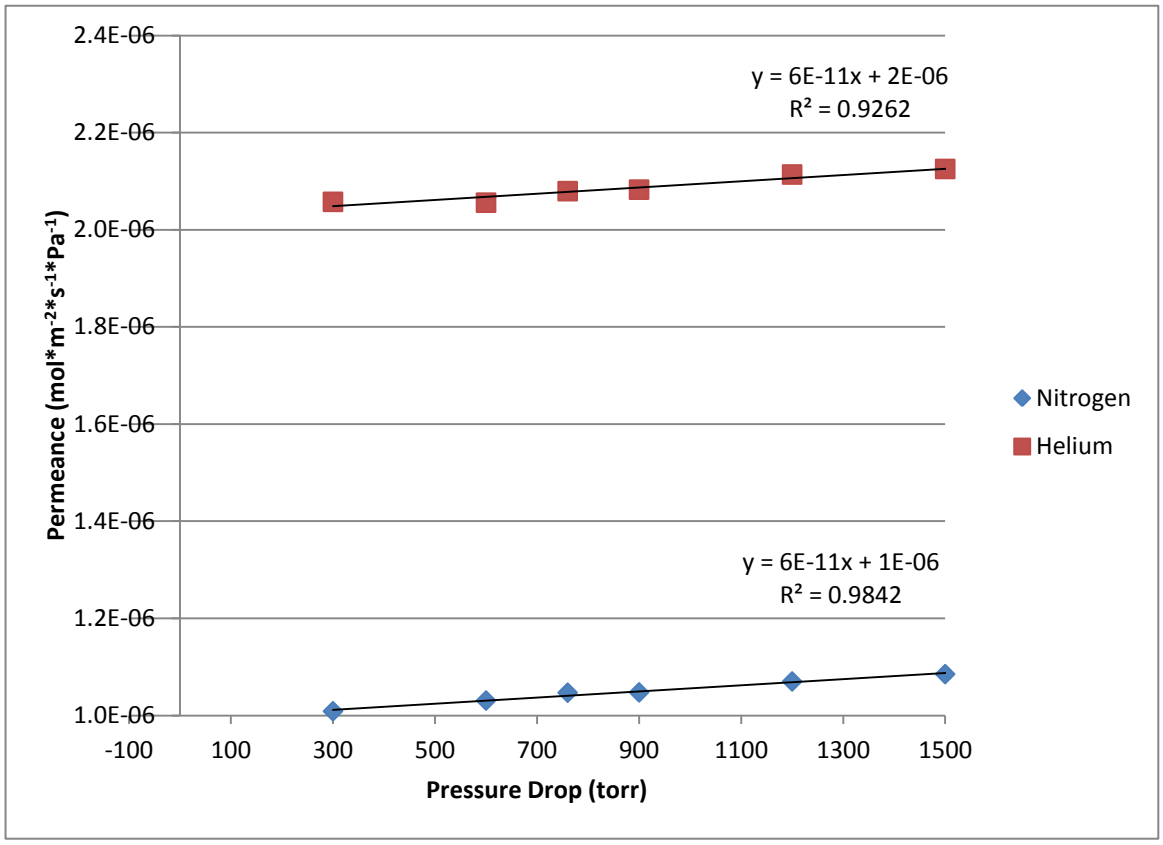

Figure 5.5 – Permeance versus pressure drop relationship for a mesoporous silica membrane

5.5 Pore Size Distribution

5.5.1 Hexane Permporometry

The membrane pore size distribution was calculated using two different methods, hexane permporometry (membranes) and nitrogen BET isotherms (powders from sol-gel). Hexane permporometry involves measuring the helium permeance of the dip-coated membrane relative to the partial pressure of hexane. Using the relationships defined in Section 4.3, the change in permeance due to pore blockage was determined and is shown in Figure 5.6. The graph shows how the permeance is reduced as the pores are successively

blocked with the increases in the activity of hexane. Over 65% of the helium permeance is attributed to pores less than 50 nm in diameter.

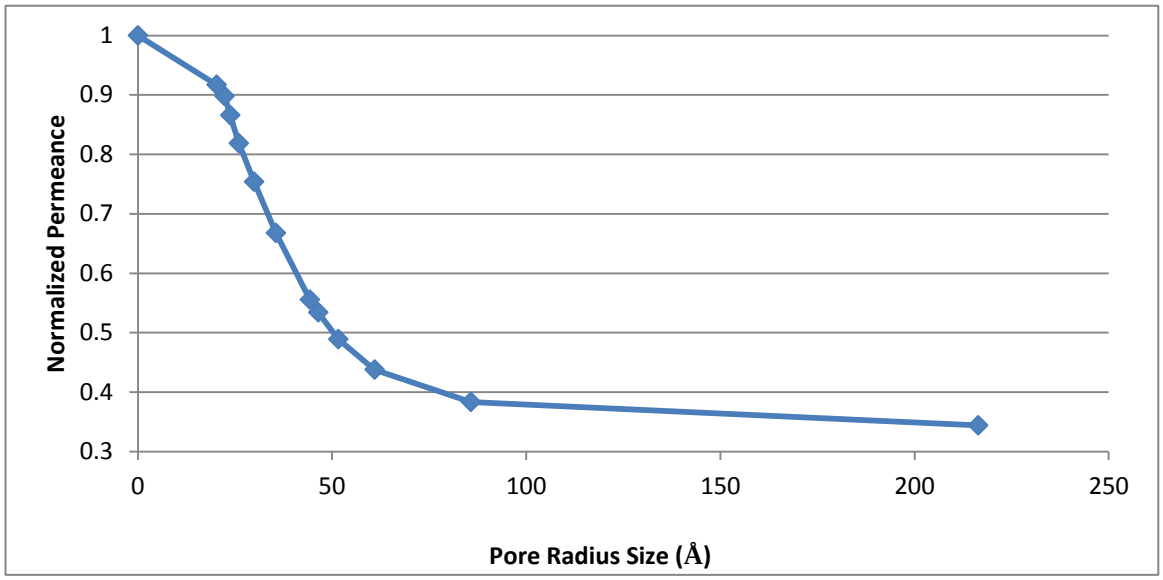

Figure 5.6 – Permeance versus radius of a mesoporous silica membrane

Using Equation 4.11, the relationship from Figure 5.6 is used to determine the pore size distribution for the active pores in the mesoporous layer of the membrane. This pore size distribution is shown in Figure 5.7. The distribution was calculated assuming a constant film thickness of 2 μm. Assuming that the film thick was variable (1-3 μm) the distribution would have a higher number of pores at areas with a thinner film and a lower number of pores at areas with a thicker film. The median pore size was 48 Å in diameter with the bulk of the pores within 1 nm of the average pore size and is independent of pore length.

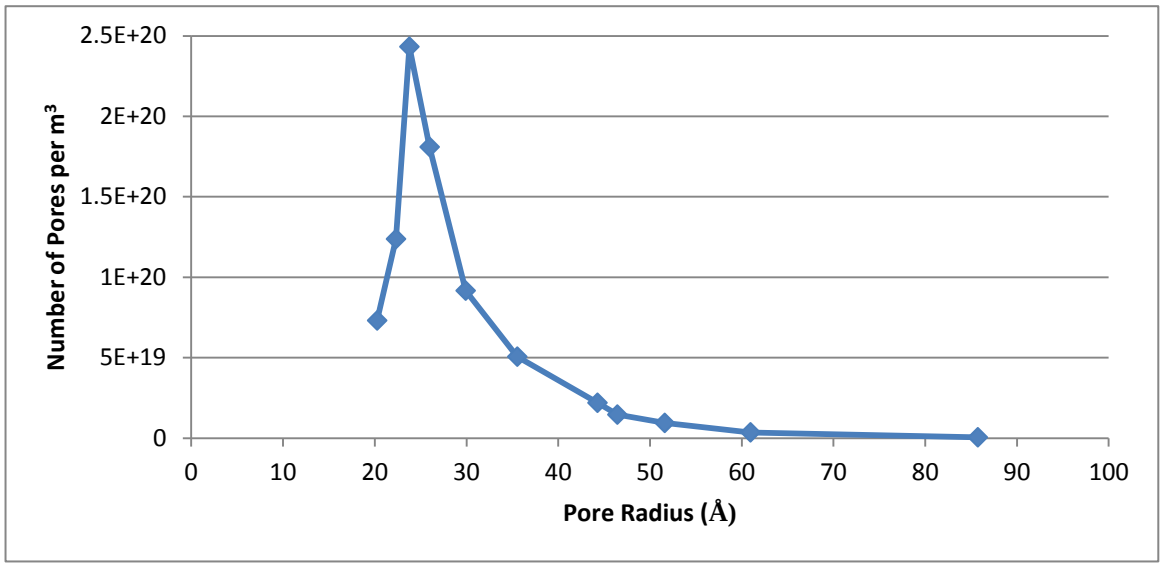

Figure 5.7 – Permporometry of a mesoporous silica membrane

5.5.2 Nitrogen Isotherm

Nitrogen isotherms offer an excellent way to determine the porosity and pore size of highly porous materials. They cannot be easily applied to a dip-coated mesoporous silica membrane because the support with pores much larger than the mesoporous range, constitutes most of the membrane. Nitrogen isotherms can be applied to the material left over from the dip-coating process. The remaining sol-gel material not deposited onto a support, was dried and calcined at 500 °C, then ground using a mortar and pestle. This material was analyzed using a BJH analysis of the nitrogen isotherm to determine the average pore size of the bulk silica. The surface area of the membrane was found to be 1027 $m^2\ g^{-1}$ with an average pore size of 3 nm in diameter. These properties are an average for the bulk of the material, but include different characteristics than the dip-coated membrane, where only active pores were evaluated. The BJH adsorption pore size distribution using a nitrogen isotherm is shown in Figure 5.8.

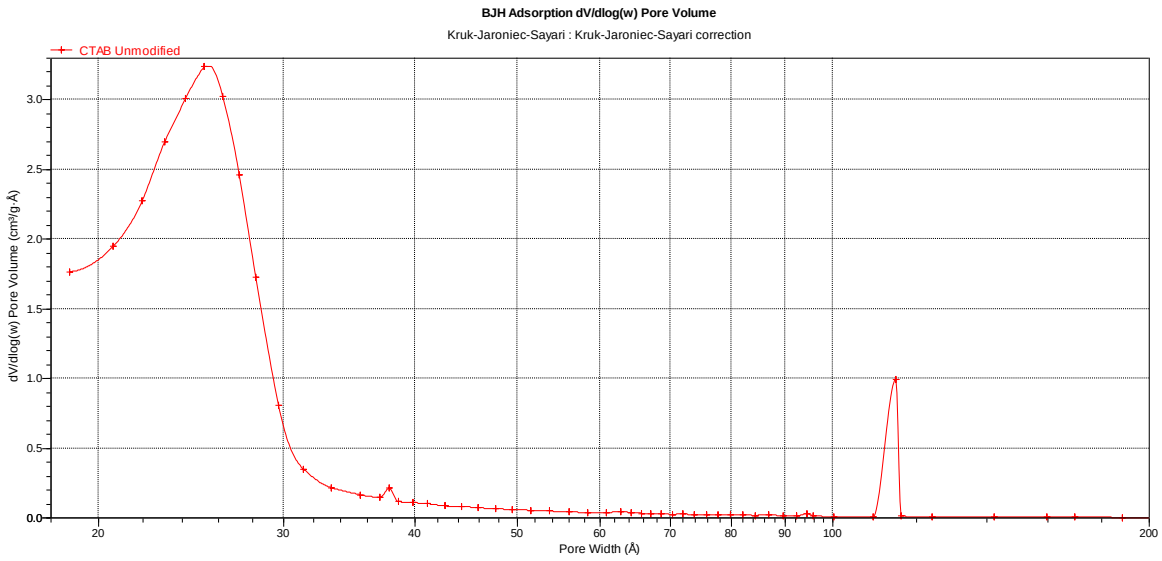

Figure 5.8 – BJH adsorption of mesoporous silica powder

5.6 Conclusions

Mesoporous silica membranes were synthesized in a repeatable fashion by dip-coating an asymmetric support in an environmentally controlled chamber. Using the chamber insured that the rate at which the membranes were dried was controlled so that the dip-coated membrane coated the support evenly and produced the desired structure. The membrane had a high permeance for He of $2.2* 10^{-6}$ mol $m^{-2}s^{-1}Pa^{-1}$ at 760 torr and with over 65% of the permeance due to pores with diameters less than 50 nm. The hexane permporometry data for the membrane indicated a median pore diameter of 4.8 nm which is slightly larger than the 3.0 nm pore diameter of the bulk mesoporous sample. The higher average pore size for the hexane permporometry could be attributed to limitations of the equipment, where pores under 2 nm were not evaluated. Also the hexane detects only the active pores, while the nitrogen isotherm measures the entire pore network, where smaller pores could dominate. The mesoporous material had a very high surface area, with a BJH adsorption surface area of 1027 m^2 g^{-1}.

CHAPTER 6

ALD REACTOR DESIGN

6.1 Overall Design

The ALD reactor was designed and built for this research project. An ALD reactor consists of three sections: precursor delivery, reactor and pumping. The design allowed for easy changes to different types of precursors, which allow the reactor to be applied also to MLD. The reaction chambers were designed so that they could be changed for the application of ALD on different types of materials. Figure 6.1 shows the process diagram for the trimethyl aluminum (TMA) and water ALD reactor.

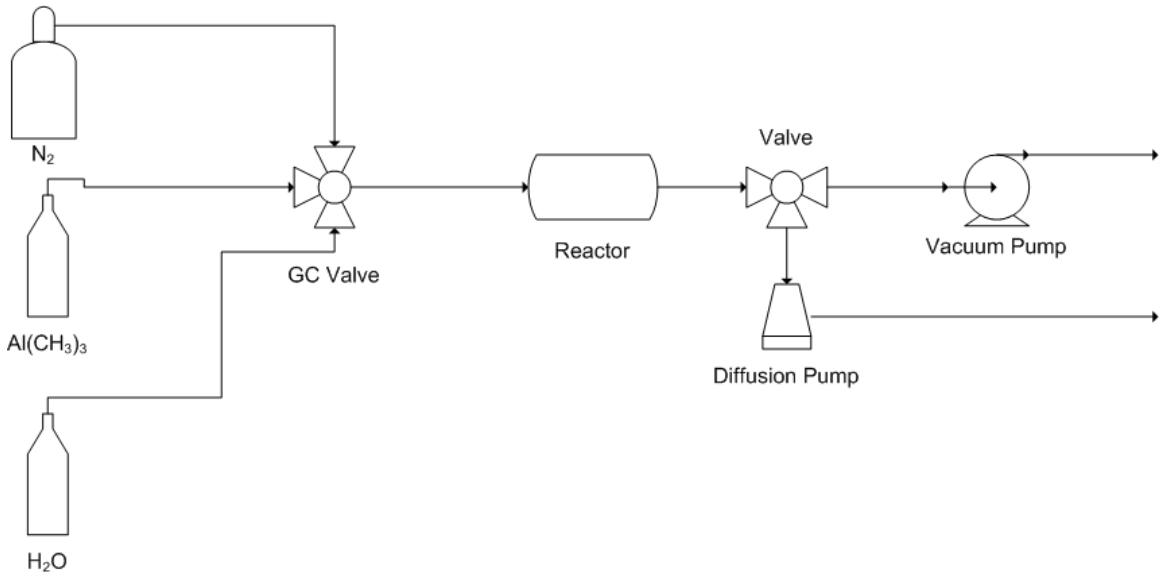

Figure 6.1 – ALD reactor design for TMA and water ALD

Two different ALD reactor systems were designed and constructed for the laboratory. One reactor was designed for catalyzed silicon tetrachloride ALD and another for conventional ALD with TMA. The design of the TMA system is described below.

6.1.1 Precursor Delivery System

In ALD, the precursors are delivered into the reactor sequentially at a specific pressure and exposure time. Typically, the minimum exposures are 0.1-5 torr for 1-60

seconds.[18, 22] For all the precursors, a vessel with one outlet was filled with the chemically pure material and the temperature was held constant to produce the desired vapor pressure. For the MLD reactions, the organic acids were solids at the operating temperatures, but sublimation of the precursors produced a high enough vapor pressure to reach the desired pressure of 2 torr.[50, 51] Each of the precursors was fed to a GC valve (Valco), as shown in Figure 6.2. The 4-port valve allowed each precursor and the sweep gas to be isolated to a set port with one common outlet. This kind of valve minimized any void space within the valve where residual precursors could be trapped. The port not in use was sealed off to prevent any leakage to or from the system.

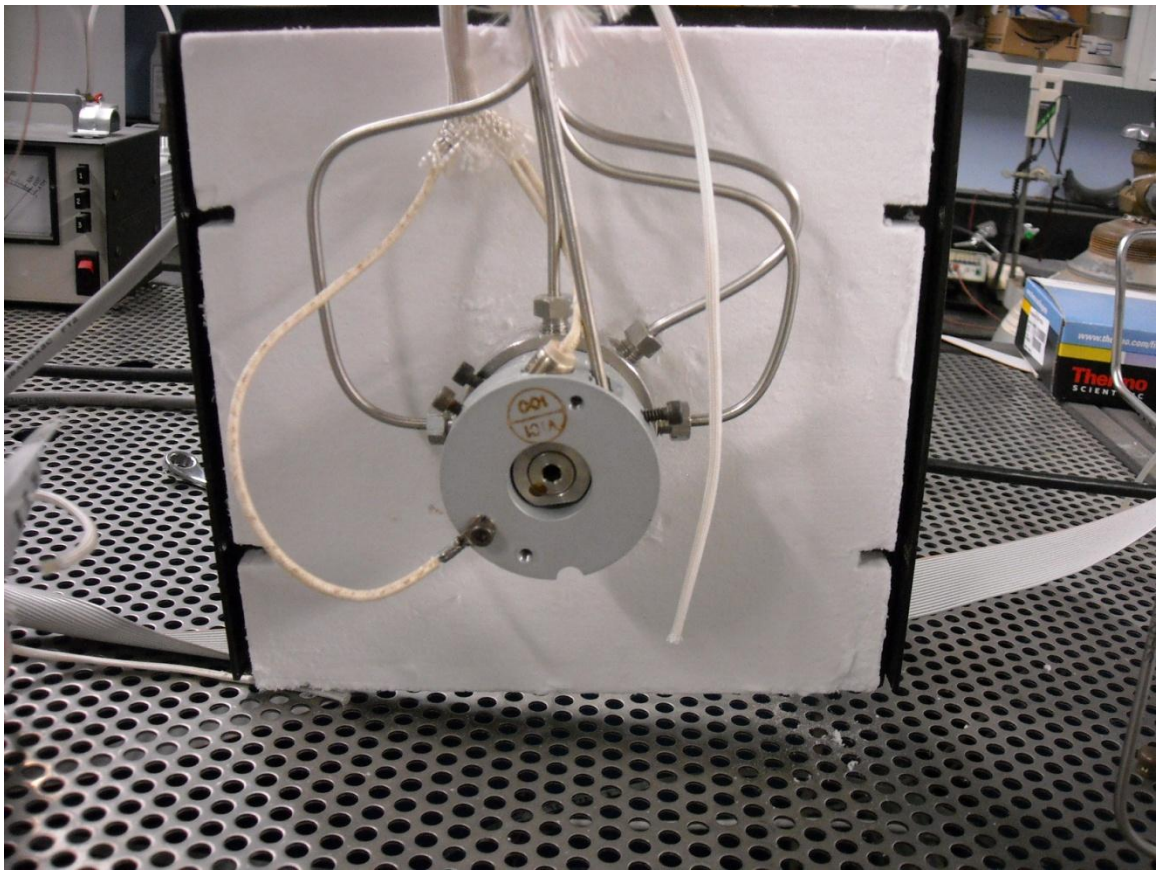

Figure 6.2 – GC valve used for ALD

Nitrogen was chosen as the inert gas which was used, along with the vacuum, to purge the system between each exposure. Nitrogen also purged the GC valve of any

remaining precursors and by-products from the ALD reaction. The GC valve switching motor was computer controlled using LabView.

6.1.2 Reactor Designs

Three different reactors were used in the system and were designed to allow for easy changing between them. The reactor for modification of porous powder materials is shown in Figure 5.3. The powder was loaded into a Pyrex glass tube fitted with a highly porous glass frit. The powder remained on top of the frit allowing for the precursors to pass through the powder.

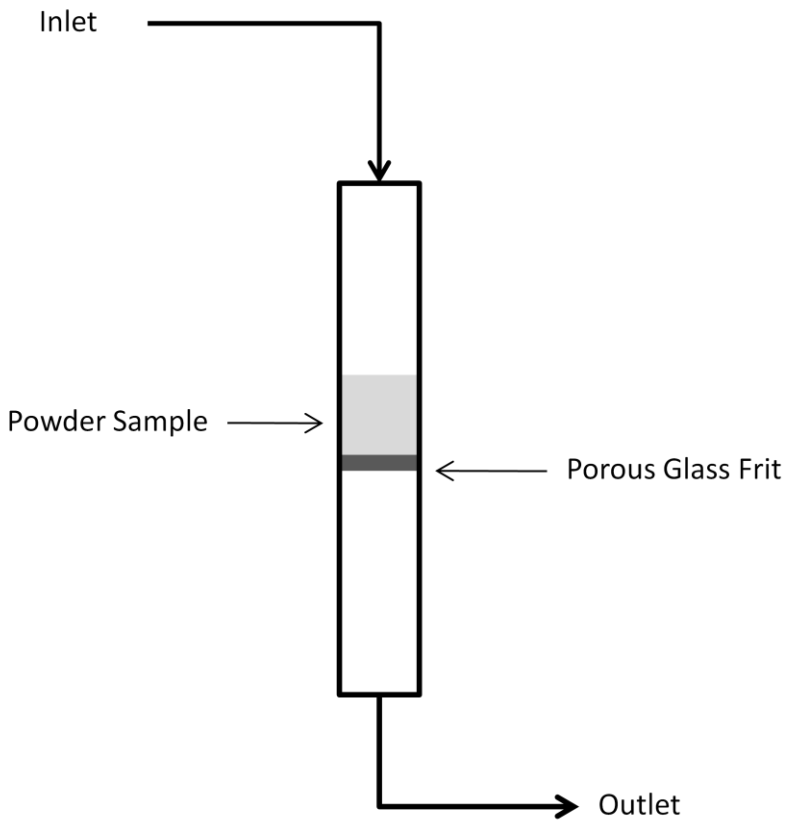

Figure 6.3 – Design of powder sample reactor

The most commonly used reactor for these studies is the membrane cell reactor shown in Figures 6.4 and 6.5. This reactor has a variety of benefits for dip coated sol-gel membrane modification. A membrane was loaded into the cell with gas inlet on the top side

of the membrane and gas outlet on both the top and bottom of the membrane. The membrane was sealed into the cell using Viton o-rings. This allows characterization of the membrane between each layer of ALD modification, without physical removal of the membrane from the reactor cell.

The extra outlet on the reactor cell offers a variety of methods for purging the membrane during ALD. Since the diffusion driving force into the membrane was weak, the precursors could be driven across the membrane while purging the back side of the membrane and without purging the top. This would help drive unreacted precursor through the membrane. Experiments in this study typically did not require this method and therefore both sides of the membrane were generally purged at the same time.

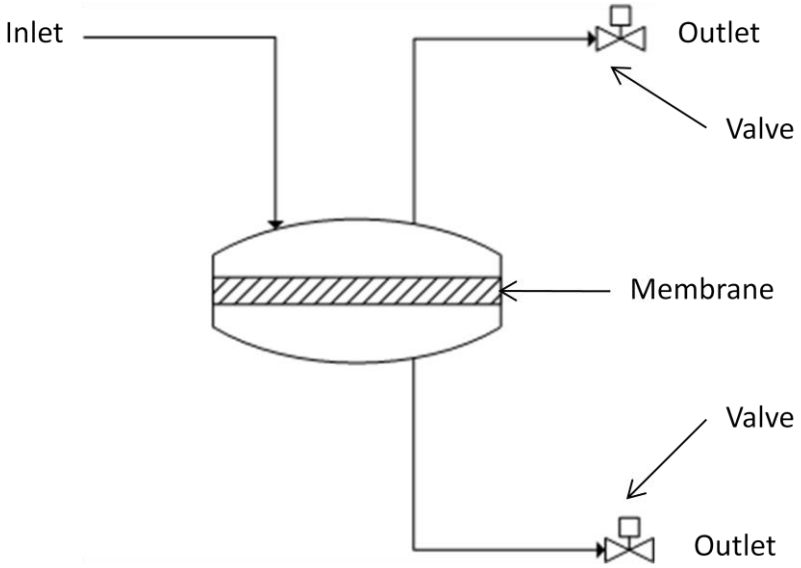

Figure 6.4 – Design of membrane cell reactor

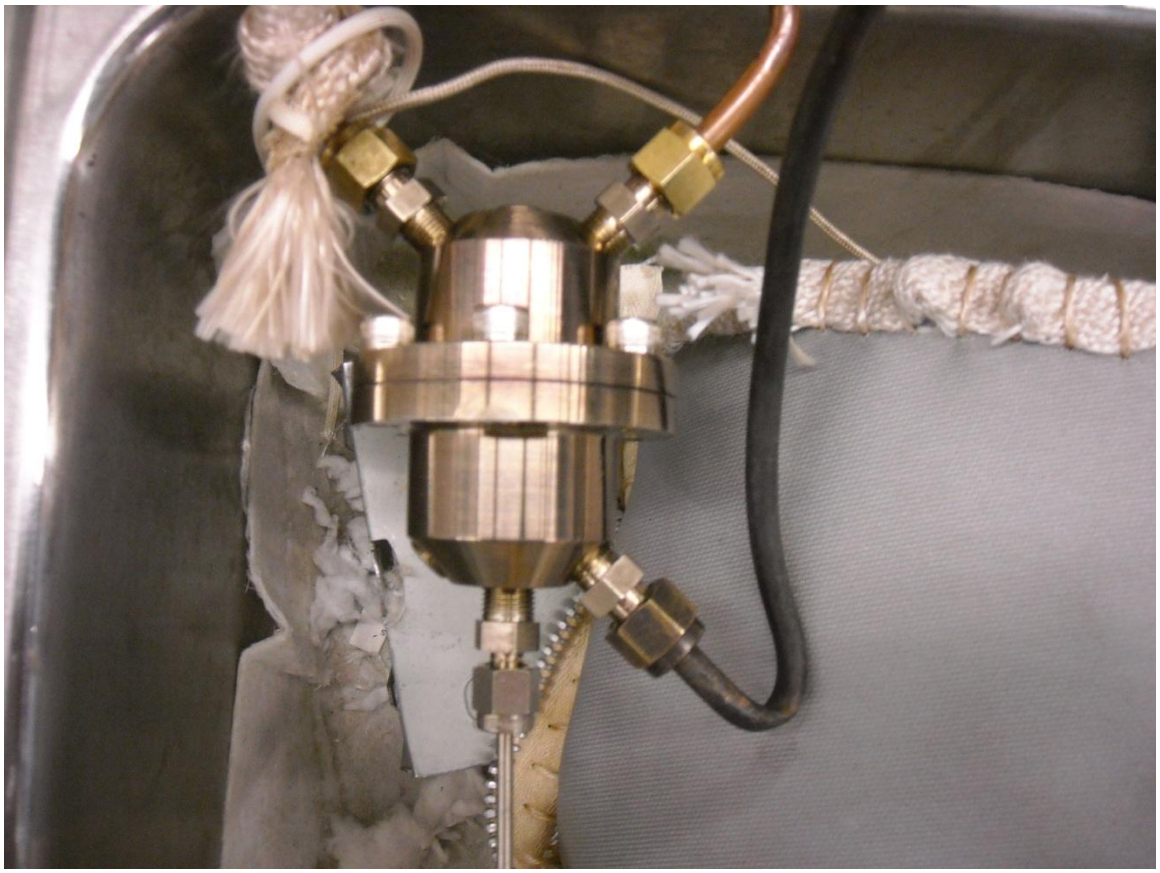

Figure 6.5 – Membrane Cell Reactor

The simplest of the reactors is a chamber designed to accommodate samples of different shapes and sizes. This reactor allowed for modification of a variety of different materials, including single crystal silicon, paper tissue fibers, and dip-coated membranes. A benefit of the chamber was that multiple samples and different types of materials could be treated at the same time.

All the reactors could be isolated from the pumping system during the precursor exposures. This allowed for the pressure to increase up to the vapor pressure of each precursor inside the reaction vessel. This concentration gradient is the driving force for precursor to pervade the pore network of the membrane.

6.1.3 Pumping System

The ALD reactor was built using both a roughing pump and a diffusion pump (see Figure 6.1). This design allows the ALD reaction chamber and entire system to be first purged using the roughing pump. The line leading into the roughing pump has a liquid nitrogen trap to prevent any excess reactants or precursors from damaging the pump.

After the system has been purged using just the roughing pump, a separate diffusion pump is run in parallel to purge the system. Using this combination of pumps and the liquid nitrogen trap allows the pressure in the reactor to be reduced to below 5 millitorr. During operation the purge times were run in excess of the minimum required in order to ensure that all remaining precursors and vapor products were removed.

6.2 Reaction Exposure Calculations

In ALD, the reaction surface must be exposed to the precursor vapor for each half-reaction. The quantity of precursor required per unit surface area is called the saturation dose, that is, the amount of precursor required to cover a unit of surface area of support. This term can be expressed in molecules per unit area. For ALD, the saturation dose, S, is directly related to the number of active sites available for chemisorption of the reactant. In ALD on silica for example, the reactive surface sites are the surface hydroxyls. In silica, this is estimated at 2.5 hydroxyls per square nanometer. If we can then estimate the flux, J, of the precursor onto the surface, we can calculate the time of precursor exposure using Equation 6.1. This assumes that all molecules striking the surface are chemisorbed or have a sticking coefficient of 1. This assumes that a single precursor reacts with the first active site it reaches, which was chosen for the calculation of a minimum exposure time. It has been shown that the sticking coefficient will decrease for high aspect ratio materials, such as membranes and larger precursors.[52] Due to the nature of a large molecules used during

the molecular layer deposition study, a lower sticking coefficient may be more relevant, ~0.01.

$$t = \frac{S}{J} \tag{6.1}$$

Assuming an ideal gas, which for the low pressures used during ALD is a reasonable assumption, kinetic theory can be applied to calculate the flux of vapor molecules striking the surface, Equation 6.2.

$$J = \frac{P}{\sqrt{2\pi mkT}} \tag{6.2}$$

Here, P is the pressure, m is the molecular mass, k is Boltzmann's constant and T is temperature.

A common measure for expressing precursor exposure is the product of pressure and time or Pt. A unit for this quantity is the Langmuir, L. One L is equivalent to 10^{-6} torr·s. Therefore, an exposure of one Langmuir is equivalent to a one second exposure of a precursor at 10^{-6} torr. Combining Equations 6.1 and 6.2 results in an expression that estimates the precursor exposure onto a flat surface, Equation 6.3.

$$Pt = S\sqrt{2\pi mkT} \tag{6.3}$$

In applying ALD to coating nanoporous materials such as membranes, the precursor flux must travel down the pore in time, t, to a specified distance, z, and deposit on the inner surface of the pore. Written incrementally, this yields Equation 6.4.

$$dt = \frac{Sc_p}{JA_p} dz \tag{6.4}$$

Where c_p and A_p are the circumference and area of the pore, respectively. In addition, the flux through the pore must be reexamined. For pores with diameters on the order of the mean free path of the diffusing molecule, the Knudsen model is used to describe the flux. For much larger pores, viscous flow is more appropriate. The expression for the Knudsen

flux through a pore is given by Equation 6.5, where R_p is the pore radius, v the molecular velocity, P, the pressure, T, the temperature, and z, the pore length.

$$J_K = \frac{2}{3}\frac{R_p v}{RT}\frac{P}{z} \tag{6.5}$$

Substituting Equation 6.5 into Equation 6.4, and integrating provides an expression of precursor exposure, Equation 6.6.

$$Pt = \frac{3}{2}\frac{SRT}{v}\frac{z^2}{R_p^2} \tag{6.6}$$

As seen in Equation 6.6 there is an involved quadratic relationship between exposure and pore radius. Using helium as an example molecule and assuming a silica surface with 2.5 hydroxyls per square nanometer, exposures can be estimated from Equations 6.3 and 6.6 for a flat surface and pore of length, z, and radius, R_p. At room temperature, the exposure of helium onto the flat surface is 2.5 x 10^{-7} torr·s or 0.25 L. For comparison, the exposure of helium required to saturate a nanopore of one micron in length and a radius of 2.5 nm, is 0.015 torr·s, 5 orders of magnitude higher. This exposure agrees with other literature values for modeling minimum exposures of mesopores.[26]

During ALD of alumina into nanopores, the exposure requirements will increase quadratically as the pore radius decreases, assuming the length of pore coating is constant. If exposures are constant throughout the ALD modification of the membrane the process could favor deposition in larger pores relative to smaller ones. Also, the thickness of the separation layer may not be uniform, as it is related to the pore diameter. In either case, it is relevant to take into account the large difference in estimating exposures for ALD deposition within nanopores.

The minimum exposure can be calculated using measured data for the helium permeance. The experimental permeance data for the mesoporous membrane incorporates tortuosity and the porosity of the membrane. The experimental permeance of the

membrane was $1*10^{-7}$mol*m^{-2}*sec^{-1}*Pa^{-1}. Use of Equation 6.7 allows for the experimental data to be applied to the exposure time.

$$P * t = \frac{S*SA_p}{\pi*SA_m} \quad (6.7)$$

The top surface area of the membrane that were pores, Sa_p, was determined from hexane permporometry and found to be $1.4*10^{-4}$ m^2. The surface area of the top membrane surface, SA_m, was $3.8*10^{-4}$ m^2. Using these experimental values an exposure time of 0.117 torr*s was calculated. The minimum exposure time is larger than the value of 0.015 torr*s for the modeled measurements as a result of the heterogeneous nature and tortuosity of the porous membrane.

6.3 Reaction Purge Measurements

The time required to purge all excess reactants involves the time that it takes to purge the general system and remove byproducts and excess precursors from the membrane pore network. For the general system purge, all the lines were purged leading up from the vacuum pumps to the reactor and to the GC Valve. Due to length and constrictions in the piping system, the purging of the system was not immediate. Based on experiments it would take approximately 45 seconds to purge the system from greater than 760 torr of nitrogen to less than 5 millitorr.

The time required to remove the leftover precursors and byproducts from inside the pore network was estimated using the exposure calculations in section 6.2. Assuming that the concentration of precursor inside the pore was 2 torr at the end of the reaction cycle, the time for the precursor to diffuse out of the pore can be estimated. It would take approximately 120 seconds to reduce the pressure to 10 millitorr. This estimated time should be much higher than actual time since the pressure inside the pore should never reach the ambient pressure during precursor exposure. The minimum purge time was 300 seconds for all ALD reactions.

Dilution of the precursors using two flushes of nitrogen gas further reduced the partial pressure of the precursors inside the reactor. After each reaction cycle the reactor was purged to below 5 millitorr and then exposed to 30 sccm of nitrogen for 30 seconds. The reactor pressure increased to over 200 torr during the nitrogen flush. The reactor was then purged to below 5 millitorr, diluting the concentration of the precursor to below 10^{-5} millitorr after the first nitrogen flush. A similar dilution effect occurred inside the pore, but would be limited due to diffusion resistance. The reactor was flushed a second time further reducing the partial pressure of any remaining precursors.

6.4 Overall Reaction Operating Procedure

Using the values determined for the exposures and for purging, a pulse/purge operating procedure was developed. The entire ALD reactor was designed and constructed to be automated using LabView. This allowed for the time of each stage to be identical e between each cycle experiment. The order of operations for ALD reactions is shown in Table 6.1.

Table 6.1 – Example of ALD reaction order of operations

Stage	Time (seconds)	Action Occurring
1	30	Nitrogen Flush
2	600	Vacuum Purge
3	600	Diffusion Vacuum Purge
4	Variable	Trimethyl Aluminum Exposure
5	600	Vacuum Purge
6	30	Nitrogen Flush
7	600	Vacuum Purge
8	30	Nitrogen Flush
9	600	Vacuum Purge
10	600	Diffusion Vacuum Purge
11	Variable	Water Exposure
12	600	Vacuum Purge
13	30	Nitrogen Flush
14	600	Vacuum Purge

The times developed were not optimized for reactor efficiency, but to ensure that any excess precursors, or byproducts, were removed. Two nitrogen flushes were used between each reactant exposure to aid in this removal. After each exposure and nitrogen flush there was a 10 minute vacuum purge using only the roughing pump. This was more than double the minimum required from the purging calculations. An extra purge before each exposure was accomplished by using the diffusion pump. The 10 minute diffusion purge would allow the system pressure to drop below 5 millitorr. After the diffusion purge, the precursor exposure would occur with the vacuum valves closed. This would allow for the pressure of the reactor to reach the vapor pressure of the precursor being exposed. The precursor exposure times were developed using the calculations shown in Section 6.2 and from literature values.[22] The exposure times were between 3-30 seconds during experiments performed in the lab.

CHAPTER 7

ATOMIC LAYER DEPOSITION MODIFIED ORDERED MESOPOROUS SILICA MEMBRANES

7.1 Introduction

A superior gas separation membrane will be ultra thin for high throughput and homogeneous in pore size with a high porosity/low tortuosity for maximum molecular sieving. In addition, many separation applications require the high thermo-chemical stability that is possible with inorganic membranes. Mesoporous silica membranes, prepared using surfactant templates and evaporation induced self-assembly, are highly porous with a majority of pores being 3-10 nm in diameter.[11, 53] Therefore, to be utilized in gas and small molecule separations, pore size reduction techniques, such as atomic layer deposition (ALD) must be applied in order to reduce the pore dimensions to the range for molecular sieving. Examples of industrially relevant gas separations include carbon dioxide/methane, carbon dioxide/nitrogen, and ethanol/water, among many others.

ALD is routinely utilized to prepare conformal coatings on high aspect ratio, non-planar supports in semiconductor manufacturing.[54] ALD has also been applied to reduce the pore size of γ-alumina membranes[21, 23, 29], anodic aluminum oxide membranes[55-59], mesoporous silica membranes[19, 37, 38, 60] and powders[39], porous substrates[61, 62] and organic membranes.[63] In all cases, ALD has proven to be a viable method for controlled pore size reduction using several reaction chemistries including SiO_2, Al_2O_3, TiO_2 and others.

In the application of ALD to membrane synthesis, the ultimate goal is to achieve highly effective molecular separations. This is achieved by tuning the final pore size and surface functionality. As the pore diameter shrinks down to molecular dimensions, the final ALD processing parameters can become highly sensitive to diffusivity reduction of reactants into the pores.[26, 64] In addition, ceramic membranes have a heterogeneous pore size

distribution that contributes to the final pore size distribution in the modified membranes. Therefore, it is important to understand the effect that ALD parameters, such as temperature, reactant exposure and reactant purging, as well as support heterogeneity, have on the pore size distribution after modification.

In this research, we applied ALD of Al_2O_3 to reduce the pore size of surfactant-templated mesoporous silica membranes prepared by dip-coating onto alumina supports. The membranes were characterized at various stages of ALD-modification, up to 50 ALD cycles, using light gas permeance and perm-porosimetry measurements. Under constant ALD reaction conditions, the deposition efficiency was reduced as the ALD cycles increased. This resulted in favorable conditions for coating larger pores within the heterogeneous support. Between 30-50 ALD cycles, the ideal separation factor for light gases was limited to that predicted by Knudsen diffusion, indicating that a significant number of remaining pores were not reduced to the molecular dimensions of the light gases probed. This can be correlated to the heterogeneity of the support as well as to the observed reduction of deposition efficiency as the number of ALD cycles increased.

7.2 Experimental

7.2.1 Membrane Synthesis

Mesoporous silica membranes were prepared with tetraethyl orthosilicate (TEOS, Sigma Aldrich) as the silica source and cetyltrimethylammonium bromide (CTAB, Sigma Aldrich) as the surfactant template. To prepare the mesoporous silica films, a solution of 7.5 ml of TEOS, 4.73 g of EtOH, 0.617 g of H_2O, and 0.057 ml of 0.03 M HCl were combined and refluxed at 60 °C for 1 hour. Following this, 10 ml of the refluxed solution was combined with 1.3 g of CTAB, 20.24g of EtOH, 1.75 g of H_2O, and 0.1 ml of 1M HCl forming a final molar ratio of 1 TEOS:20.52 EtOH:5.25 H_2O:0.144 CTAB:0.00409 HCl. This solution was allowed to set for 1 week at ≈3°C in a sealed container.

Inside a controlled environment chamber at 30°C and 50% humidity, an asymmetric alpha alumina support disk with a 20 μm top layer of 100 nm pore size (HiTK, Germany) was dipped into the solution for 15 seconds, using a dipping apparatus. The membrane was allowed to dry inside the chamber for 24 hr. The surfactant was removed by sintering at 500°C for 4 hr in air with a ramp rate of 1°C/min. The dip and calcination procedure was repeated 3 additional times to build up the membrane thickness to cover the support.

7.2.2 Atomic Layer Deposition Modification

The membrane/support disc was placed in a custom-built stainless-steel cell that sealed the membrane using Viton O-rings, allowing both membrane modification and characterization without membrane removal. ALD was carried out at 100°C and ≤5 mtorr using trimethyl aluminum (TMA, Sigma Aldrich) and H_2O as reactants. The TMA and H_2O were held at 0°C, producing vapor pressures of 2.56 and 4.60 torr, respectively. The membrane was dosed with each precursor for 1 second over the top of the membrane for exposures of 2.5 and 4.6 Langmuirs, respectively. Here, our goal was to provide a thin separation layer confined to the surface of the membrane. The exposure times used in this study approaches the minimal values for alumina ALD within a nanoporous membrane, as estimated from continuum transport modeling.[64] In two other membrane modification experiments, exposures of TMA and water were increased to 77 and 138, and 100 and 197 Langmuirs in order to examine the effects of increased exposure on membrane modification. To evacuate the cell, it was first held under vacuum for 10 minutes on both sides of the membrane. Then, N_2 was purged for 30 seconds at 30 sccm over the top of the membrane. This purge cycle was repeated to remove all non-adsorbed reactant from the pore network. The typical coating cycle sequence was: dose TMA, evacuate excess TMA, N_2 purge, evacuate, N_2 purge, evacuate, dose H_2O, evacuate excess H_2O, N_2 purge, evacuate, N_2

purge, and evacuate. This complete cycle resulted in one monolayer of Al_2O_3 deposited within the pores. Up to 50 complete cycles were applied to modify the support membranes.

7.2.3 Characterization

The membranes were characterized using single gas permeation and porosimetry. Single gas permeation was measured with helium and nitrogen at 25°C at pressure drops between 300 and 1800 torr. The hexane perm-porosimetry measurement apparatus and procedure is described in greater detail elsewhere.[40] Briefly, as the hexane vapor pressure is exposed to the membrane, capillary condensation occurs in the pores governed by the Kelvin equation. As the activity of hexane is increased, successively larger pores are blocked, and the He permeance through the membrane is reduced. From these data, a pore size distribution can be calculated.[45] The hexane perm-porosimetry measurement was carried out with the membrane and hexane bubbler at 25°C and a pressure drop of 300 torr. These measurements were completed on an unmodified membrane and after 1, 2, 3, 4, 5, 10, 15, 20, 30, 40, and 50 cycles of ALD.

7.3 Results

Mesoporous silica membranes were formed on alumina supports by dip-coating and subsequent thermal treatments to remove the surfactant template, leaving behind a porous layer. Membranes were formed with four dip/fire cycles to minimize large cracks, commonly formed from film shrinkage and the unevenness of the alumina support. Figure 7.1 shows a cross-sectional view of a fractured, fabricated membrane. This view reveals the asymmetric support consisting of two layers; a thicker, highly porous layer supporting a 20 μm thick layer with 100 nm pores. This asymmetric support provided a relatively smooth layer for dip-coating the thin, mesoporous silica membranes with pore diameters less than 5 nm. The thin, 1-3 μm, top mesoporous silica layer, prepared by dip-coating is also shown

in Figure 7.1. This design aided in minimization of the thickness of the separation layer as required for a high-flux membrane.

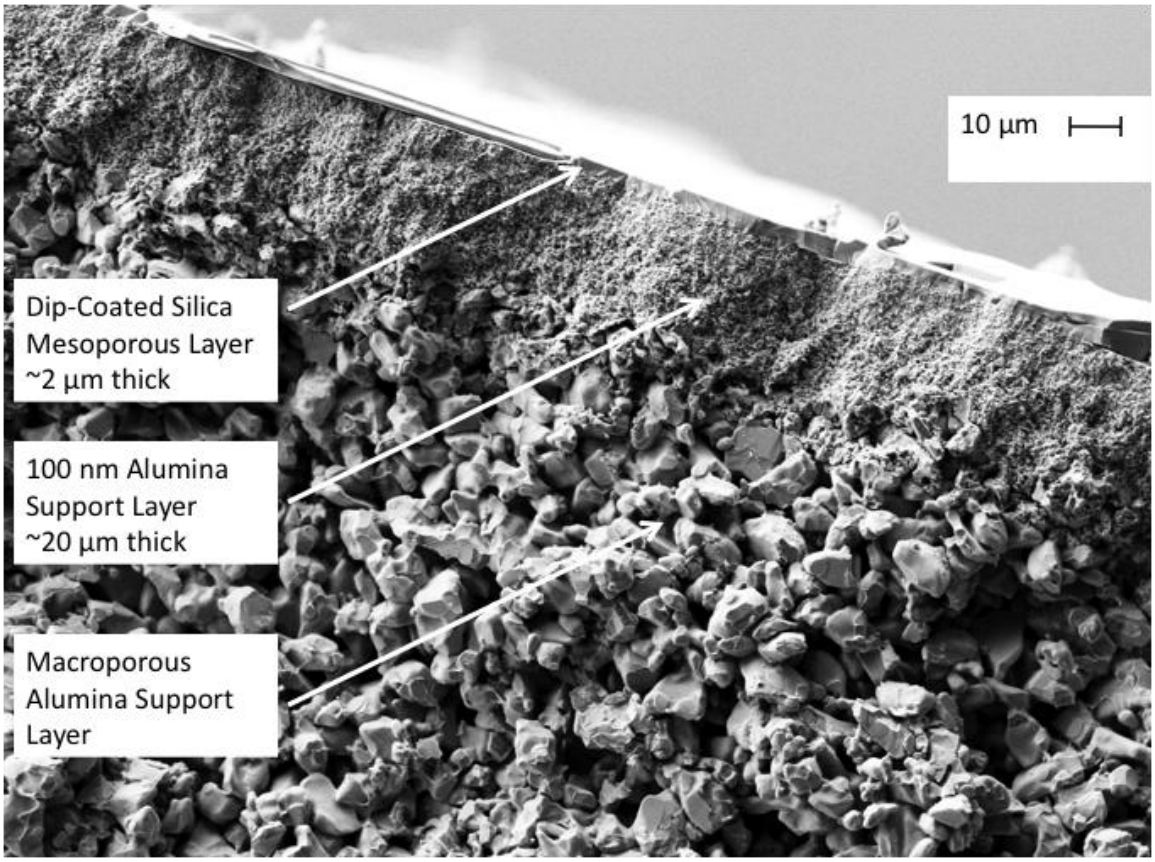

Figure 7.1 - Cross-sectional view of the asymmetric alumina membrane support coated with a mesoporous silica membrane

Evidence for pore size reduction via ALD of alumina within mesoporous silica membranes is provided in Figure 7.2. Here, the He permeance, normalized to the unmodified membrane, is shown for the first 4 ALD cycles with different precursor exposures.

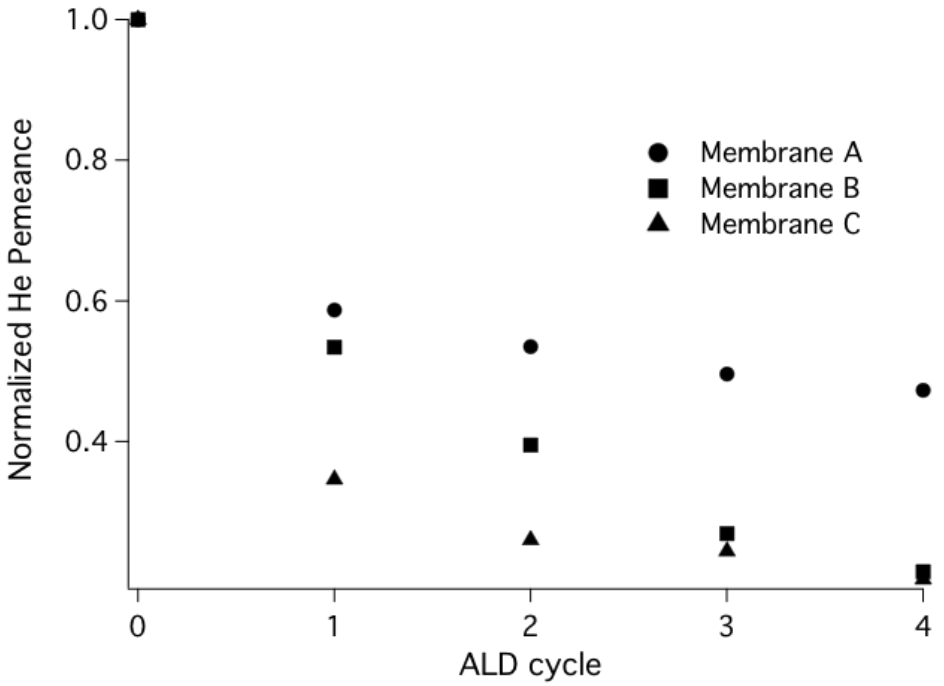

Figure 7.2 - He permeance reduction in mesoporous silica membranes during alumina ALD modification

Experimental data are shown in Table 7.I. Clearly, an increase in precursor exposure decreases the relative He permeance, presumably as a result of both pore size reduction and pore blocking.

Table 7.1 - He permeance data for ALD-modified mesoporous silica membranes with different precursor exposures

Membrane	TMA (Langmuirs)	H_2O (Langmuirs)	π_{He} 0-ALD (10^6 mol $m^{-2}s^{-1}Pa^{-1}$)	π_{He} 4-ALD (10^6 mol $m^{-2}s^{-1}Pa^{-1}$)
A	2.5	4.6	4.0	1.9
B	77	138	8.7	1.9
C	100	197	4.6	1.0

On one sample, permeance and pore size distribution data were collected for 50 sequential ALD cycles (membrane A). Overall, the He permeance decreased continually from 4.0 $x10^{-6}$ to 6.6 $x10^{-8}$ mol m^{-2} s^{-1} Pa^{-1} through the 50 ALD cycles. Figure 7.3 shows the pore size distributions calculated from perm-porosimetry data taken at different stages of ALD modification for membrane A. The unmodified mesoporous silica membrane had a majority

of pores with diameter ~4 nm. The unmodified membrane also had a 20% residual He permeance through pores larger than 50 nm, indicative of defects in the membrane. As shown in Figure 7.3, the pore size distribution shifted to lower pore diameters along with a porosity decrease as the number of ALD cycles increased.

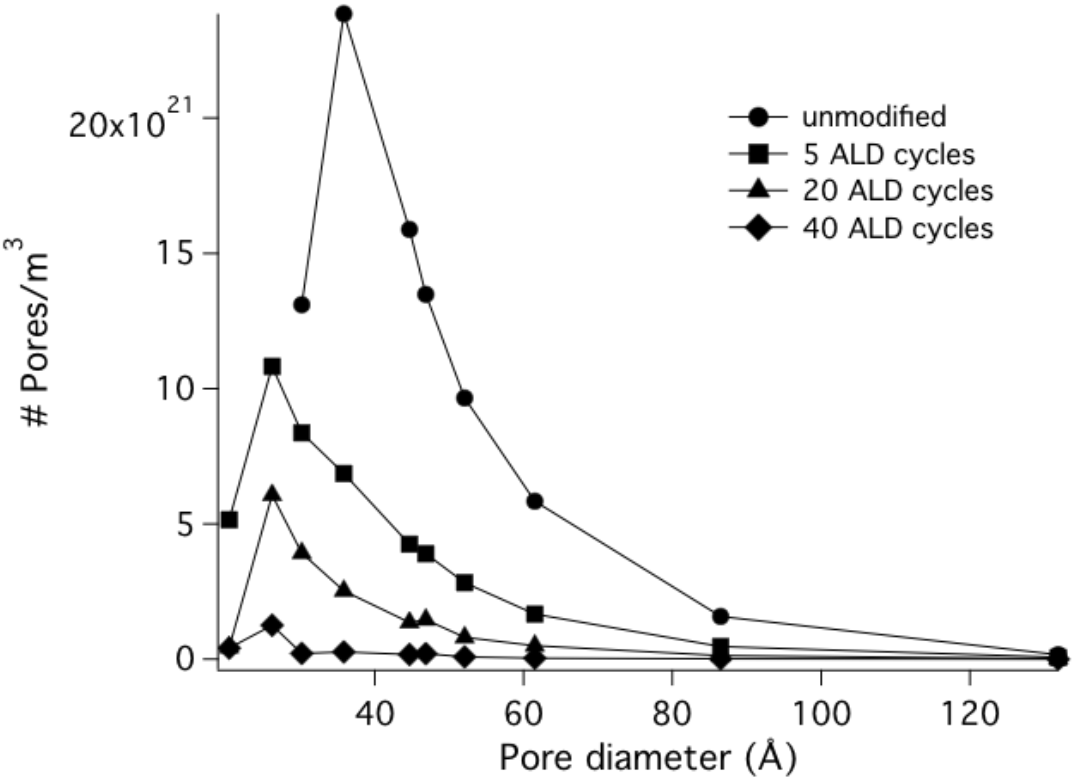

Figure 7.3 - Pore size distributions calculated from perm-porosimetry measurements on ALD modified mesoporous silica membranes

The improvement in membrane performance after ALD modification is shown in Figure 7.4. The experimental ideal separation factor, α, for He/N_2 (ratio of single gas permeance values) is compared to the theoretical Knudsen separation factor of 2.65, calculated from $\alpha = \sqrt{M_1 / M_2}$ where M_1 and M_2 are the molecular weights of N_2 and He, respectively. For pore diameters between 2-10 nm and at atmospheric pressure, molecule-pore wall interactions become significant and the transport mechanism is largely Knudsen flow. The Knudsen permeance is proportional to the inverse square root of the molecular

weight of the permeating molecule. Initially, the ideal separation factor was lower than the theoretical separation factor, indicating that there were larger pores and defects present in the membrane.[28] This is consistent with the perm-porosimetry data shown in Figure 7.3. Between 20 and 30 ALD cycles, the ideal separation factor increased to a value slightly greater than the Knudsen value indicating that the majority of defects had been reduced to pores with diameters small enough for Knudsen flow to be dominant. Separation factors slightly larger than the theoretical value can result from transport through pores with pore sizes at the lower limit of the occurrence of Knudsen flow, ~1 nm. However, at values approaching the molecular diameters of the permeating gases, separation factors can increase greatly due to molecular sieving. For nitrogen, the molecular diameter is ~0.37nm. From 30 to 50 ALD cycles, the measured ideal separation factor was constant, suggesting that while pore sizes continued to decrease, there must be a significant fraction of pores that transported both nitrogen and helium.

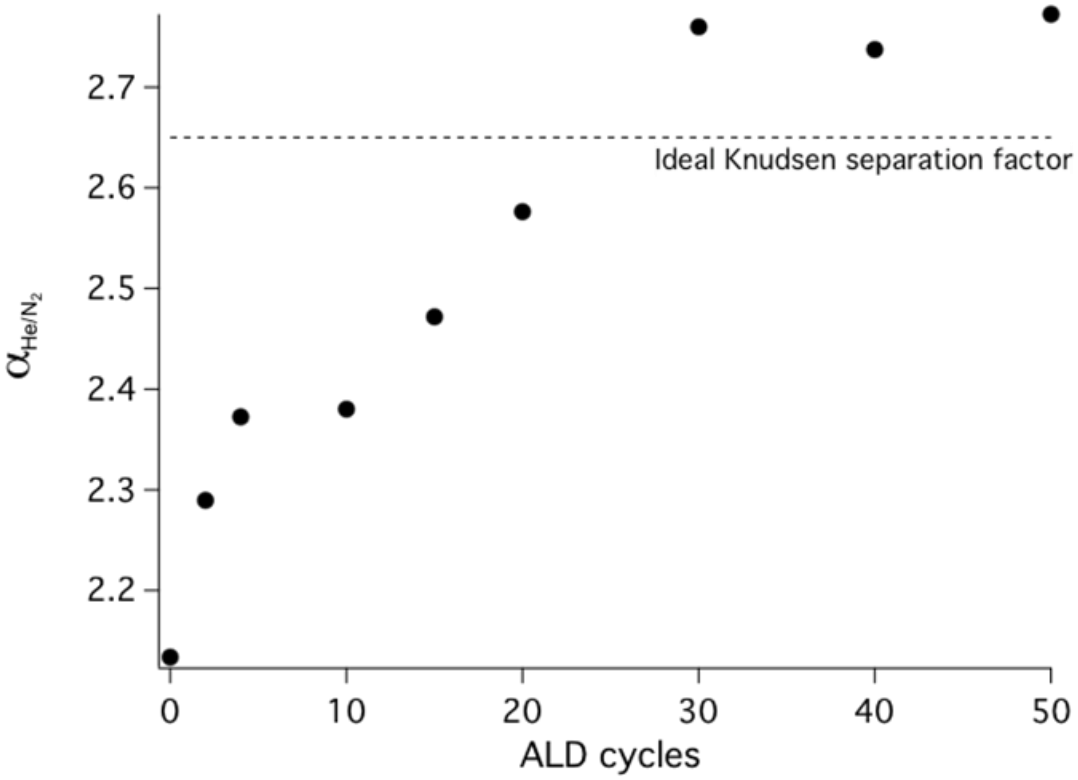

Figure 7.4 - The effect of ALD cycles on the measured ideal separation factor compared to the ideal Knudsen separation factor for He/N_2

7.4 Discussion

The decrease in measured He permeance with subsequent ALD cycles provides evidence for film growth within the pores of the membrane. Initially, the He permeance decreased significantly, but the rate of decrease gradually tapered off. This large initial decrease in permeance was also reported by George's group.[21] As the pore size decreased through film growth, the porosity also decreased.

Porosity is defined as the volume fraction of the membrane available for molecular transport. In the perm-porosimetry measurement, only active pores contribute to the pore size distribution. Therefore, the pore size distribution, calculated at a fixed membrane thickness, provides a measure of the two-dimensional porosity of the membrane (the fraction of pore area available for transport). The cumulative pore area, assuming the pores

are cylinders, can be estimated by summing the pore areas from the pore size distribution data. The cumulative pore area, calculated at specific ALD cycles, can similarly be calculated and normalized to the unmodified pore area. The decrease in normalized cumulative pore area will be similar to the decrease in normalized two-dimensional porosity. The decrease in normalized two-dimensional porosity is plotted against ALD cycles in Figure 7.5.

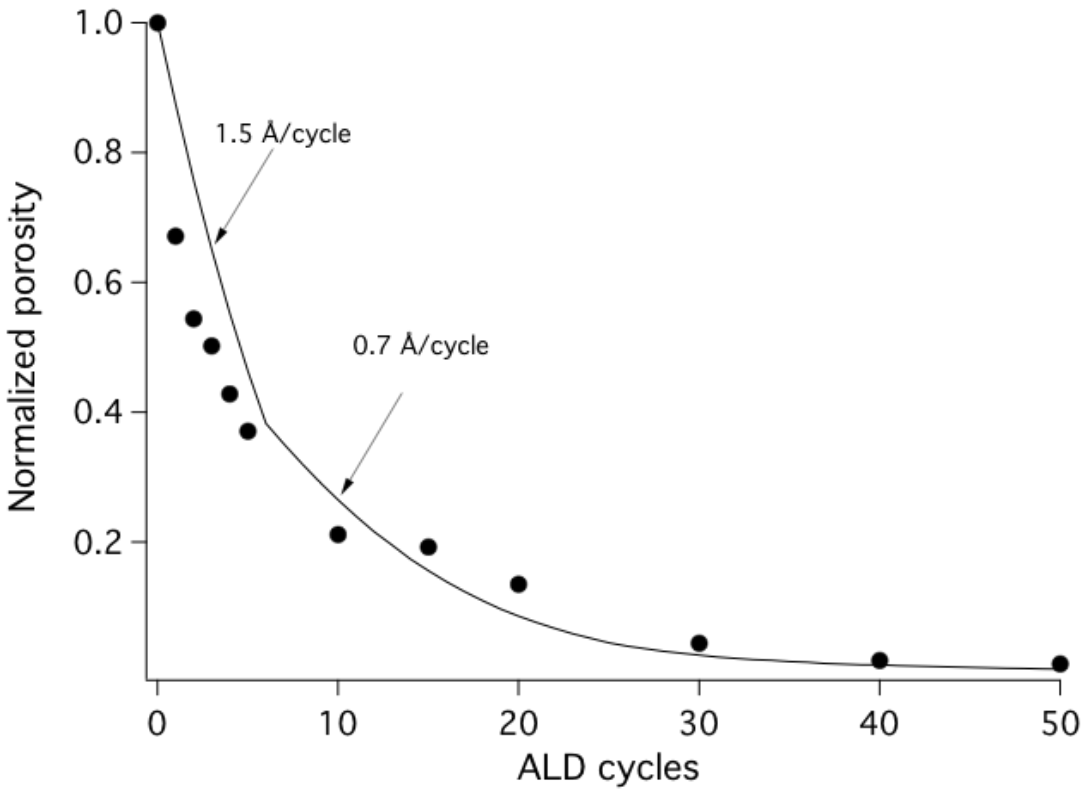

Figure 7.5 - Normalized porosity decrease with increasing ALD cycles with a constant growth rate model fit

The reduction in two-dimensional porosity per ALD cycle was modeled using a constant ALD growth rate per cycle, applied to the pore size distribution data for the unmodified membrane. For each ALD cycle, the pores at each measured pore size were reduced with a constant growth rate. The cumulative pore area was then calculated and normalized against the unmodified data per ALD cycle, shown in Figure 7.5 as the solid line. Over the complete range of data, it is clear that one ALD growth rate is not adequate to

describe the pore size reduction. As shown in Figure 7.5, for the first 7 ALD cycles, the data compared reasonably well to a porosity decrease predicted with a ~1.5 Å per cycle growth rate. For the subsequent ALD cycles, the growth rate used to fit the model to the data decreased to ~0.7 Å per cycle, indicating a decrease in growth rate with decreasing pore size. The 0.7 Å per cycle growth rate is well below the 1.3 Å per cycle growth rate cited for planar substrates.[64]

There are several possible reasons for the decrease in growth rate under constant reaction conditions as the ALD layer grows within the pores. In order for reaction to occur, the reactants must diffuse into the membrane pore network. The intrinsic diffusivity of reactants into the pores will decrease as the radius decreases. In our membranes, reactant diffusion into the intrinsic pores (mesopores) will occur largely by Knudsen diffusion, while diffusion through the larger, defect pores will have some pressure-driven diffusion. Knudsen diffusion occurs when the mean free path between particle-particle collisions is larger than a characteristic length in the system, in our case the pore diameter. The Knudsen number is defined as a ratio of the mean free path of the diffusing molecule to a characteristic length and quantifies gas rarefaction. Estimating the mean free paths of both water and TMA to be ~10^{-5} m at 373K and 5 torr, the respective Knudsen numbers would be on the order of 10^3 for a pore diameter of 4nm. Knudsen numbers of this order suggest that molecule-wall interactions are more probable than molecule-molecule interactions and that Knudsen diffusion of the reactants into the pores is therefore the probable mechanism. Knudsen and pressure-driven diffusivities are both dependent upon pore radius ($D_K \sim r$ and $D_P \sim r^2$, respectively) and are additive.[28] Therefore, as the pore size decreases during ALD, a longer diffusion time is required for surface coverage. In addition, it is expected that due to curvature, the number of surface sites available for reaction will be reduced in greater proportion than the reduction in surface area because of steric hindrance.

In order to estimate the ALD rate as a function of pore size we fitted the pore size distribution for a 20 ALD cycle-modified membrane (membrane A) with a pore size distribution calculated by shifting the unmodified pore size distribution with different ALD rates. Figure 7.6 shows the measured pore size distribution fitted with two ALD rates: a constant rate and a rate that varied linearly with pore radius. For supporting calculations for the growth rate models, see Appendix A. The constant rate used was 0.5 Å per ALD cycle, which resulted in a uniform 10 Å pore size reduction applied to all pores. The variable rate used to fit the pore size distribution was R = 0.018r + 0.001, where *R* is the growth rate in Å/cycle and *r* is the pore radius in Å. The constant growth rate aligns the peak of the pore size distribution with the measure data, but the larger pores are not reduced sufficiently to fit the measured data. Applying a growth rate that varied with the pore radius provides a better data fit, as seen in Figure 7.6.

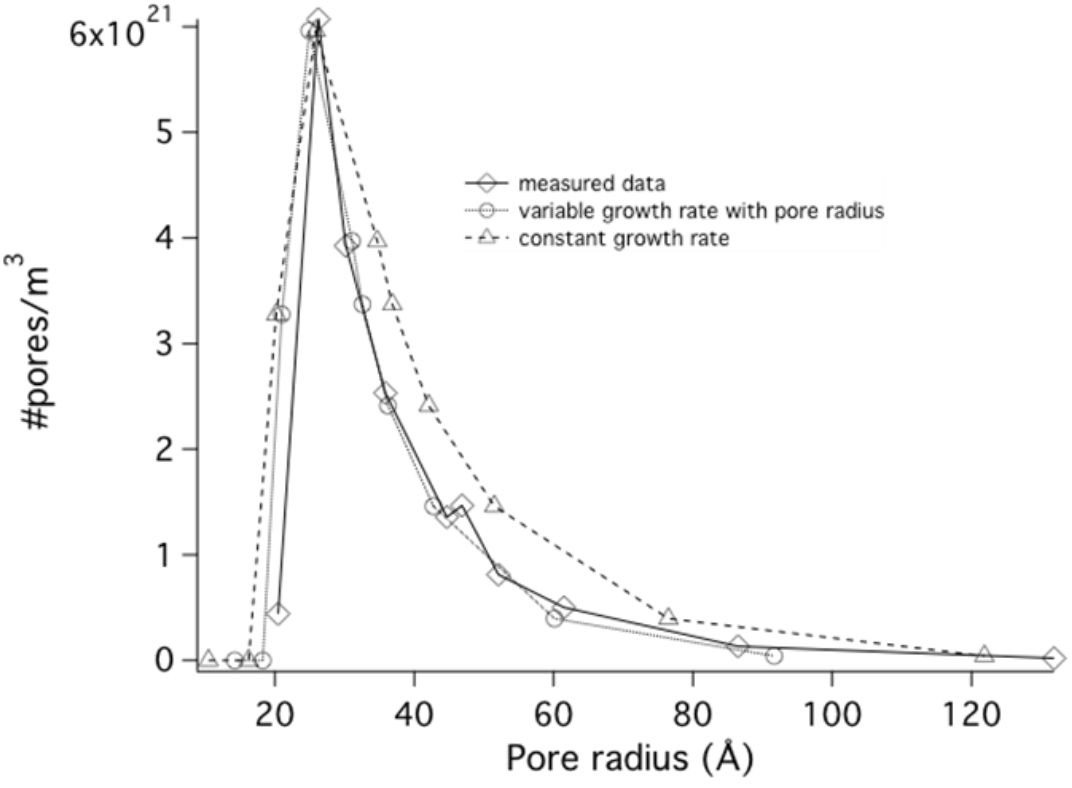

Figure 7.6 – Comparing variable and constant growth rate models for ALD deposition rates

The ALD reaction under our reaction conditions clearly favored larger pores. This is evident from the data in Figures 7.3-7.6. The data indicate that there may be a limit to pore reduction above the kinetic diameters of the reactants. Figure 7.4 indicates that the final pore size distribution results in permanent gas transport characterized by Knudsen flow. It is interesting that the separation factor plateaus between 30 and 50 ALD cycles. There are two possible explanations for this: self-limiting pore size reduction based on reduction in deposition efficiency or the presence of significant defects where 50 ALD cycles were insufficient to close pores. The above data also suggest that pore modification can be controlled to some degree, based on controlling the reaction conditions during modification. If larger pore removal is desired, for example, reactant exposure conditions can be reduced to limit modification of the smaller pores.

Self-limiting pore size reduction is an important concept in engineering a membrane for a particular separation based on molecular sieving. In previous work, we demonstrated that using base-catalyzed ALD of silica was successful in self-limiting pore size reduction based on the size of the amine catalyst.[37, 38] However, this reaction requires a third ALD cycle with the removal of an amine salt during synthesis, thus increasing the complexity. The alumina ALD reaction here is both less complex and can be applied to a wide variety of supports. Previous work with alumina ALD modification of porous materials has not provided the detailed analysis (including porosimetry measurements) to indicate the effect of ALD on pore size distribution change and deposition efficiency as pores decrease to the lower limits of the mesoporous range.[23, 29]

7.5 Conclusions

We have modified ordered mesoporous silica membranes, prepared by dip-coating surfactant-templated silica sols onto porous alumina disks, by atomic layer deposition of aluminum oxide layers within the porous network of the membrane. Light gas permeance

measurements taken at different stages (up to 50 ALD cycles) of modification provide evidence of pore modification. Perm-porosimetry data taken at different stages of modification provide information regarding the pore size shift and porosity changes in the membranes. The porosity change per ALD cycle deviate from that predicted assuming a constant growth rate per ALD cycle. Our data indicate that after 7 ALD cycles, the growth rate per cycle decreased significantly. This is possibly explained by limited diffusivity of reactants into the pores and decreasing reaction sites. These data suggest that membrane modification by ALD is very sensitive to ALD reaction conditions. Applications include controlled defect reduction and controlled deposition layer thickness in membranes.

CHAPTER 8

MOLECULAR LAYER DEPOSITION MODIFICATION OF MESOPOROUS SILICA MEMBRANES

8.1 Introduction

Mesoporous silica prepared using surfactants as templating structures provides a potential framework for hybrid organic-inorganic membranes by providing a relatively narrow pore size distribution in the mesoporous range, 2-10 nm diameter pores, and high pore volume for further chemical functionalization and property modification for gas separations.[11, 40, 53] The incorporation of organic functionality into the mesoporous membrane provides the potential for increasing separation of gas mixtures by enhancing adsorption of one molecule over another and reducing pore sizes below the lower limit of mesoporous silicas. These pore sizes, relative to gas molecules, result in Knudsen transport, with separation limited by the square root of the molecular weight ratio. The mesoporous silica framework, on the other hand, can provide thermal and chemical stability to the membrane.

There are two general strategies for incorporating organic functionality into mesoporous silica membranes: post-synthesis grafting or insertion of molecules that react with the silica surface, for example functionalized silanes or dendrimers [65-67]; and incorporating chemical functionalities into the framework of the mesoporous silica.[68-71] Post-synthesis grafting strategies have included reactions in solution, vapor-phase and supercritical fluid between functionalized silanes and surface silanols.[40, 69] By selective specific silanes, the modified silica surface may consist either of a polymerized layer or a single, surface-limited functionalized layer.[69]

A second strategy for preparing hybrid organic-inorganic membranes, organic functionalities can be incorporated into the silica framework. In synthesizing a mesoporous

silica membrane, a molecular source of silica is used, typically tetraethyl orthosilicate (TEOS), that condenses around surfactant templates forming a mesoporous silica structure. Reactions of TEOS and functionalized silanes that take part in this condensation reaction result in incorporating the functional groups into the silica framework.[72] If the surfactant is eliminated, a dense functionalized silica layer is formed.

In this work, we present an alternative strategy for preparing organic-inorganic mesoporous silica membranes based on atomic layer deposition (ALD) explained in detail in Chapter 3. Atomic layer deposition is a method tailored for the deposition of inorganic layers into structures with high aspect ratios or porous materials.[22, 23, 37] Atomic layer deposition consists of forming a layer through two consecutive half-reactions that are surface reaction-limited. These reactions typically occur from the vapor phase onto the solid surface. Combining these two sequential half-reactions results in one monolayer of material formed on the surface. Repetition of this reaction sequence results in increasing the thickness of the layer. Atomic layer deposition has been applied to membranes primarily as a method to reduce pore size in a controlled manner.[21-23, 37, 39, 48] Typically, ALD has been limited to inorganic layers. An example of ALD reaction chemistry for the formation of aluminum oxide includes the reaction of trimethyl aluminum with surface hydroxyls (first half-reaction) and the regeneration of surface hydroxyls with water (second half-reaction).

In order to create a hybrid organic-inorganic layer by ALD, researchers recently have substituted water with an organic molecule containing two hydroxyl groups, where one hydroxyl reacts with the surface and the other provides a surface site for the next set of reactions.[50, 73-77] This method is commonly termed molecular layer deposition or MLD and results in incorporating organic spacer molecules between the inorganic oxide components. Figure 8.1 compares conventional ALD of alumina with MLD using two

different precursors. Reaction 1 consists of trimethyl aluminum and water and results in aluminum oxide deposition. Reactions 2 and 3 replace the water with oxalic and o-phthalic acid, respectively, providing hydroxyls to react with surface methyl groups and leaving one hydroxyl for the next trimethyl aluminum cycle. The resulting layers now have organic spacers between the aluminum oxide units resulting in a hybrid organic-inorganic structural unit that is built up in consecutive layers through MLD.

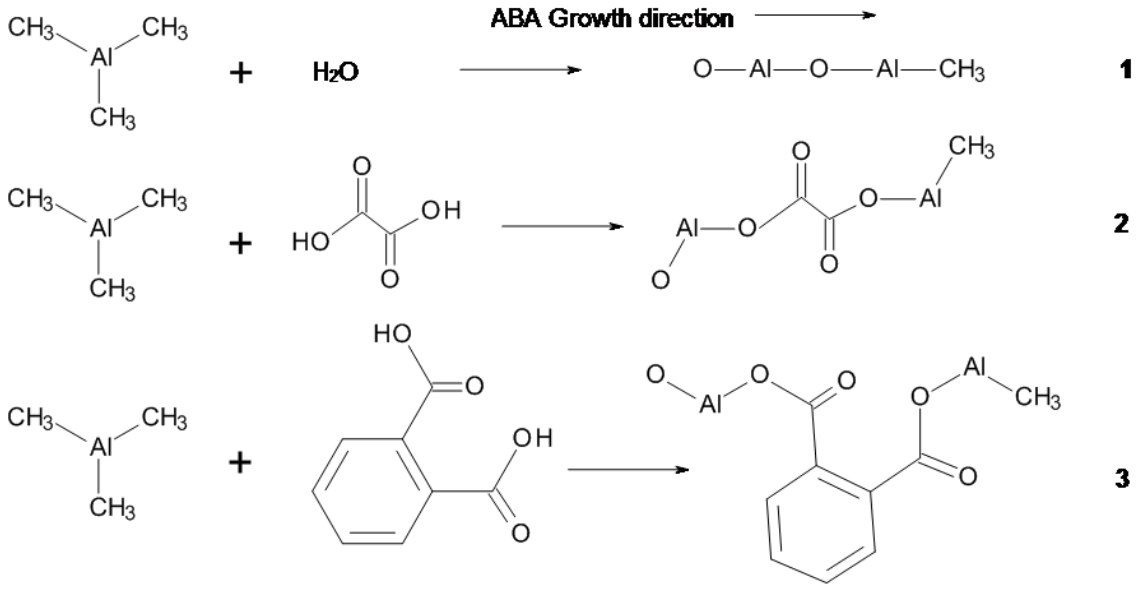

Figure 8.1 - ALD and MLD reaction schemes using trimethly aluminum and water (1), oxalic acid (2), and o-phthalic acid (3) as reactants

Molecular layer deposition offers an opportunity to both reduce the pore size of a mesoporous silica framework in a controlled manner similar to ALD, and simultaneously impart chemical functionality to the membrane. Molecular layer deposition on flat substrates using trimethyl aluminum has been previously studied using glycols and organic acids.[50, 73, 75, 76] These studies have provided a demonstration of the MLD reaction chemistry, growth rates as a function of temperature, and film property characterization. In this work, we have extended the MLD method to modify mesoporous silica membranes using oxalic and o-phthalic acids as precursor molecules. These precursors were chosen for

their previous feasibility on flat silicon surfaces and lower minimum operating temperatures.[50, 73] We report the relationship between the number of MLD cycles and membrane properties such as permeance of light gases and comparing this to ALD of alumina using water as a reactant. This synthesis technique provides an alternative method for creating organic-inorganic membranes that could provide unique separation capabilities based on controlling both the final pore size and chemical functionality within pores less than 2 nm in diameter.

8.2 Experimental

8.2.1 Membrane Synthesis

Mesoporous silica membranes were prepared using cetyltrimethylammonium bromide as the surfactant and tetraethyl orthosilicate as the silica source. The preparation method was previously explained in detail in Section 7.2.1.[48]

8.2.2 Molecular Layer Deposition Modification

The dip-coated membrane/support was placed in a custom-built reaction cell. The reaction cell allowed for membrane modification and characterization without membrane removal, which could damage the active layer. The membrane was sealed with silicon O-rings for oxalic acid (Sigma Aldrich) MLD and Kalrez (Dow) O-rings for the 1,2-benzene dicarboxylic acid (o-phthalic acid, Sigma Aldrich) MLD. For all MLD reactions the aluminum source was trimethyl aluminum (TMA, Sigma Aldrich) and it was held at 5°C. The molecular layer deposition operation followed the protocol conditions developed by Klepper el al.[50, 73] Oxalic acid and o-phthalic acid were held at 100°C and 177°C, respectively. All the lines and valves leading into the reaction cell from the precursors were heated to a least 10°C above the temperature of the organic precursor. In order to minimize the temperature dependence the reaction cell was operated above the minimum temperature required for MLD. For oxalic acid MLD, the reaction cell was held at 190°C and at 240°C for o-phthalic

acid. The exposure times for all the precursors was 30 seconds to ensure diffusion into the pores of the membrane, which was well above the minimum required for the reaction to take place on a flat surface (under 5 seconds).

The reaction purge cycle between each exposure of precursor involved: 10 minutes of being held under vacuum, followed by a 30 second N_2 flush over the top of the membrane. This purge cycle was repeated to remove any non-reacted precursors and byproducts from the pore network. The coating cycle sequence for molecular layer deposition was: dose TMA, evacuate excess TMA, N_2 purge, evacuate, N_2 purge, evacuate, dose organic acid, evacuate excess acid, N_2 purge, evacuate, N_2 purge, and evacuate. This complete cycle of MLD adds one monolayer of the organic-inorganic hybrid aluminum layer deposited within the pores. Up to 20 cycles were applied to modify the support membranes.

8.2.3 Characterization

The membranes were characterized using single gas permeation and perm-porosimetry. Single gas permeation was measured with helium and nitrogen at 30°C at pressure drops between 300 and 1800 torr. Single gas permeance was also measured for argon, methane and sulfur hexafluoride at 30°C and a single pressure drop between 760-1800 torr, depending on the total permeance. The hexane perm-porosimetry measurement apparatus and procedure is described in greater detail elsewhere.[78] Briefly, as the hexane vapor pressure is exposed to the membrane, capillary condensation occurs in the pores governed by the Kelvin equation. As the activity of hexane is increased, successively larger pores are blocked, and the He permeance through the membrane is reduced. From this data, a pore size distribution can be calculated.[79] The hexane perm-porosimetry was carried out with the membrane at 30°C and hexane bubbler at 25°C and a pressure drop of 300 torr. These measurements were completed on an unmodified membrane and after: 1, 2, 3, 4, 5,

and 10 cycles of MLD for oxalic acid and after: 1, 3, 5, 10, and 20 cycles of o-phthalic acid MLD.

8.3 Results and Discussion

The mesoporous silica membranes synthesized in our laboratory had properties similar to those reported elsewhere.[8, 11, 37] The membranes used in this study, prepared using CTAB as a template, had a maximum number of pores with diameter 2.5 nm, as determined using perm-porosimetry. The permeance versus pressure drop data indicated essentially Knudsen-based transport within the membranes. The permeances of light gases through the mesoporous support are shown in Table 8.1.

Table 8.1 – Permeance (mol $m^{-2}s^{-1}Pa^{-1}$) of light gases through unmodified and modified (after 10 cycles) mesoporous silica membranes

	TMA/Water		TMA/o-phthalic acid		TMA/oxalic acid	
	Unmodified	Modified	Unmodified	Modified	Unmodified	Modified
He (10^7)	39.87	12.08	9.70	1.95	13.59	1.77
N_2 (10^7)	18.69	5.08	3.95	0.66	6.06	0.37
Ar (10^7)	--	--	3.86	0.66	5.39	0.29
CH_4 (10^7)	--	--	5.67	1.84	9.72	0.50
SF_6 (10^7)	--	--	2.19	0.32	--	0.19

In this study, mesoporous silica membranes were subjected to successive MLD cycles and periodically characterized using permeance and perm-porosimetry in order to examine the effect of MLD cycle number on pore size reduction. Figure 8.2 shows the reduction of permeance resulting from MLD modification using both oxalic (OA) and o-phthalic (PA) acids, in comparison to ALD of aluminum oxide. Table 8.1 provides the permeance values of the unmodified and modified mesoporous silica membranes after 10 MLD or ALD cycles. In all cases, the reduction of permeance indicates that the MLD reaction is effective in pore size reduction, however, the oxalic acid reaction is clearly more effective in reducing pore size and permeance. Compared to ALD of alumina, this is somewhat

expected due to the larger reaction rate reported for OA MLD relative to alumina ALD (5Å/cycle vs. 1.3Å/cycle). The PA MLD, however, resulted in markedly less pore size and permeance reduction than the OA MLD.

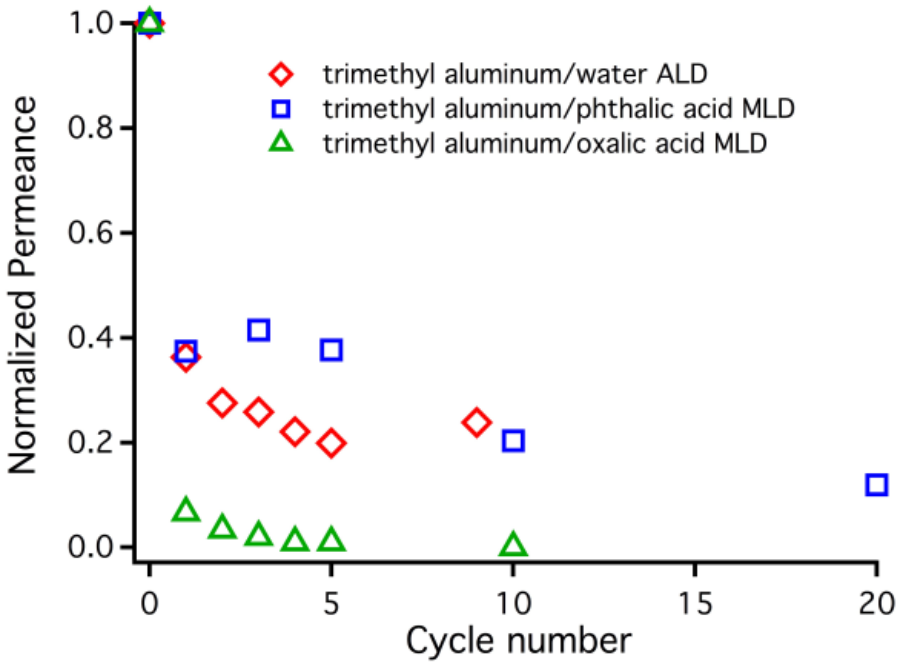

Figure 8.2 - Nitrogen permeance decrease during ALD and MLD modification of mesoporous silica membranes

Figure 8.3 shows the experimental ideal selectivities for He/N_2 calculated with the measured single gas permeance values at room temperature at different deposition cycles for both OA and PA MLD modification of mesoporous silica. The line for the theoretical Knudsen selectivity, assuming Knudsen flow, is shown for comparison. After one MLD cycle, both membrane selectivities increase above the Knudsen value. The OA MLD modified membrane selectivity plateaus near a value of 5 whereas the PA MLD selectivity increases to near 4 and then decreases slightly. At this time, we have no explanation for the slight decrease in measured selectivity. The selectivity values above the theoretical value could suggest a pore size shift into diameters where the diffusivity transitions more toward molecular flow. Alternatively, this could be an effect of the presence of surface flow. In this

case, nitrogen could have a lower surface flow on the MLD membranes, although this would not be expected.

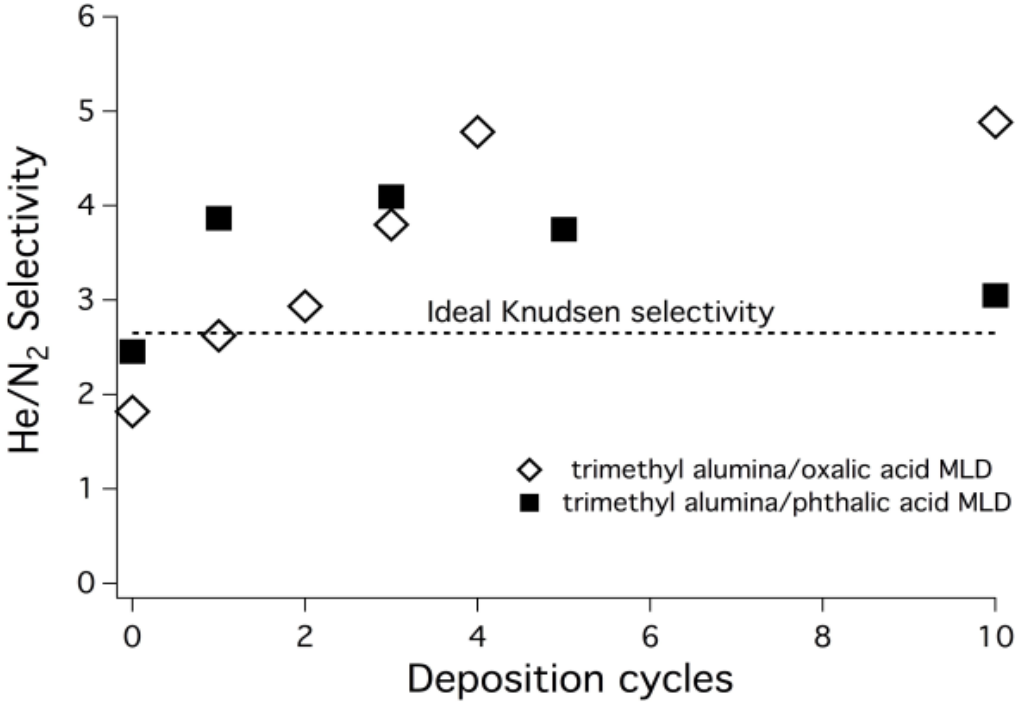

Figure 8.3 - Experimental ideal He/N_2 selectivities of MLD modified mesoporous silica membranes

The transport through the MLD modified membranes could occur as some combination of surface flow, Knudsen diffusion and viscous flow. Ignoring surface flow, there could be some contribution to the transport from viscous flow, particularly through the unmodified layer and the support. Given the reduced values of permeance and the separation factors measured (Figure 8.3), the transport through the MLD modified layers is essentially governed by Knudsen diffusion. Analysis of the support resistance indicated that it was more than two orders of magnitude smaller than the MLD layer resistance and it is therefore neglected in the following analysis. For pure Knudsen flow the permeance is given by the expression:

$$\pi\left(\frac{mol}{m^2 \cdot s \cdot Pa}\right) = \frac{N}{\Delta P} = \frac{\varepsilon}{\tau} \cdot \frac{D_K}{z} \cdot \frac{1}{RT} \cong \frac{97}{R} \cdot \left(\frac{\varepsilon \bar{r}}{\tau z}\right) \cdot \frac{1}{\sqrt{TM}} \qquad (8.1)$$

where ε is the porosity, τ is the tortuosity, D_K is the Knudsen diffusivity, z is the membrane thickness and M is the molecular weight.

In accordance with Equation 8.1, the permeance for several light gases (He, CH_4, N_2, Ar and SF_6) at room temperature plotted against the inverse root of molecular weight is shown in Figure 8.4 for PA MLD. Data are plotted so that the slopes of the linear fits are equivalent to the parameter $\frac{\varepsilon \bar{r}}{\tau z}$ for the membrane at different MLD cycles. Clearly, this parameter decreases as MLD proceeds, again providing evidence that the membrane properties are altered through MLD.

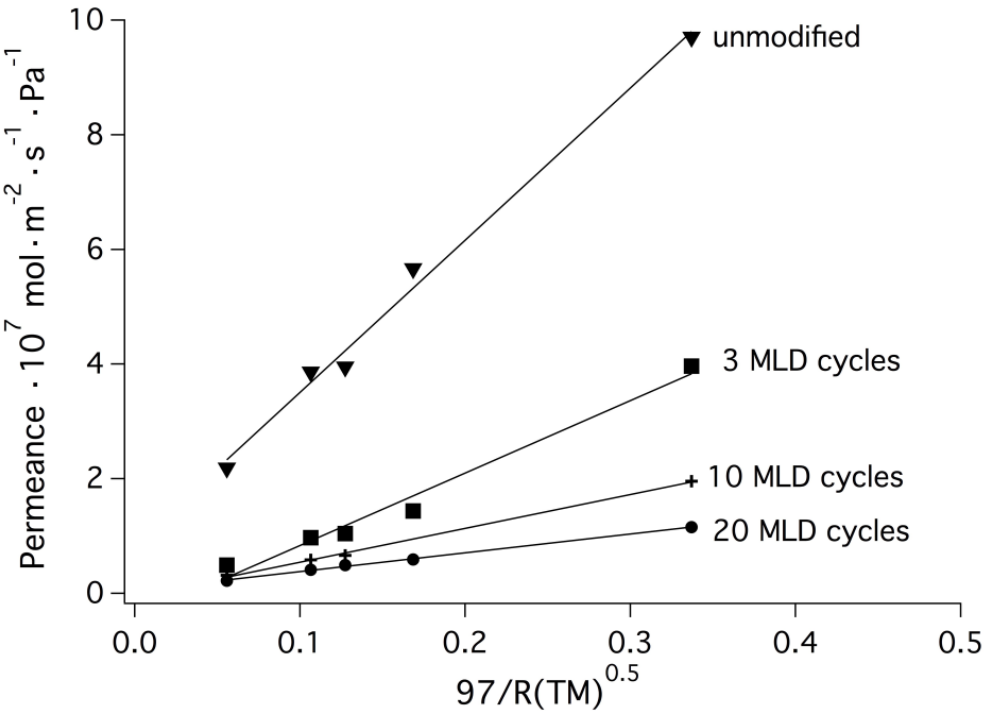

Figure 8.4 - Permeance data for different gases fitted to ideal Knudsen flow

The relationship between the different variables in the parameter $\frac{\varepsilon \bar{r}}{\tau z}$ can provide a better understanding of the membrane modification process by MLD. Of the four parameters, τ, the tortuosity, is assumed to remain essentially constant during modification. The membrane thickness, z, is difficult to determine experimentally. The initial mesoporous

silica membrane is between 1-3μm thick. The MLD of TMA and PA may not coat uniformly to this depth and as deposition continues and pore size decreases, the effective thickness may decrease further. To simplify the analysis, however, we will assume initially that membrane thickness also remains constant throughout MLD modification. Experimental data were obtained for the porosity, ε, during MLD modification by hexane perm-porosimetry, shown in Figure 8.5. This data is limited to the contribution of pores greater than 2 nm to the pore size distribution, the practical limit of the Kelvin equation.[40, 79]

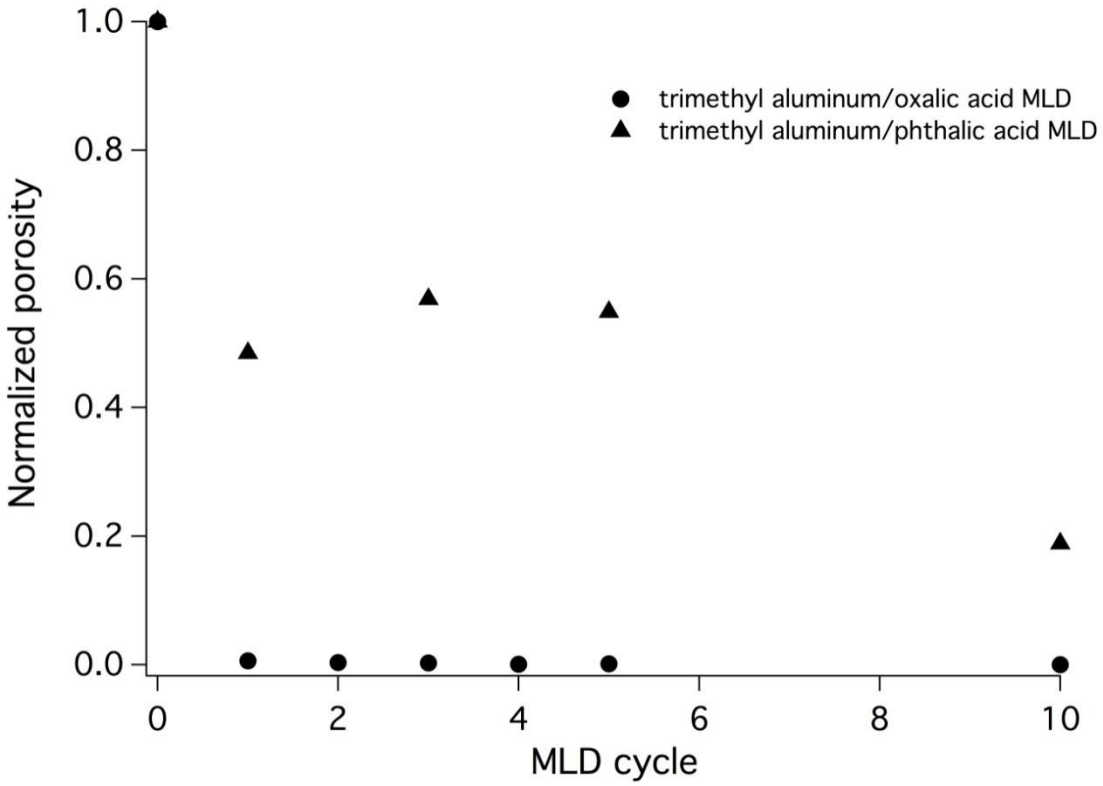

Figure 8.5 - Porosity changes with MLD cycle for OA and PA modified membranes

Starting with a simple model that assumes the porosity decrease is due only to the reduction of the diameters of cylindrical pores, that can measured by the hexane perm-porosimetry, a pore diameter reduction can be determined for each MLD cycle. The data for the OA MLD indicates a significant decrease, >95%, in porosity during the first cycle. As a result, a very high growth rate, 30 Å/cycle of TMA/OA during the first cycle is calculated

from the model. After the second and third cycle and out to the twentieth cycle, a lower growth rate, ~2Å/cycle, is calculated.

The change in porosity with PA MLD is quite different from the OA MLD. The PA MLD modification resulted in significantly less porosity change over 20 MLD cycles relative to the OA MLD. Here, the large relative porosity decrease during the first several cycles was markedly reduced and fitted with a growth rate of 2.5Å/cycle over the first 5 cycles. The remaining 15 cycles were fitted with a growth rate of 1.5Å/cycle. Except for the very large growth rate calculated for the first deposition cycle using OA MLD, the growth rates predicted are in reasonable agreement with values from the literature for MLD using OA and PA on flat substrates.[50, 73]

In order to further examine the relationship between porosity and mean pore radius, the parameter $\frac{\varepsilon\bar{r}}{\tau z}$ is plotted against ε using experimentally determined values of relative porosity for TMA/PA MLD as shown in Figure 8.6. The porosity, ε, is determined by $\zeta\varepsilon_0$ where ζ is the relative porosity and ε_0 is the porosity of the unmodified membrane. The relative porosity is calculated using hexane permporometry characterization. If the data fit is linear, that would indicate that the reduction in the parameter, $\frac{\varepsilon\bar{r}}{\tau z}$ is due to the porosity decrease with the mean pore radius remaining constant (again, assuming constant membrane thickness, z). However, it is not clear that a linear fit would best describe the relationship between $\frac{\varepsilon\bar{r}}{\tau z}$ and ε, particularly during the transition between initial modification and subsequent modification, indicating that the decrease of $\frac{\varepsilon\bar{r}}{\tau z}$ could be a combination of both porosity and mean pore radius reduction. This could be further

corroborated by the results shown in Figure 8.3 where ideal separation factors of He/N_2 are greater than the theoretical Knudsen value.

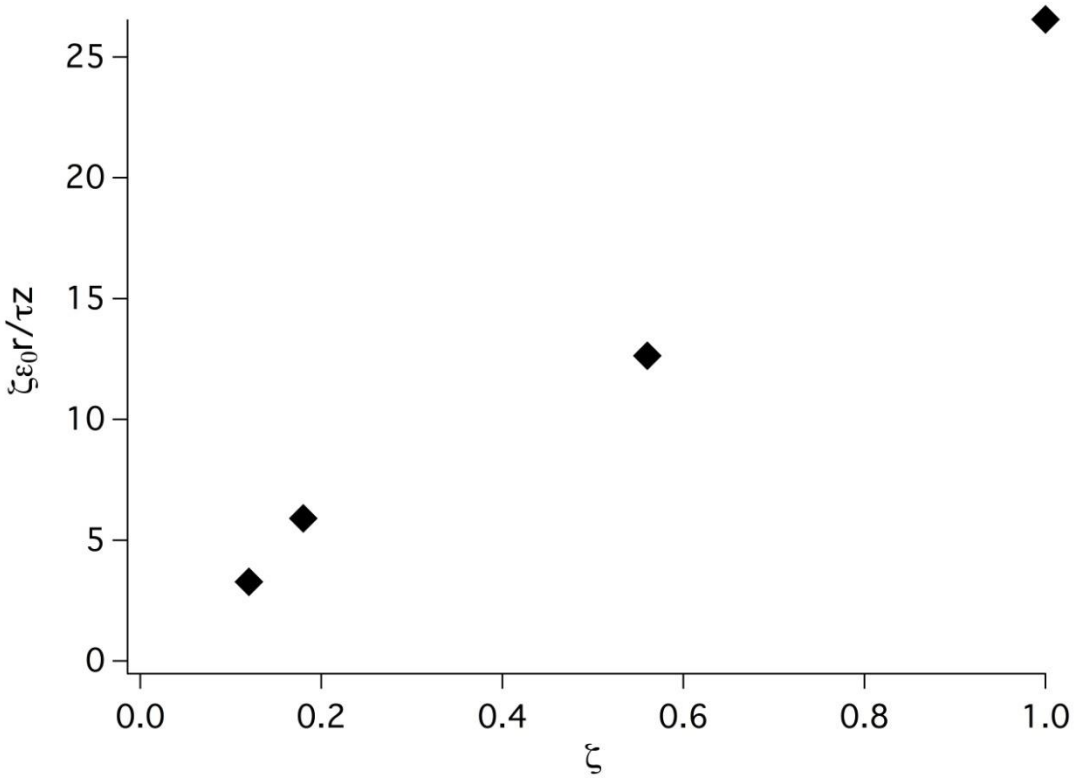

Figure 8.6 - Pore radius dependence on porosity change

8.3.1 Effect of Membrane Thickness

The above analysis assumes that the reduced permeance with increasing MLD cycles is independent of membrane thickness and tortuosity. This may not be the case, particularly with respect to membrane thickness. As pores become more constricted and porosity decreases, diffusion of the precursor molecules into the pores will become increasingly difficult. Thus the length of pore being modified would decrease as the modification becomes more extensive. A decrease in membrane thickness with increasing MLD modification would require a further decrease in the mean pore radius beyond that suggested by the above analysis.

8.3.2 Possibility of Micropores

The above analysis also assumed that the porosity was completely determined by pores greater than 2 nm. In MCM-48, micropores are not known to contribute strongly to the porosity of this material.[8] However, membrane synthesis of MCM-48 proceeds differently from bulk synthesis. Membranes in this study were prepared using evaporation induced self-assembly, EISA, of silica sols that were aged a specified time prior to deposition. In EISA, the initial silica/surfactant solution is dilute, in order to facilitate dip-coating of the membrane. During the drying process through evaporation of solvent, the surfactants continually reorganize as the solution becomes a gel. The final organization of the surfactants is determined by many factors including initial surfactant/silicon ratio, and humidity and temperature during evaporation. All this drying takes place at the interface of an alumina support. Because of the very different synthesis conditions for the mesoporous silica, the presence of micropores may be possible.

If a significant quantity of micropores were present, these could be easily blocked during the very early stages of MLD. Micropores could also provide high energy adsorption sites for MLD reactants facilitating a rapid blocking of larger pores as well. The rapid reduction of porosity during the first MLD cycle could, in part, be explained by the presence of micropores and their removal by MLD during the first cycle. The trapping of excess reactants within the pores could also contribute to a large initial pore blockage. When this occurs, chemical vapor deposition (CVD) can take place where a thicker, non-controlled layer is deposited.[24, 55]

8.3.3 Differences in PA and OA MLD Modified Membranes

The MLD of mesoporous silica membranes using PA and OA as precursors with TMA resulted in membranes that were, in some respects very different. The OA MLD modified membrane had a significantly reduced permeance to light gases; 10 times less than PA MLD

modified membranes. This could be due to several reasons related to the diffusivity and reactivity of PA MLD vs. OA MLD. Within porous supports, the larger PA molecule would have increasing difficulty diffusing into pores. The molecular diameters of PA and OA are estimated at 7.6 and 4.5 Å, respectively. O-phthalic acid MLD was reported to have a lower growth rate, despite its larger molecular size relative to OA. On flat supports, this could be due to lower surface coverage efficiency. Within porous supports, the larger PA molecule would have increased difficulty diffusing into pores.

It is interesting that both MLD modified membranes have similar ideal separation factors (Figure 8.3) for He/N_2, yet the permeance values after 10 deposition cycles are significantly lower for the OA MLD modified membrane. The limitations of PA to diffuse and react, could limit the reaction only near the mouth of the pore, resulting in a very thin separation layer, and hence, a higher permeance despite similar separation. Additionally, pore blockage could be more complete with OA MLD, resulting in a decreased number of active pores allowing transport.

8.3.4 Self-limiting Pore Size Reduction and Relationship to TMA/H_2O ALD Modification

Reacting precursors within porous materials to reduce the pore size can be self-limiting due to size exclusion of the precursor from the shrinking pore.[37, 80] The reduction of permeance of OA MLD relative to TMA/H_2O ALD shown in Figure 8.1 would not initially support this mechanism. The OA molecule is larger than water and if deposition was pore size self-limited we would expect to observe a higher permeance after complete modification, relative to ALD of alumina. The ALD of alumina, even after 50 modification cycles, had a higher permeance of light gases. In contrast, the PA MLD permeance decrease could, in part, be explained by a pore size self-limited reaction given the higher values of permeance relative to alumina ALD.

8.3.5 Opportunities for MLD Modified Mesoporous Silica Membranes

MLD offers many potential opportunities for modification of mesoporous silica membranes, particularly due to the nearly limitless number of organic molecules that could be applied to MLD. There are many different aromatic and linear molecules which, provided that a self-limiting effect can be produced, might offer new ways to tailor the final pore size of a mesoporous membrane. The use of organics adds functionality to the membrane and can be incorporated into chemically selective separations for gas phase and pervaporation processes. The organic linkers in MLD could also be removed through calcination leaving behind the inorganic framework with high porosity and small micropores templated by the organic precursors. MLD also offers more opportunities to grow films at many different thicknesses per cycle than is possible using ALD, and thus can help tailor the desired thickness and increase the efficiency.

Metal-organic frameworks (MOFs) are highly porous crystalline organic-inorganic hybrid materials. The crystal structure of MOFs produces intrinsic pores that are defined by the length and structure of the organic linkers. In order to apply MOFs as membranes, Zhao group reported needing a thick coating of over 15 μm and Bux et al reported a 30 μm thick layer in their synthesis of a comparable zeolitic sub-class of MOFs.[81, 82] In the synthesis of zeolite membranes of similar properties, the membrane was reported to be over 1.2 mm thick. [83] The thick layer of material is needed to coat defects and cracks between the different crystalline lattices and reduces the performance of the membrane. MLD offers a way to synthesize MOF-like organic-inorganic structures. The structure would not be identical to MOFs, but could have the same cage structure with similar functionality. MLD offers a method to grow a uniform film on many different supporting materials (mesoporous silica and alumina) with a much finer control on the thickness of the layer.

MOF-like material templated onto a mesoporous silica support could have a thickness of less than 1 μm.

8.4 Conclusions

Mesoporous silica membranes dip-coated onto an alumina support with a mean pore radius of 2.5 nm, were subsequently modified using molecular layer deposition, MLD. An inorganic/organic material was deposited within the membrane resulting in a reduction in permeance values of light gases. The MLD reactions studied were trimethyl aluminum with oxalic acid (OA MLD) and with o-phthalic acid (PA MLD). The reactions took place in sequential order, similar to ALD, where a self-limiting process occurs that controls film deposition. The OA MLD modification of mesoporous silica resulted in a membrane that had its porosity reduced significantly (>95%) in the first deposition cycle and after 10 deposition cycles had a permeance value 233 times lower than the unmodified membrane. The PA MLD modification of mesoporous silica resulted in a membrane with a less pronounced decrease in porosity than the OA MLD membrane and a permeance of N_2 after 10 deposition cycles that was considerably higher (28 times) than the 10 cycle OA MLD membrane. Both modified membranes had a He/N_2 selectivity greater than the theoretical Knudsen value. Analysis of the permeance data for both membranes indicated that transport occurred largely by Knudsen diffusion. The permeance reduction in the MLD modified membranes was due to a combination of porosity and mean pore radius decrease. Molecular layer deposition provides an alternative synthesis technique for creating inorganic/organic membranes.

CHAPTER 9

HYDROTHERMAL STABILITY OF MESOPOROUS SILICA MEMBRANES MODIFIED BY ALUMINA ALD

9.1 Introduction

The choice of an inorganic membrane in preference to a polymer membrane is generally decided by considerations of the thermal/chemical stability. One problem with silica membranes, however, is their hydrothermal instability, which makes them unsuitable for many applications. Many studies have shown membrane degradation under varying hydrothermal conditions. It has been shown that the permeance decreased over time for membranes exposed to traces of water vapor.[43, 44] For example, in a hydrogen separation with traces of water vapor at 600 °C, the permeance declined to about 10% of its initial value after 48 hours exposure indicating membrane degradation.[84] In the presence of water vapor at elevated temperatures, it is thought that the membranes undergo a process called densification. It has been hypothesized that steam catalyzes reactions between surface silanols leading to a blocking of the small pores within the membrane.[85, 86] In another study, the Kim group was able to show that MCM-48 completely degrade in liquid water at 100 °C.[87]

In addition to pore blocking under hydrothermal conditions, it has been shown that pores can also expand under hydrothermal treatment. In Coppens work, they applied a vapor phase hydrothermal treatment to MCM-48 to expand the pore diameter from 2.6 to 4.2 nm.[86] The MCM-48 maintained its high porosity due its thicker pore walls than other mesoporous silicas, such as MCM-41.[88]

Studies have been directed to modifying silica membranes in order to increase their hydrothermal stability. Since it is known that some ceramic membranes are more hydrothermally stable, attempts have been made to coat the surface of silica membranes

with different materials such as alumina, titania, and zirconia.[85, 89, 90] These ceramics were added in variety of different ways. Adding these materials to the silica sol-gel solution before dip-coating the membrane increased the hydrothermal stability. Replacing some of the free surface silicas with other ceramics was thought to prevent the water molecules from catalyzing the reaction of adjacent silica molecules to collapse on each other, thus improving the hydrothermal stability.

ALD offers another method for adding alumina to the surface of silica mesoporous membrane pores and could change the hydrothermal stability of the membrane. In this study, the hydrothermal stability of mesoporous silica membranes was compared to 10 cycle ALD modified mesoporous silica membranes. The membranes were subjected to hydrothermal treatment in a membrane cell holder at 200 °C with a trace amount of water. The initial results suggest that coating the mesoporous silica with alumina by ALD improves hydrothermal stability in the membrane.

9.2 Experimental

9.2.1 Membrane Synthesis

Mesoporous silica membranes were produced by the method described in Section 7.2.1. The membranes were dip-coated onto an α-alumina support. This support was selected because of its hydrothermal stability and asymmetric structure. Four dip-coating cycles were used to synthesize the membrane for both the unmodified and alumina ALD modified membrane.

9.2.2 ALD Modification

The modification of the ALD membrane was carried out at 100°C for 10 cycles using TMA and water. The membrane modification process followed the procedure described in section 7.2.2.

9.2.3 Hydrothermal Treatment

The hydrothermal treatment of the mesoporous membrane was carried out to mimic conditions for membranes exposed to trace water content. This method was chosen to prevent water from condensing inside the pores during the permeance measurements, enabling all permeance change to be correlated with hydrothermal stability. The treatment was carried out at 200°C with a 1 torr partial vapor pressure of water. The total flow rate entering the membrane cell was 105 sccm, with helium as a carrier gas, and a 300 torr pressure drop across the membrane was maintained. The membrane was exposed to these conditions for 5 days, while monitoring the permeance at regular intervals. Any remaining water inside the pore network was removed by exposing the membrane to dry helium gas for 1 day at 200 °C, and the membrane permeance was then characterized.

9.2.4 Characterization

The membranes were characterized before and after the hydrothermal treatment of the membrane. The characterization involved collecting permeance versus pressure drop data for nitrogen and helium, as well as hexane permporometry data. The characterizations were carried out at 30 °C for both the permeance and permporometry.

9.3 Results and Discussion

The plots of permeance versus pressure for nitrogen and helium for an unmodified silica membrane before and after hydrothermal treatment are shown in Figure 9.1. The permeance values for helium and nitrogen decreased during the hydrothermal treatment of the unmodified membrane. For comparison, the alumina ALD modified membrane permeance data, before and after hydrothermal treatment are shown in Figure 9.2. Comparing Figures 9.1 and 9.2, there is a noticeable difference in the change in permeance due to the hydrothermal treatment. The permeance at a pressure drop of 760 torr for the unmodified mesoporous silica membrane was reduced by 19% for nitrogen and 16% for

helium, while the ALD modified membrane showed a negligible reduction in the permeance of the membrane (less than 1%). The larger permeance reduction of the unmodified membrane for nitrogen relative to helium suggests a reduction in the pore diameter, specifically of the larger pores. The ALD modified membrane did not show any real reduction in the permeance, suggesting no change in the average pore size. The helium permeance of the ALD modified membrane was $5.8*10^{-7}$ mol $m^{-2}s^{-1}Pa^{-1}$ at a 760 torr pressure drop whereas the permeance of the unmodified membrane was substantially higher at $2.1*10^{-6}$ mol $m^{-2}s^{-1}Pa^{-1}$. The lower permeance was due to the ALD modification. The alumina coating may have sealed the silica membrane preventing the water from catalyzing the surface silicas and thereby increasing the hydrothermal stability.

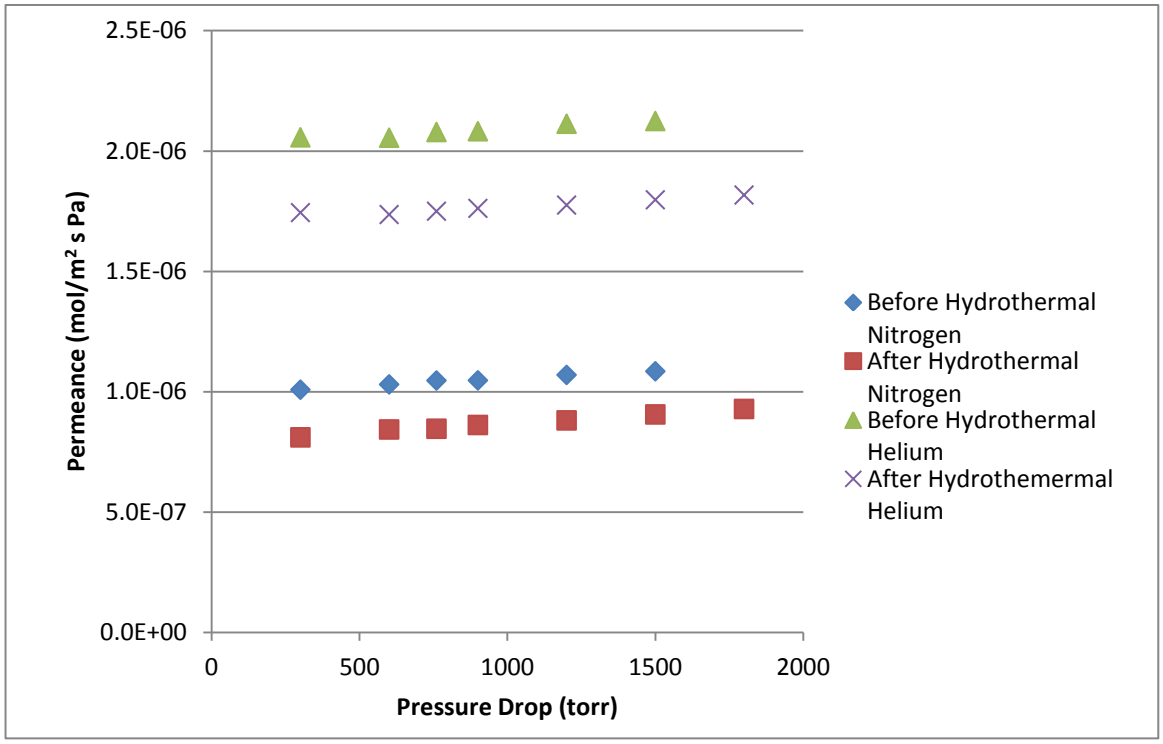

Figure 9.1 – Permeance versus pressure drop for an unmodified silica membrane

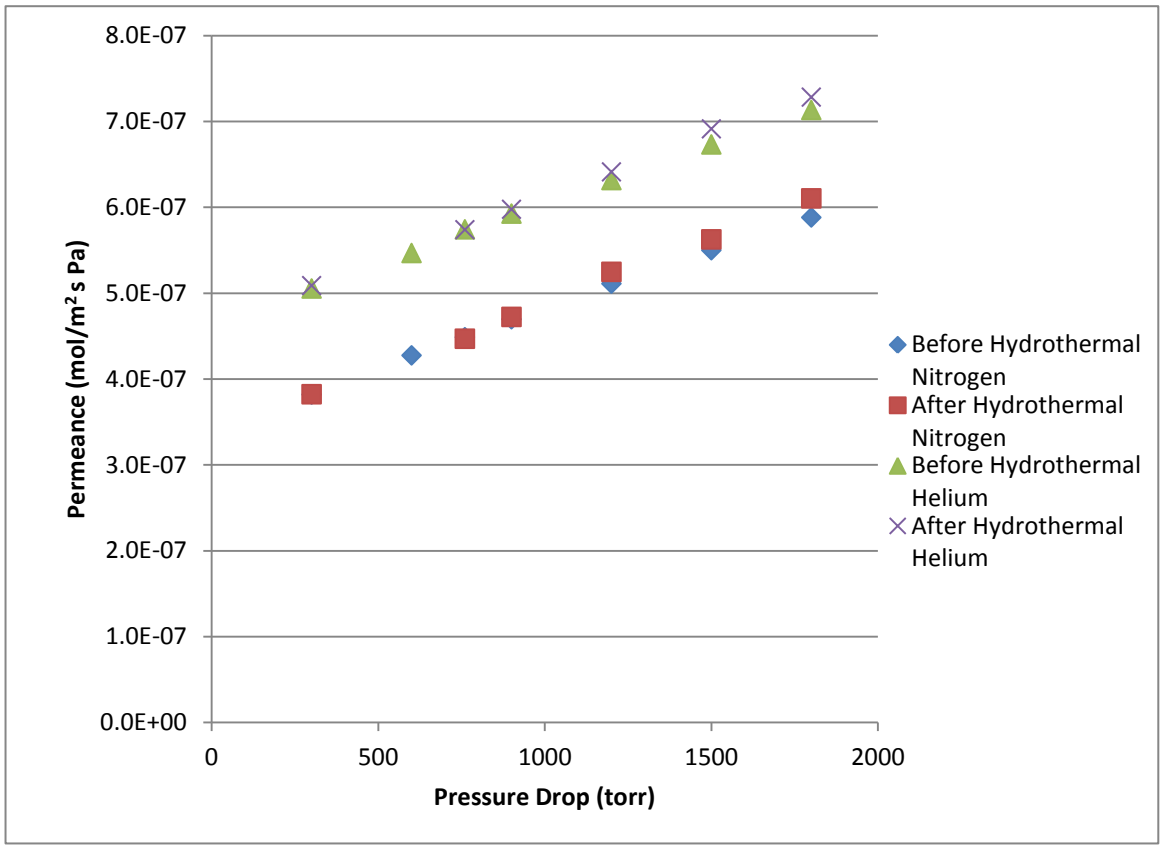

Figure 9.2 – Permeance versus pressure drop for an ALD modified silica membrane

There was a shift in the pore size distribution due to the hydrothermal treatment for the unmodified membrane, shown in Figure 9.3. There was a collapse of the pore size distribution, with a total porosity reduction of 41%, which is comparable to other hydrothermal studies on MCM-41 where the porosity decreased by 40-50% over 120 hrs.[88] The reason that there was no shift in the pore size could be due to the limitations of the hexane permporometry experiment in which pores less than 2 nm are not analyzed.

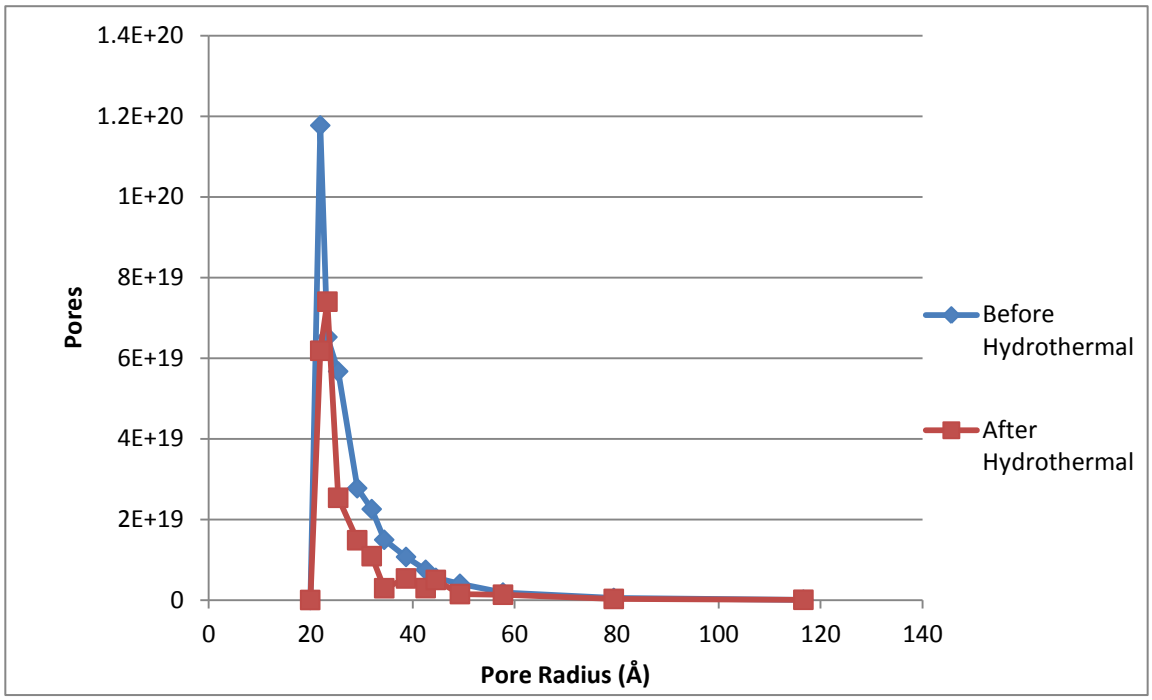

Figure 9.3 – Pore size distribution before and after hydrothermal treatment of a mesoporous silica membrane

The pore size distribution for the ALD modified membrane, shown in Figure 9.4, did not show the same collapse. There porosity remained relatively constant and any variation in the distribution was attributed to experimental noise. This demonstrates that the ALD modified membrane's pore structures are more stable during hydrothermal conditions at 200 °C.

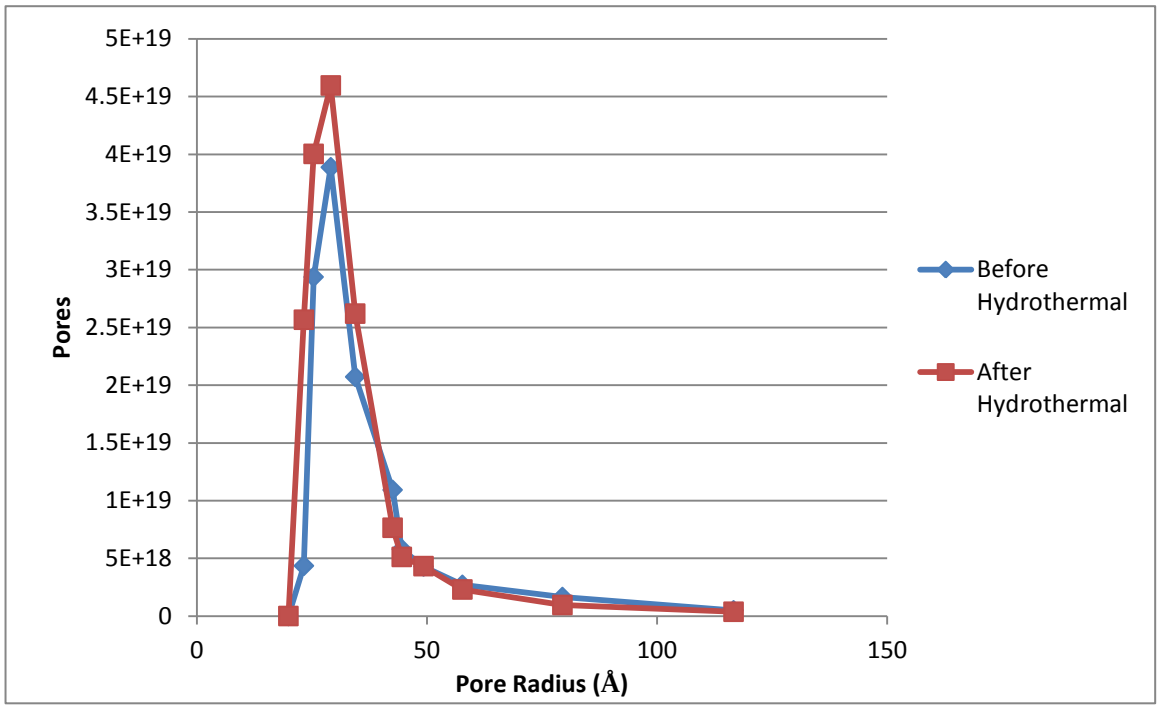

Figure 9.4 – Pore size distribution before and after hydrothermal treatment of an alumina ALD modified mesoporous silica membrane

9.4 Conclusions

The hydrothermal stability of CTAB surfactant template mesoporous silica membranes at 200°C under conditions of trace water content was examined. The helium permeance decreased by 16% but the porosity of the membrane dropped by over 42%. The average pore size remained constant with a net reduction in the total number of pores. ALD modified membranes performed better during hydrothermal treatments without a reduction in the permeance or porosity of the membrane. The viscous contribution to the total flux of the membrane did slightly increase for the ALD modified membrane, suggesting some degradation on the membrane surface during the hydrothermal treatment.

CHAPTER 10

CONCLUSIONS

10.1 Mesoporous Silica

Mesoporous silica membranes were synthesized to act as a support for ALD to reduce the pore size of a membrane to below 2 nm in diameter. The mesoporous silica membranes were dip-coated onto an α-alumina asymmetric support using a sol-gel solution derived from CTAB, TEOS, ethanol, water, and dilute hydrochloric acid. The membrane was produced through dip-coating using a technique called evaporated induced self-assembly, which produced an ordered membrane structure. The membranes were dip-coated at 30 °C and 50% humidity to produce the desired membrane with minimal defects in a reproducible manner. The CTAB surfactant was removed through calcination at 500 °C, leaving behind a porous network. Four dip-coating cycles were needed to produce a defect free mesoporous layer on top of the 100 nm support. The mesoporous layer was 1-3 μm thick with an average pore size of ~4 nm in diameter.

10.2 Atomic Layer Deposition

The mesoporous silica membrane was modified using trimethyl aluminum and water with up to 50 cycles of ALD. The membrane permeance and porosity decreased with each subsequent cycle of ALD. The selectivity of He/N_2 of the membrane increased gradually during the first 30 cycles of ALD, from 2.1 to ~2.7 and leveled off at about ~2.7 through the remainder of the cycles. This corresponded to a reduction in the viscous contribution to the permeance and after 30 cycles of modification, the permeance was predominately Knudsen, close to the theoretical selectivity of 2.65. The growth rate was higher during the initial cycles, 1.5 Å/cycle during the first 7 cycles, and subsequently decreased to 0.7 Å/cycle thereafter. Diffusion limitations could have contributed to the decreasing growth rate. Comparing the unmodified and the 20 ALD cycle membrane pore

size distributions, revealed that the growth rate was not constant for all pores; larger pores were favored. The variable growth rate as a function of pore radius was estimated to be R=0.018r + 0.001, where R is the growth rate in Å/cycle and r is the pore radius in Å.

10.3 Molecular Layer Deposition

The MLD was carried out using two different organic acids, oxalic and o-phthalic acid, with trimethyl aluminum. Oxalic acid is a saturated linear dicarboxylic acid and was chosen due to its smaller molecular size, lower temperature of reaction, and exposure time required for MLD. O-phthalic acid is an aromatic acid and was chosen for its larger molecular size, while still requiring a lower operating temperature and exposure time.

The oxalic acid and trimethyl aluminum MLD showed a very high initial growth rate, ~30 Å/cycle, where He permeance reduced by over 95% in the first two cycles. After 3 cycles of MLD, the growth rate dropped to ~2 Å/cycle which corresponds more closely to the expected growth rate. The membrane He/N_2 selectivity increased during the modification from 1.9 to 4.5 after 4 cycles, significantly larger than the ideal Knudsen selectivity value of 2.65.

The o-phthalic acid and trimethyl aluminum MLD showed a growth rate similar to that of traditional ALD with TMA and water. The permeance declined by 80% over 10 cycles, with a growth rate of ~2.5 Å/cycle for the first 5 cycles and ~ 1.5 Å/cycle afterward.

10.4 Hydrothermal Stability

A preliminary study into the hydrothermal stability of mesoporous silica membranes showed degradation of the pores of a mesoporous silica membrane when exposed to a trace amount of water at 200°C. The nitrogen permeance declined by 19% during the 5 days that the membrane was exposed to 1 torr of water vapor at 200°C. There was also a collapse of the pore size distribution with the porosity decreasing to 41% for pores between 2 nm and 40 nm. The mesoporous silica membrane modified by 10 cycles of

alumina ALD using TMA and water was less affected by the hydrothermal treatment. The membrane permeance for both helium and nitrogen remained constant before and after modification, with a reduction of under 1%.

10.5 Proposed Future Work

The purpose of this study was to determine the effects of atomic and molecular layer deposition on the modification of mesoporous silica membranes. This has been accomplished, but a better understanding of the minimum pore size would also be desirable. These deposition techniques offer a way to a have a self-limiting effect on the final pore size of a membrane corresponding to the precursors used for modification. Especially in MLD, there are many opportunities for applying this self-limiting effect. The oxalic acid did not demonstrate this effect as well as the o-phthalic acid, so other aromatics could be selected as the focus of future work. Different aromatics could be used to tailor different final pore sizes.

The other possible product that could be produced using MLD would be a MOF like material on the top surface of a mesoporous membrane. MOFs offer a way to produce a microporous membrane with high functionality and control over the pore size dictated by the organic linker molecules. However, currently MOF membranes must be fairly thick to minimize the effects of defects on transport. An MLD synthesized MOF like material could have these similar properties, considering that oxalic and o-phthalic acid are used in MOF synthesis as well as MLD. MLD could synthesize a sub 1 μm thick membrane of this material with a similar organic-inorganic linker type structure for membrane separations processes.

Another possible way to produce a microporous membrane deposited onto a mesoporous membrane support would be to remove the deposited organic linkers after MLD modification. MLD could be used to plug the membrane and deposit a thin layer of the organic-inorganic material on the top surface of the membrane. The organics would be

removed using calcination, leaving behind a highly porous alumina network with the pore size dictated by the size of the organic precursor used.

BIBLIOGRAPHY

1. Burggraaf, A.J. and L. Cot, eds. Fundamentals of Inorganic Membrane Science and Technology. Vol. 4. 1996, Elsevier: Amsterdam. 690.

2. Di Renzo, F., H.l.n. Cambon, and R. Dutartre, A 28-year-old synthesis of micelle-templated mesoporous silica. Microporous Materials, 1997. **10**(46): p. 283-286.

3. Kresge, C., et al., Ordered Mesoporous Molecular Sieves Synthesized by a Liquid. Nature, 1992. **359**(6397): p. 710-710.

4. Beck, J.S., et al., A new family of mesoporous molecular-seives prepared with liquid-crystal templates. Journal of the American Chemical Society, 1992. **114**(27): p. 10834-10843.

5. Monnier, A., et al., Cooperative formation of inorganic-organic interfaces in the synthesis of silicate mesostructures. Science, 1993. **261**(5126): p. 1299-1303.

6. Huo, Q.S., et al., Generalized synthesis of periodic surfactant inorganic composite-materials. Nature, 1994. **368**(6469): p. 317-321.

7. Huo, Q.S., et al., Organization of organic-molecules with inorganic molecular-species into nanocomposite biphase arrays. Chemistry of Materials, 1994. **6**(8): p. 1176-1191.

8. Vartuli, J.C., et al., Effect of surfactant silica molar ratios on the formation of mesoporous molecular sieves inorganic mimicry of surfactant liquid-cystal phases and mechanistic implications. Chemistry of Materials, 1994. **6**(12): p. 2317-2326.

9. Zhao, D.Y., et al., Triblock copolymer syntheses of mesoporous silica with periodic 50 to 300 angstrom pores. Science, 1998. **279**(5350): p. 548-552.

10. Kim, Y.S. and S.M. Yang, Preparation of continuous mesoporous silica thin film on a porous tube. Advanced Materials, 2002. **14**(15).

11. McCool, B.A., et al., Synthesis and characterization of mesoporous silica membranes via dip-coating and hydrothermal deposition techniques. Journal of Membrane Science, 2003. **218**(1-2): p. 55-67.

12. Coasne, B., et al., Gas adsorption in mesoporous micelle-templated silicas: MCM-41, MCM-48, and SBA-15. Langmuir, 2006. **22**(26): p. 11097-11105.

13. Innocenzi, P., et al., Order-Disorder in Self-Assembled Mesostructured Silica Films: A Concepts Review. Chemistry of Materials, 2009. **21**(13): p. 2555-2564.

14. Gibaud, A., et al., Evaporation-controlled self-assembly of silica surfactant mesophases. Journal of Physical Chemistry B, 2003. **107**(25): p. 6114-6118.

15. Urade, V.N., et al., Controlling interfacial curvature in nanoporous silica films formed by evaporation-induced self-assembly from nonionic surfactants. II. Effect of processing parameters on film structure. Langmuir, 2007. **23**(8): p. 4268-4278.

16. Suntola, T., Method for producing compound thin films. 1977, United States Patent: Finland.

17. Ahonen, M., M. Pessa, and T. Suntola, Study of ZNTE films grown on glass substrates using an atomic layer evaporation method. Thin Solid Films, 1980. **65**(3): p. 301-307.

18. George, S.M., Atomic Layer Deposition: An Overview. Chemical Reviews, 2010. **110**(1): p. 111-131.

19. Jiang, Y.B., et al., Nanometer-thick conformal pore sealing of self-assembled mesoporous silica by plasma-assisted atomic layer deposition. Journal of the American Chemical Society, 2006. **128**(34): p. 11018-11019.

20. Soto, C. and W.T. Tysoe, The reaction pathway for the growth of alumina on high surface-area alumina and in ultrahigh-vacuum by a reaction between trimethyl aluminum and water. Journal of Vacuum Science & Technology a-Vacuum Surfaces and Films, 1991. **9**(5): p. 2686-2695.

21. Cameron, M.A., et al., Atomic layer deposition of SiO2 and TiO2 in alumina tubular membranes: Pore reduction and effect of surface species on gas transport. Langmuir, 2000. **16**(19): p. 7435-7444.

22. Ott, A.W., et al., Modification of porous alumina membranes using Al2O3 atomic layer controlled deposition. Chemistry of Materials, 1997. **9**(3): p. 707-714.

23. Berland, B.S., et al., In situ monitoring of atomic layer controlled pore reduction in alumina tubular membranes using sequential surface reactions. Chemistry of Materials, 1998. **10**(12): p. 3941-3950.

24. Pan, M., et al., CVD modification and vapor gas separation properties of nanoporous alumina membranes. Journal of Membrane Science, 1999. **158**(1-2): p. 235-241.

25. Ebrahimi, M., Atomic Layer Deposition (ALD). 2006, University of Waterloo.

26. Gordon, R.G., et al., A kinetic model for step coverage by atomic layer deposition in narrow holes or trenches. Chemical Vapor Deposition, 2003. **9**(2): p. 73-78.

27. Kang, J.K. and C.B. Musgrave, Mechanism of atomic layer deposition of SiO2 on the silicon (100)-2x1 surface using SiCl4 and H2O as precursors. Journal of Applied Physics, 2002. **91**(5): p. 3408-3414.

28. Higgins, S., W. DeSisto, and D. Ruthven, Diffusive transport through mesoporous silica membranes. Microporous and Mesoporous Materials, 2009. **117**(12): p. 268-277.

29. Cooper, C.A. and Y.S. Lin, Microstructural and gas separation properties of CVD modified mesoporous gamma-alumina membranes. Journal of Membrane Science, 2002. **195**: p. 35-50.

30. Jin, T., et al., Preparation of surface-modified mesoporous silica membranes and separation mechanism of their pervaporation properties. Desalination, 2011. **280**(13): p. 139-145.

31. Diaz, D.J., et al., Electroless deposition of gold and platinum for metallization of the intrapore space in porous gallium nitride. Thin Solid Films, 2006. **514**(1-2): p. 120-126.

32. Berland, B.S., et al., In situ monitoring of atomic layer controlled pore reduction in alumina tubular membranes using sequential surface reactions. Chemistry of Materials, 1998. **10**: p. 3941-3950.

33. Cameron, M.A., et al., Atomic layer deposition of SiO2 and TiO2 in alumina tubular membranes: pore reduction and effect of surface species on gas transport. Langmuir, 2000. **16**: p. 7435-7444.

34. Klaus, J.W., et al., Atomic layer deposition of SiO2 using catalyzed and uncatalyzed self-limiting surface reactions. Surface Review and Letters, 1999. **6**(3-4): p. 435-448.

35. Klaus, J.W., O. Sneh, and S.M. George, Growth of SiO2 at room temperature with the use of catalyzed sequential half-reactions. Science, 1997. **278**(5345): p. 1934-1936.

36. Du, Y., X. Du, and S.M. George, SiO2 film growth at low temperatures by catalyzed atomic layer deposition in a viscous flow reactor. Thin Solid Films, 2005. **491**(1-2): p. 43-53.

37. McCool, B.A. and W.J. DeSisto, Synthesis and characterization of silica membranes prepared by pyridine-catalyzed atomic layer deposition. Industrial & Engineering Chemistry Research, 2004. **43**(10): p. 2478-2484.

38. McCool, B.A. and W.J. DeSisto, Self-limited pore size reduction of mesoporous silica membranes via pyridine-catalyzed silicon dioxide ALD. Chemical Vapor Deposition, 2004. **10**(4): p. 190-+.

39. Mahurin, S., et al., Atomic layer deposition of TiO(2) on mesoporous silica. Journal of Non-Crystalline Solids, 2006. **352**(30-31): p. 3280-3284.

40. Higgins, S., et al., Preparation and characterization of non-Ionic block co-polymer templated mesoporous silica membranes. Journal of Membrane Science, 2006. **279**(1-2): p. 669-674.

41. Elliot, J., Diffusion in Polymers. 2004.

42. Li, K., Ceramic membranes for separation and reaction. 2007: John Wiley and Sons. 77-79.

43. Sea, B.K., et al., Hydrogen recovery from a H-2-H2O-HBr mixture utilizing silica-based membranes at elevated temperatures. 1. Pre of H2O- and H-2-selective membranes. Industrial & Engineering Chemistry Research, 1998. **37**(6): p. 2502-2508.

44. Tsuru, T., et al., Methane steam reforming by microporous catalytic membrane reactors. Aiche Journal, 2004. **50**(11): p. 2794-2805.

45. Cao, G.Z., et al., Permporometry study on the size distribution of active pores in porous ceramic membranes. Journal of Membrane Science, 1993. **83**(2): p. 221-235.

46. Joyner, L.G., E.P. Barrett, and R. Skold, The Determination of Pore Volume and Area Distributions in Porous Substances II. Journal of the American Chemical Society, 1951. **73**(7): p. 3155-3158.

47. Jaroniec, M., et al., Modification of surface and structural properties of ordered mesoporous silicates. Adsorption-Journal of the International Adsorption Society, 1999. **5**(1): p. 39-45.

48. Cassidy, D.E. and W.J. DeSisto, Atomic layer deposition modified ordered mesoporous silica membranes. Chemical Vapor Deposition, 2012(Accepted for Publication).

49. Siegfriedt, A., Evaluation of membrane performance on separating acetic acid from water compared to competing technologies, in Chemical Engineering. 2011, University of Maine: Orono.

50. Klepper, K.B., et al., Atomic layer deposition of organic-inorganic hybrid materials based on saturated linear carboxylic acids. Dalton Transactions, 2011. **40**(17): p. 4636-4646.

51. Noyes, W.A. and D.E. Wobbe, The vapor pressure of anhydrous oxalic acid. Journal of the American Chemical Society, 1926. **48**: p. 1882-1887.

52. Rose, M. and J.W. Bartha, Method to determine the sticking coefficient of precursor molecules in atomic layer deposition. Applied Surface Science, 2009. **255**(13-14): p. 6620-6623.

53. Guliants, V.V., M.A. Carreon, and Y.S. Lin, Ordered mesoporous and macroporous inorganic films and membranes. Journal of Membrane Science, 2004. **235**(12): p. 53-72.

54. Ritala, M. and M. Leskela, Handbook of Thin Film Materials. 2002: Academic Press.

55. Alsyouri, H.M., et al., Cyclic CVD modification of straight pore alumina membranes. Langmuir, 2003. **19**(18): p. 7307-7314.

56. Narayan, R.J., et al., Atomic layer deposition-based functionalization of materials for medical and environmental health applications. Philosophical Transactions of the Royal Society a-Mathematical Physical and Engineering Sciences, 2010. **368**(1917): p. 2033-2064.

57. Alessandri, I., et al., Tailoring the Pore Size and Architecture of CeO(2)/TiO(2) Core/Shell Inverse Opals by Atomic Layer Deposition. Small, 2009. **5**(3): p. 336-340.

58. Perez, I., et al., TEM-based metrology for HfO2 layers and nanotubes formed in anodic aluminum oxide nanopore structures. Small, 2008. **4**(8): p. 1223-1232.

59. Velleman, L., et al., Structural and chemical modification of porous alumina membranes. Microporous and Mesoporous Materials, 2009. **126**(1-2): p. 87-94.

60. Jiang, Y.B., et al., Sub-10 nm thick microporous membranes made by plasma-defined atomic layer deposition of a bridged silsesquioxane precursor. Journal of the American Chemical Society, 2007. **129**(50).

61. Ritala, M., et al., Rapid coating of through-porous substrates by atomic layer deposition. Chemical Vapor Deposition, 2006. **12**(11): p. 655-658.

62. Kemell, M., et al., Coating of Highly Porous Fiber Matrices by Atomic Layer Deposition. Chemical Vapor Deposition, 2008. **14**(11-12): p. 347-352.

63. Liang, X.H., et al., Modification of nanoporous supported lyotropic liquid crystal polymer membranes by atomic layer deposition. Journal of Membrane Science, 2010. **349**(1-2): p. 1-5.

64. Adomaitis, R.A., Development of a multiscale model for an atomic layer deposition process. Journal of Crystal Growth, 2010. **312**(8): p. 1449-1452.

65. Chew, T.L., A.L. Ahmad, and S. Bhatia, Ordered mesoporous silica (OMS) as an adsorbent and membrane for separation of carbon dioxide (CO(2)). Advances in Colloid and Interface Science, 2009. **153**(1-2): p. 43-57.

66. Yoo, S., et al., Reverse-selective membranes formed by dendrimers on mesoporous ceramic supports. Journal of Membrane Science, 2009. **334**(1-2): p. 16-22.

67. Kumar, P. and V.V. Guliants, Periodic mesoporous organic-inorganic hybrid materials: Applications in membrane separations and adsorption. Microporous and Mesoporous Materials, 2010. **132**(1-2): p. 1-14.

68. Williams, J.J., N.A. Seaton, and T. Duren, Influence of Surface Groups on the Diffusion of Gases in MCM-41: A Molecular Dynamics Study. Journal of Physical Chemistry C, 2011. **115**(21): p. 10651-10660.

69. McCool, B.A. and W.J. DeSisto, Amino-functionalized silica membranes for enhanced carbon dioxide permeation. Advanced Functional Materials, 2005. **15**(10): p. 1635-1640.

70. Hao, S.Y., et al., One-Pot Synthesis of Amino-Functionalized SBA-15 and Their CO(2)-Adsorption Properties. Chinese Journal of Inorganic Chemistry, 2011. **26**(6): p. 982-988.

71. Linares, N., et al., Incorporation of chemical functionalities in the framework of mesoporous silica. Chemical Communications, 2011. **47**(32): p. 9024-9035.

72. Lim, M.H., C.F. Blanford, and A. Stein, Synthesis and Characterization of a Reactive Vinyl-Functionalized MCM-41:â€‰ Probing the Internal Pore Structure by a Bromination Reaction. Journal of the American Chemical Society, 1997. **119**(17): p. 4090-4091.

73. Klepper, K.B., O. Nilsen, and H. Fjellvag, Deposition of thin films of organic-inorganic hybrid materials based on aromatic carboxylic acids by atomic layer deposition. Dalton Transactions, 2010. **39**(48): p. 11628-11635.

74. Klepper, K.B., et al., Atomic Layer Deposition of Organic-Inorganic Hybrid Materials Based on Unsaturated Linear Carboxylic Acids. European Journal of Inorganic Chemistry, 2011(34): p. 5305-5312.

75. Dameron, A.A., et al., Molecular layer deposition of alucone polymer films using trimethylaluminum and ethylene glycol. Chemistry of Materials, 2008. **20**(10): p. 3315-3326.

76. George, S.M., B. Yoon, and A.A. Dameron, Surface Chemistry for Molecular Layer Deposition of Organic and Hybrid Organic-Inorganic Polymers. Accounts of Chemical Research, 2009. **42**(4): p. 498-508.

77. Yoon, B., et al., Molecular Layer Deposition of Hybrid Organic-Inorganic Polymer Films using Diethylzinc and Ethylene Glycol. Chemical Vapor Deposition, 2009. **15**(4-6): p. 112-121.

78. Higgins, S., et al., Preparation and characterization of non-ionic block co-polymer templated mesoporous silica membranes. Journal of Membrane Science, 2006. **279**: p. 669-674.

79. Cao, G.Z., et al., Permporometry study on the size distribution of active pores in UF membranes. Journal of Membrane Science, 1993. **83**: p. 221-235.

80. McCool, B.A. and W.J. DeSisto, Self-limited pore size reduction of mesoporous silica membranes via pyridine-catalyzed silicon dioxide ALD. Chemical Vapor Deposition, 2004. **10**(4).

81. Zhao, Z.X., et al., Synthesis, characterization and gas transport properties of MOF-5 membranes. Journal of Membrane Science, 2011. **382**(1-2): p. 82-90.

82. Bux, H., et al., Zeolitic Imidazolate Framework Membrane with Molecular Sieving Properties by Microwave-Assisted Solvothermal Synthesis. Journal of the American Chemical Society, 2009. **131**(44).

83. An, W., et al., Selective separation of hydrogen from C1/C2 hydrocarbons and CO2 through dense natural zeolite membranes. Journal of Membrane Science, 2011. **369**: p. 414-419.

84. Leboda, R. and E. Mendyk, Hydrothermal modification of porous structure of silica adsorbents. Materials Chemistry and Physics, 1991. **27**(2): p. 189-212.

85. Fotou, G.P., Y.S. Lin, and S.E. Pratsinis, Hydrothermal stability of pure and modified microporous silica membranes. Journal of Materials Science, 1995. **30**(11): p. 2803-2808.

86. Sun, J.H. and M.O. Coppens, A hydrothermal post-synthesis route for the preparation of high quality MCM-48 silica with a tailored pore size. Journal of Materials Chemistry, 2002. **12**(10): p. 3016-3020.

87. Kim, J.M. and R. Ryoo, Disintegration of mesoporous structures of MCM-41 and MCM-48 in water. Bulletin of the Korean Chemical Society, 1996. **17**(1): p. 66-68.

88. Cassiers, K., et al., A detailed study of thermal, hydrothermal, and mechanical stabilities of a wide range of surfactant assembled mesoporous silicas. Chemistry of Materials, 2002. **14**(5): p. 2317-2324.

89. Gu, Y.F. and S.T. Oyama, Permeation properties and hydrothermal stability of silica-titanic membranes supported on porous alumina substrates. Journal of Membrane Science, 2009. **345**(1-2): p. 267-275.

90. Araki, S., et al., Preparation and pervaporation properties of silica-zirconia membranes. Desalination, 2011. **266**(1-3): p. 46-50.

APPENDIX A

CALCULATIONS FOR THE PORE SIZE REDUCTION

Calculation of the pore size reduction with constant growth rate

Raw data input from permporosimetry

$i := 0..9$

$$r0 := \begin{pmatrix} 20.42198413 \\ 26.19750331 \\ 30.15850301 \\ 35.83714683 \\ 44.65507083 \\ 46.84158741 \\ 52.05097116 \\ 61.48295552 \\ 86.47455321 \\ 131.8495752 \end{pmatrix} \quad np0 := \begin{pmatrix} 0 \\ 0 \\ 1.31096E+19 \\ 2.38567E+19 \\ 1.58863E+19 \\ 1.34879E+19 \\ 9.65431E+18 \\ 5.84169E+18 \\ 1.58641E+18 \\ 1.69734E+17 \end{pmatrix} \quad np1 := \begin{pmatrix} 9.68193E+18 \\ 1.63575E+19 \\ 1.67593E+19 \\ 1.21872E+19 \\ 7.43766E+18 \\ 8.5932E+18 \\ 4.81676E+18 \\ 2.92038E+18 \\ 8.39878E+17 \\ 1.04822E+17 \end{pmatrix} \quad np2 := \begin{pmatrix} 4.04822E+18 \\ 1.4482E+19 \\ 1.64881E+19 \\ 1.02056E+19 \\ 5.91178E+18 \\ 5.76124E+18 \\ 3.89829E+18 \\ 2.4405E+18 \\ 6.9488E+17 \\ 9.39023E+16 \end{pmatrix}$$

$$np4 := \begin{pmatrix} 1.88634E+18 \\ 1.48458E+19 \\ 1.11932E+19 \\ 7.03364E+18 \\ 4.50698E+18 \\ 4.79965E+18 \\ 3.50221E+18 \\ 1.84E+18 \\ 5.19233E+17 \\ 8.01475E+16 \end{pmatrix} \quad np5 := \begin{pmatrix} 5.15731E+21 \\ 1.08221E+22 \\ 8.36587E+21 \\ 6.87112E+21 \\ 4.25654E+21 \\ 3.90389E+21 \\ 2.82896E+21 \\ 1.67292E+21 \\ 4.72125E+20 \\ 7.3424E+19 \end{pmatrix} \quad np15 := \begin{pmatrix} 3.7091E+18 \\ 5.46667E+18 \\ 4.06609E+18 \\ 3.55879E+18 \\ 2.09047E+18 \\ 2.58959E+18 \\ 1.34027E+18 \\ 7.24664E+17 \\ 2.33879E+17 \\ 3.4064E+16 \end{pmatrix}$$

$$np20 := \begin{pmatrix} 4.41737E+20 \\ 6.07259E+21 \\ 3.92626E+21 \\ 2.5318E+21 \\ 1.35845E+21 \\ 1.46738E+21 \\ 8.13461E+20 \\ 5.01781E+20 \\ 1.34094E+20 \\ 2.02056E+19 \end{pmatrix} \quad np40 := \begin{pmatrix} 4.16732E+20 \\ 1.25661E+21 \\ 2.15622E+20 \\ 2.69252E+20 \\ 1.7854E+20 \\ 2.07724E+20 \\ 9.05669E+19 \\ 4.34694E+19 \\ 1.54902E+19 \\ 2.52204E+18 \end{pmatrix} \quad np50 := \begin{pmatrix} 5.06E+20 \\ 2.51E+20 \\ 4.81E+20 \\ 2.03E+20 \\ 9.72E+19 \\ 2.05E+20 \\ 5.28E+19 \\ 2.26E+19 \\ 9.39E+18 \\ 1.36E+18 \end{pmatrix}$$

$np0 := np0 \cdot 100($
$np1 := np1 \cdot 100($
$np2 := np2 \cdot 100($
$np3 := np3 \cdot 100($
$np4 := np4 \cdot 100($
$np10 := np10 \cdot 100($
$np15 := np15 \cdot 100($

Calculation of porosity from the distribution data: The PSD is integrated to sum up the overall pore areas of each membrane. The relative porosity change is determined by normalizing to the pore area for the unmodified membrane. The assumption here is that the pores are all cylinders and the calculation just the 2D porosity change, that is a cross sectional porosity change. In effect, it assumes the membrane thickness is uniform if translated to a 3D porosity calculation.

PSD data are fitted to a function and then integrated to calculate 2D pore areas for each membrane.

Subscripts on the variable *Area*, refer to the number of ALD cycles used for modification.

$S := \text{lspline}(r0, np0)$ $\quad np0fit(z) := \text{interp}(S, r0, np0, z)$ $\quad z := 10..150$

$$Area_0 := \pi \cdot \int_{27}^{150} z^2 \cdot np0fit(z)\, dz = 5.046 \times 10^{27}$$

Calculation of relative porosity per ALD cycle

$S_1 := \text{lspline}(r0, np1)$ $\quad np1fit(z) := \text{interp}(S_1, r0, np1, z)$

$$Area_1 := \pi \cdot \int_{13}^{95} z^2 \cdot np1fit(z)\, dz = 2.732 \times 10^{27}$$

$S_2 := \text{lspline}(r0, np2)$ $\quad np2fit(z) := \text{interp}(S_2, r0, np2, z)$

$$E_1 := \frac{Area_1}{Area_0} = 0.542$$

$$Area_2 := \pi \cdot \int_{19}^{150} z^2 \cdot np2fit(z)\, dz = 2.411 \times 10^{27}$$

$S_3 := \text{lspline}(r0, np3)$ $\quad np3fit(z) := \text{interp}(S_3, r0, np3, z)$

$$E_2 := \frac{Area_2}{Area_0} = 0.478$$

$$Area_3 := \pi \cdot \int_{20}^{150} z^2 \cdot np3fit(z)\, dz = 2.204 \times 10^{27}$$

$S_4 := \text{lspline}(r0, np4)$ $\quad np4fit(z) := \text{interp}(S_4, r0, np4, z)$

$$E_3 := \frac{Area_3}{Area_0} = 0.437$$

$$Area_4 := \pi \cdot \int_{20}^{150} z^2 \cdot np4fit(z)\, dz = 1.909 \times 10^{27}$$

$$E_4 := \frac{Area_4}{Area_0} = 0.378$$

$S_5 := \text{lspline}(r0, np5)$ $\quad np5fit(z) := \text{interp}(S_5, r0, np5, z)$

$$Area_5 := \pi \cdot \int_{17}^{150} z^2 \cdot np5fit(z)\, dz = 1.707 \times 10^{27}$$

$$E_5 := \frac{Area_5}{Area_0} = 0.338$$

$S_{10} := \text{lspline}(r0, np10) \qquad np10fit(z) := \text{interp}(S_{10}, r0, np10, z)$

$$Area_{10} := \pi \cdot \int_{24}^{150} z^2 \cdot np10fit(z)\, dz = 9.674 \times 10^{26} \qquad E_{10} := \frac{Area_{10}}{Area_0} = 0.192$$

$S_{15} := \text{lspline}(r0, np15) \qquad np15fit(z) := \text{interp}(S_{15}, r0, np15, z)$

$$Area_{15} := \pi \cdot \int_{20}^{150} z^2 \cdot np15fit(z)\, dz = 7.925 \times 10^{26} \qquad E_{15} := \frac{Area_{15}}{Area_0} = 0.157$$

$S_{20} := \text{lspline}(r0, np20) \qquad np20fit(z) := \text{interp}(S_{20}, r0, np20, z)$

$$Area_{20} := \pi \cdot \int_{21}^{150} z^2 \cdot np20fit(z)\, dz = 5.39 \times 10^{26} \qquad E_{20} := \frac{Area_{20}}{Area_0} = 0.107$$

$S_{30} := \text{lspline}(r0, np30) \qquad np30fit(z) := \text{interp}(S_{30}, r0, np30, z)$

$$Area_{30} := \pi \cdot \int_{20}^{150} z^2 \cdot np30fit(z)\, dz = 1.228 \times 10^{26} \qquad E_{30} := \frac{Area_{30}}{Area_0} = 0.024$$

$S_{40} := \text{lspline}(r0, np40) \qquad np40fit(z) := \text{interp}(S_{40}, r0, np40, z)$

$$Area_{40} := \pi \cdot \int_{20}^{150} z^2 \cdot np40fit(z)\, dz = 6.61 \times 10^{25} \qquad E_{40} := \frac{Area_{40}}{Area_0} = 0.013$$

$S_{50} := \text{lspline}(r0, np50) \qquad np50fit(z) := \text{interp}(S_{50}, r0, np50, z)$

$$Area_{50} := \pi \cdot \int_{20}^{150} z^2 \cdot np50fit(z)\, dz = 3.328 \times 10^{25} \qquad E_{50} := \frac{Area_{50}}{Area_0} = 6.597 \times 10^{-3}$$

Examples of some of the fitted functions that were integrated

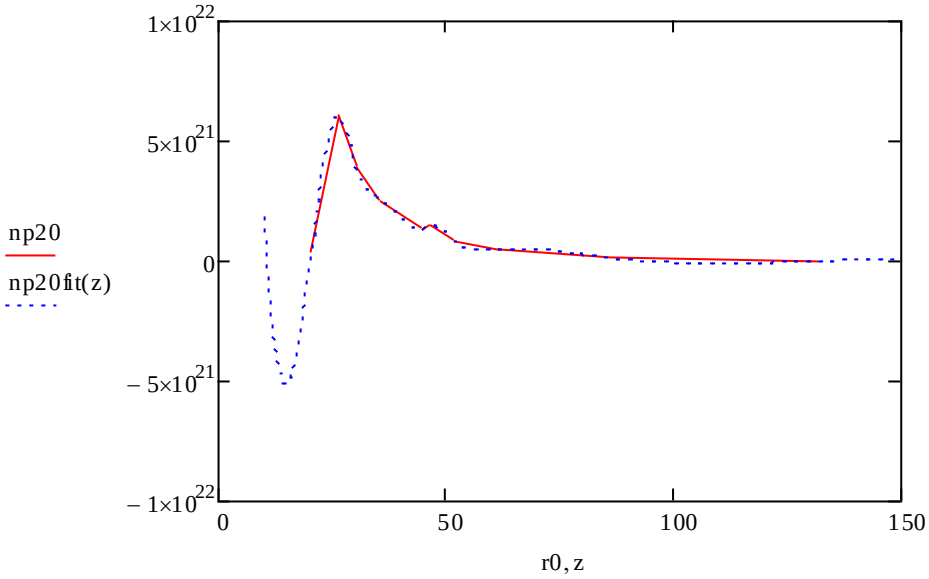

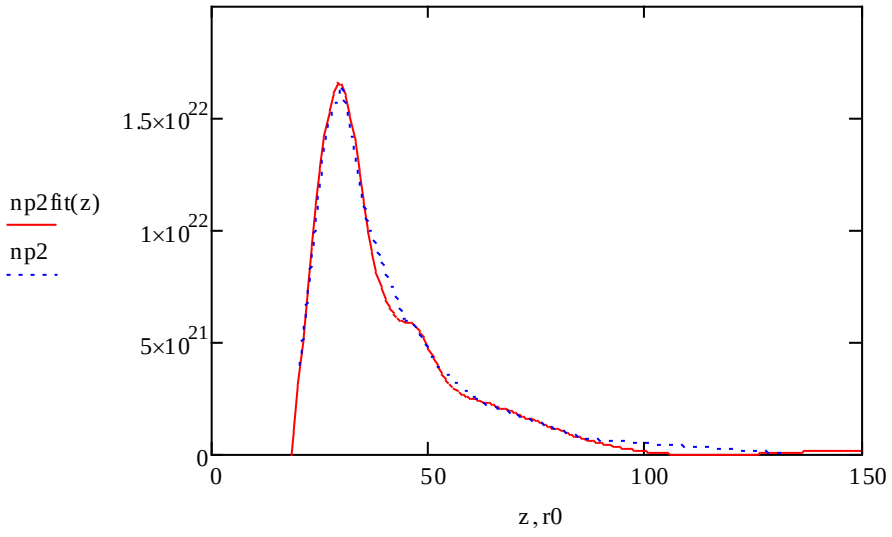

Experimental data from ALD: relative porosity (datarp) change as a function of cycle number (datan)

$$datarp := \begin{pmatrix} 1 \\ 0.671374717 \\ 0.544037263 \\ 0.502157055 \\ 0.428300278 \\ 0.37081376 \\ 0.211711755 \\ 0.192652063 \\ 0.135265524 \\ 0.044219766 \\ 0.017741343 \\ 0.012274491 \end{pmatrix} \quad datan := \begin{pmatrix} 0 \\ 1 \\ 2 \\ 3 \\ 4 \\ 5 \\ 10 \\ 15 \\ 20 \\ 30 \\ 40 \\ 50 \end{pmatrix} \quad datarp1 := \begin{pmatrix} 1 \\ E_1 \\ E_2 \\ E_3 \\ E_4 \\ E_5 \\ E_{10} \\ E_{15} \\ E_{20} \\ E_{30} \\ E_{40} \\ E_{50} \end{pmatrix} \quad datan1 := \begin{pmatrix} 0 \\ 1 \\ 2 \\ 3 \\ 4 \\ 5 \\ 10 \\ 15 \\ 20 \\ 30 \\ 40 \\ 50 \end{pmatrix}$$

Plot shows the relative porosity change calculated from permeance reduction, datarp, as a function of cycle number as well as the relative porosity change calculated from integrating PSD's, datarp1. The data are in reasonable agreement, suggesting that the permeance reduction is largely due to porosity change after modification. At the early cycles the permeance does not drop as one might predict from the porosity decrease alone.

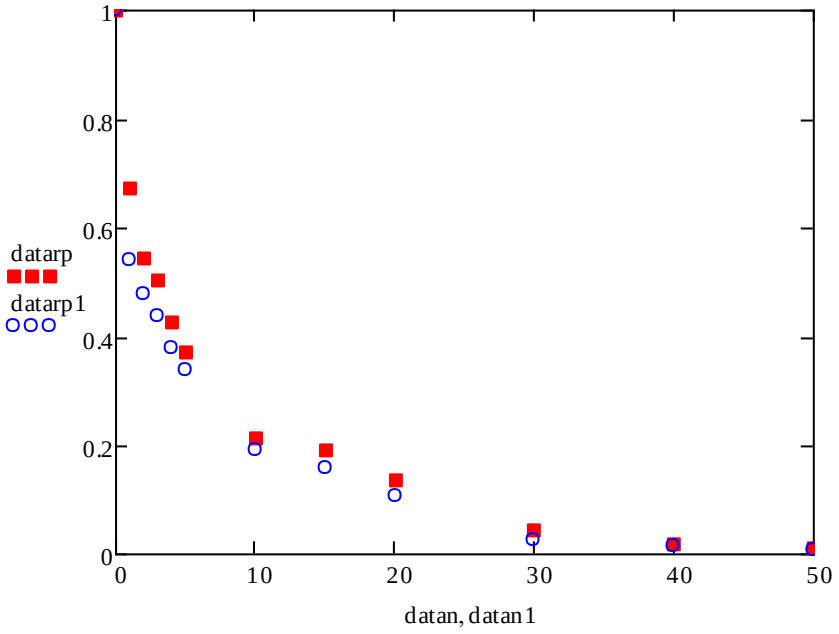

The calculation below determines the reduction in pore area per ALD cycle, and assumes a constant ALD growth rate per cycle, R1 and R2.

$R1 := 1.5$

growth rate 1

$n := 0..60$

$$\text{Area1}(n) := \pi \cdot \left[\sum_i \left[\left[\frac{\left[\left(r0_i - n \cdot R1 \right) + \overrightarrow{\left| r0_i - n \cdot R1 \right|} \right]}{2} \right]^2 \cdot np0_i \right] \right]$$

Program to calculate a changing radius as a function of variable growth rate. The function, r(r,n) is the new radii (from the original r) after n ALD cycles. An ALD growth rate per cycle can be given as a function of pore radius.

Growth rate as a function of pore radius

$\underset{\wedge\wedge\wedge}{R}(r) := 1.5$

$\underset{\wedge\wedge\wedge}{R}(r) := 0.015 \cdot r + .01$

Calculation of new radii as a function of starting radii and number of ALD cycles

$i := 0..9$

$$r(r,n) := \left| \begin{array}{l} \text{for } i \in 0..\text{rows}(r) - 1 \\ \quad x_i \leftarrow r_i \\ \text{for } n \in 1..n \\ \quad \left| \begin{array}{l} \text{for } i \in 0..\text{rows}(r) - 1 \\ \quad x_i \leftarrow \text{if}\left(x_i > R\left(x_i\right), x_i - R\left(x_i\right), 0 \right) \end{array} \right. \\ x \end{array} \right.$$

Examples of pore size distribution data fitted to a growth rate that is dependent on pore radius Note that the decrease in occurrence of all pores had to be adjusted by the division factor seen in the y-axis data. The blue curves are experimental data. The red curves are fitted data. The growth rate is a compromise and here shows a better fit in the middle ALD cycles.

2 ALD cycles of modification

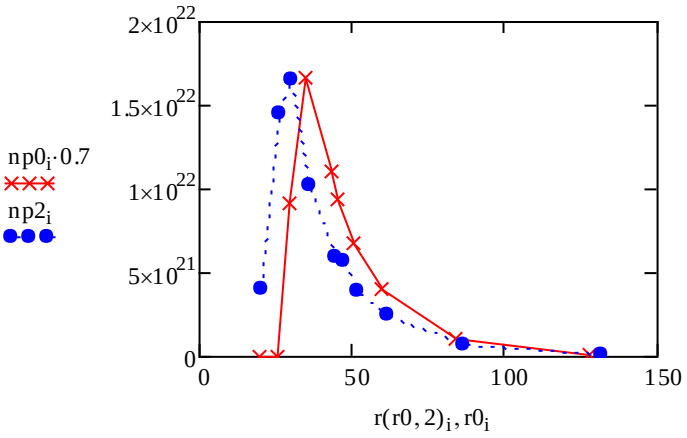

5 ALD cycles modification, fit not as good reflecting the higher growth rate here.

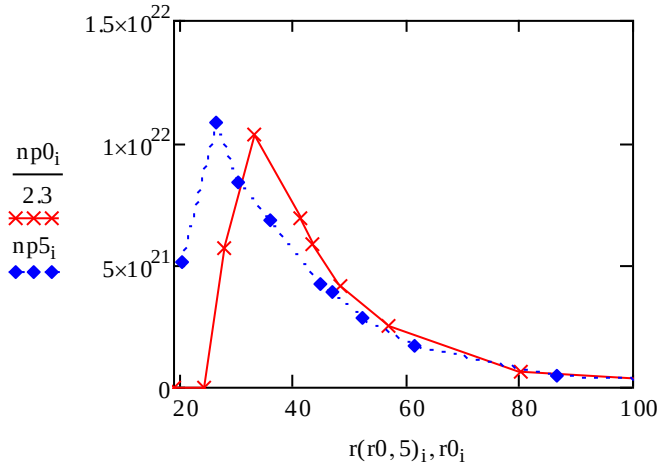

10 ALD cycles modification

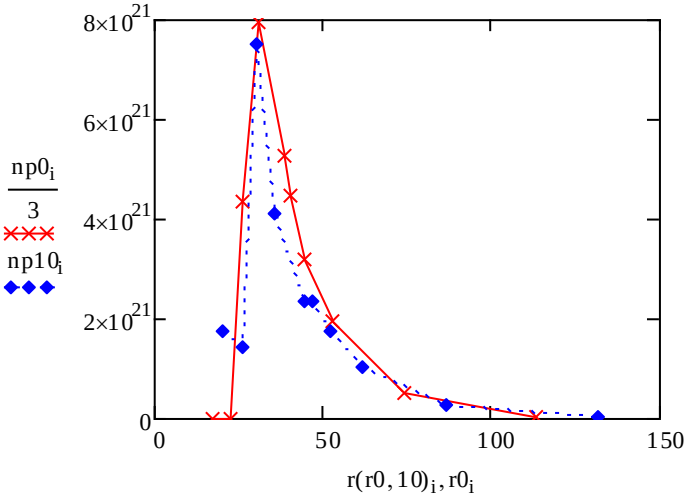

20 ALD cycles modification

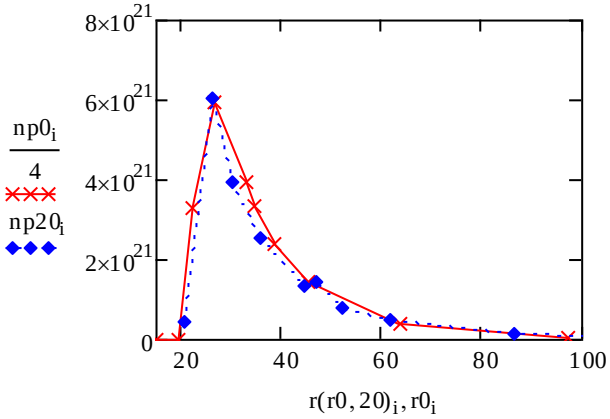

40 ALD cycles modification

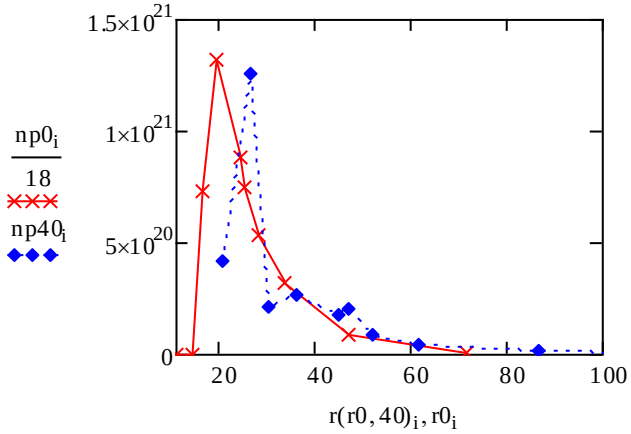

Calculation of cumulative pore area for the fitted data numerically using a Reimann sum method

$$Area5fit := \frac{\pi \cdot \left[\sum_i \left[\left(r(r0,5)_i \right)^2 \cdot \frac{np0_i}{2.3} \right] \right]}{Area1(0)} = 0.373$$

$$Area20fit := \frac{\pi \cdot \left[\sum_i \left[\left(r(r0,20)_i \right)^2 \cdot \frac{np0_i}{4} \right] \right]}{Area1(0)} = 0.135$$

$$Area40fit := \frac{\pi \cdot \left[\sum_i \left[\left(r(r0,40)_i \right)^2 \cdot \frac{np0_i}{4} \right] \right]}{Area1(0)} = 0.073$$

$$Area50fit := \frac{\pi \cdot \left[\sum_i \left[\left(r(r0,50)_i \right)^2 \cdot \frac{np0_i}{4} \right] \right]}{Area1(0)} = 0.053$$

Calculation of the area under the fitted data (fitted to a growth rate) by first fitting the data to a spline function and then integrating that function. Some fits created functions that were negative below a certain pore radius. Checks on this were done graphically to provide the starting pore radius for integration. These numbers could be compared with the above values done simply by a Reimann sum method. Again, subscripts refer to number of ALD cycles.

$$Sf_2 := \text{lspline}\left(r(r0,2), \frac{np0}{1.5}\right) \qquad np2fit_m(z) := \text{interp}\left(Sf_2, r(r0,2), \frac{np0}{1.5}, z\right)$$

$$Area_{2m} := \pi \cdot \int_{26}^{150} z^2 \cdot np2fit_m(z)\, dz = 3.065 \times 10^{27} \qquad \frac{Area_{2m}}{Area_0} = 0.607$$

$$Sf_5 := \text{lspline}\left(r(r0,5), \frac{np0}{2.3}\right) \qquad np5fit_m(z) := \text{interp}\left(Sf_5, r(r0,5), \frac{np0}{2.3}, z\right)$$

$$Area_{5m} := \pi \cdot \int_{26}^{130} z^2 \cdot np5fit_m(z)\, dz = 1.724 \times 10^{27} \qquad \frac{Area_{5m}}{Area_0} = 0.342$$

$$Sf_{10} := \text{lspline}\left(r(r0,10), \frac{np0}{3}\right) \qquad np10fit_m(z) := \text{interp}\left(Sf_{10}, r(r0,10), \frac{np0}{3}, z\right)$$

$$Area_{10m} := \pi \cdot \int_{13}^{130} z^2 \cdot np10fit_m(z)\, dz = 1.064 \times 10^{27} \qquad \frac{Area_{10m}}{Area_0} = 0.211$$

$$Sf_{20} := \text{lspline}\left(r(r0,20), \frac{np0}{4}\right) \qquad np20fit_m(z) := \text{interp}\left(Sf_{20}, r(r0,20), \frac{np0}{4}, z\right)$$

$$Area_{20m} := \pi \cdot \int_{10}^{100} z^2 \cdot np20fit_m(z)\, dz = 4.951 \times 10^{26} \qquad \frac{Area_{20m}}{Area_0} = 0.098$$

Example of data fitting using lspline to calculate the area under the curve. This is for the 20 ALD cycle membrane.

$$Y := \frac{np0}{4} =$$

	0
0	0
1	0
2	$3.277 \cdot 10^{21}$
3	$5.964 \cdot 10^{21}$
4	$3.972 \cdot 10^{21}$
5	$3.372 \cdot 10^{21}$
6	$2.414 \cdot 10^{21}$
7	$1.46 \cdot 10^{21}$
8	$3.966 \cdot 10^{20}$
9	$4.243 \cdot 10^{19}$

$X := r(r0, 20)$

$S := lspline(X, Y)$

$fit(z) := interp(S, X, Y, z)$

$z := 0..150$

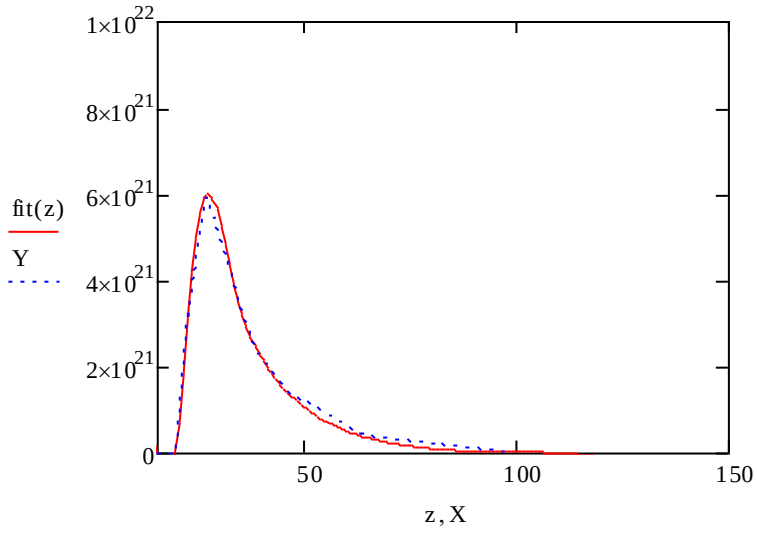

$$\int_{20}^{150} fit(z)\,dz = 9.391 \times 10^{22}$$

Plot of the relative porosity change for the fitted and raw pore size distributions. Again, the data plotted is the normalized area decrease as a function of ALD cycles. Here, the normalized area is assumed to correlate with the normalized porosity (in 2D)

$$datafit := \begin{pmatrix} 1 \\ \frac{Area_{2m}}{Area_0} \\ \frac{Area_{5m}}{Area_0} \\ \frac{Area_{10m}}{Area_0} \\ \frac{Area_{20m}}{Area_0} \end{pmatrix} \quad dataX := \begin{pmatrix} 0 \\ 2 \\ 5 \\ 10 \\ 20 \end{pmatrix} \quad dataraw := \begin{pmatrix} 1 \\ \frac{Area_2}{Area_0} \\ \frac{Area_5}{Area_0} \\ \frac{Area_{10}}{Area_0} \\ \frac{Area_{20}}{Area_0} \end{pmatrix}$$

$$\frac{Area_{5m}}{Area_0} = 0.342$$

$$\frac{Area_5}{Area_0} = 0.338$$

xx:= 0..40

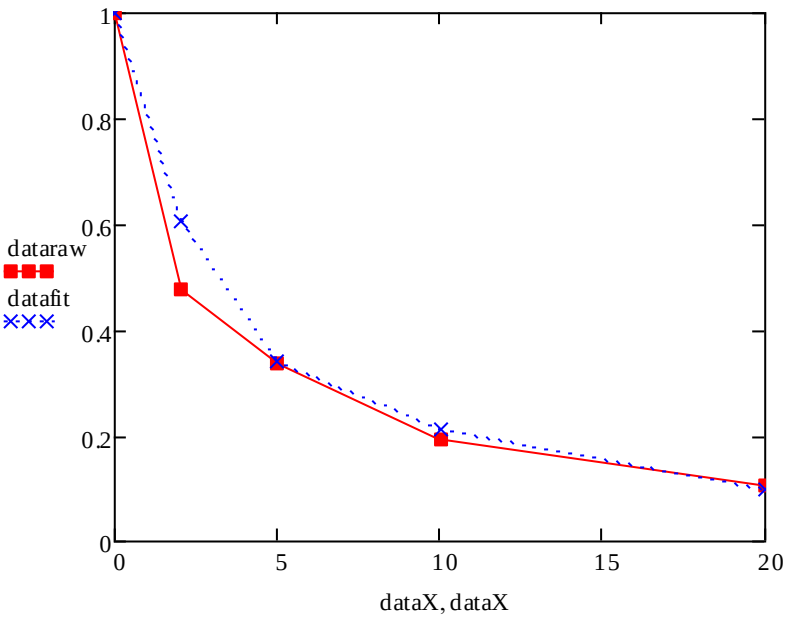

$$datafit = \begin{pmatrix} 1 \\ 0.607 \\ 0.342 \\ 0.211 \\ 0.098 \end{pmatrix}$$

$$dataraw = \begin{pmatrix} 1 \\ 0.478 \\ 0.338 \\ 0.192 \\ 0.107 \end{pmatrix}$$

As seen from the fits of the pore size distributions generated using the variable growth rate above, the growth rate chosen has a better fit at cycles greater than 5. Data beyond 20 ALD cycles was neglected as the PSD data was less reliable due to low porosity.

BIOGRAPHY OF THE AUTHOR

David Emmett Cassidy was born and raised in Bangor, Maine. He graduated from John Bapst Memorial High School (Bangor, ME) in 2002, and went on to attend Clarkson University in Potsdam, New York where he graduated in 2006 with a Bachelor of Science in Chemical Engineering with a Minor in Business. After graduation, he completed a 6 month sailing voyage in 2006 on s/v Fleana, a 38' yawl built in 1961. This journey took him from Bangor, Maine, USA to Bangor, Northern Ireland, where he along with his father Daniel Cassidy, delivered the key to the city of Bangor, Maine to the Mayor of Bangor, Northern Ireland. On the return trip 2007, they delivered the Crest of Bangor, Northern Ireland to Bangor, Maine. David then entered the Chemical Engineering graduate program at the University of Maine in November 2006 to study under Dr. William J. DeSisto. Extracurricular pursuits include ice and rock climbing, canoeing and backcountry skiing. He is a candidate for the Doctor of Philosophy degree in Chemical Engineering from the University of Maine in May, 2012.